THESIS

A TECHNO-ECONOMIC STUDY ON THE WASTE HEAT RECOVERY OPTIONS FOR WET COOLED NATURAL GAS COMBINED CYCLE POWER PLANTS

Submitted by

Achyut Paudel

Department of Mechanical Engineering

In partial fulfillment of the requirements

For the Degree of Master of Science

Colorado State University

Fort Collins, Colorado

Summer 2018

Master's Committee:

Advisor: Todd M. Bandhauer

Jason C. Quinn
Kenneth F. Reardon

ABSTRACT

A TECHNO-ECONOMIC STUDY ON THE WASTE HEAT RECOVERY OPTIONS FOR WET COOLED NATURAL GAS COMBINED CYCLE POWER PLANTS

Increasing ambient temperature is known to have negative impacts on the performance of gas turbine and combined cycle power plants. There have been multiple approaches to mitigate this performance reduction. One such method involves cooling of the gas turbine inlet air. There are several different commercial techniques available, but they are energy intensive and require large capital investments. One potential option for cost reduction is to recover the waste heat emanating from the power plants to operate thermally activated cooling systems to cool the turbine inlet air. In this study, a 565 MW natural gas combined cycle power plant subjected to different waste heat recovery scenarios and gas turbine inlet chilling is assessed. A simplified thermodynamic and heat transfer model is developed to predict the performance of an evaporatively cooled NGCC power plant at varying ambient conditions. By taking typical meteorological year (TMY3) hourly weather data for two different locations – Los Angeles, California and Houston, Texas – the yearly output for this plant is predicted at a 100% capacity factor. The feasibilities of different waste heat recovery (WHR) systems including a gas turbine exhaust driven absorption chiller, a flue gas driven absorption chiller, a steam driven absorption chiller, and an electrically driven vapor compression chiller are assessed by calculating the Levelized Cost of Electricity (LCOE) for each scenario. In each of these cases, a parametric analysis was performed on the COP and the costs (\$ per kW_{th}) of the system. In these cases, the COP was varied from 0.2 to 2.0 (increments of 0.2), whereas the costs were varied logarithmically

from \$10 to \$10,000 per kW_{th}. The results of the analysis showed that for a fixed WHR system cost (i.e., \$ per kW_{th}), the system powered by flue gas generated the lowest LCOE, followed by the electrically-driven vapor compression chiller, steam-heated chiller, and finally, the gas turbine exhaust driven chiller for both geographic locations at all COP combinations. The analysis also investigated the impact of fixed investment cost, and the flue gas system again yielded the smallest LCOE and yielded a lower LCOE than the baseline case (no WHR) over a wide range of COPs. The maximum costs each of these systems could tolerate before the LCOE is higher than the baseline case was also determined. The flue gas driven absorption system had the highest tolerable costs at all COP combinations, followed by the vapor compression, steam, and gas turbine exhaust driven systems. As such, the flue gas powered system was identified as the most economic system to reduce the LCOE from the baseline case for a wide range of COP combinations at high tolerable costs for these two locations.

ACKNOWLEDGEMENTS

First of all, I would like to thank my advisor Dr. Todd Bandhauer for his valuable insights that helped me initiate, work through, and complete my research. The opportunity to work with him has helped me grow intellectually and communicate well technically. During my time working with him, I gained a lot of confidence and lessons that will serve throughout my professional career. In addition, I would like to thank my committee member Dr. Jason Quinn for his valuable insights that he provided during our multiple meetings in the Powerhouse Energy Campus. I would also like to thank Dr. Kenneth Reardon for being in my committee.

I would like to thank my mentor Dr. Nawa Raj Baral who helped me with much of the economic model generation and visual basic programming in excel. I would also like to thank the members and fellow students of the Interdisciplinary Thermal Science Lab for their help and insightful thoughts through this endeavor. Specifically, I would like to thank Derek Young, Shane Garland and David Hobby as I have spent multiple hours working in the lab with them and talking about the prospects of my research. They have also helped me review my works and provide positive comments.

Finally, I am thankful to my family and friends who supported me throughout my graduate studies. Without the support from my family and friends, it wouldn't have been possible to be staying abroad and completing my studies and research.

TABLE OF CONTENTS

LIST OF TABLES

LIST OF FIGURES

LIST OF SYMBOLS

Symbol	Description	Units
A	Area	m^2
a_s	Stoichiometric Coefficient	-
B	Breadth	m
d_d	Drop Diameter	m
D	Diameter, Diffusion Coefficient, Discount Rate	m,m^2 s^{-1},%
dP	Pressure Drop	kPa
dT	Temperature Differential	°C
C	Heat Capacity	J $K^{-1}s^{-1}$
c_p	Specific Heat Capacity	J $kg^{-1}K^{-1}$
C_r	Ratio of Heat Capacities	-
FA	Fuel Air Ratio	-
g	Gravitational Acceleration	m s^{-2}
G	Mass Velocity	kg $m^{-2}s^{-1}$
h	Heat Transfer Coefficient	W $m^{-2}K^{-1}$
H	Height	m
h_d	Mass Transfer Coefficient	kg $m^{-2}s^{-1}$
i	Enthalpy	J kg^{-1}
K	Loss Coefficient	-
L	Length	m

LPn	Levelization Period	years
$\dot{m}$	Mass flow rate	kg s^{-1}
Me	Merkel's Number	-
MW	Molecular Weight	kg mol^{-1}
$\dot{n}$	Molar Flow	mol s^{-1}
N	Nominal Escalation Rate	%
NTU	Number of Transfer Units	-
p	Pressure	kPa
PR	Pressure Ratio	-
Pr	Prandtl Number	-
$\dot{Q}$	Heat Transfer Rate	W
r	Radius	m
R	Gas Constant	J $kg^{-1}K^{-1}$
Re	Reynold's Number	-
RH	Relative Humidity, Reheater	-
Ry	Characteristic Flow Parameter	m^{-1}
Sc	Schmidt Number	-
T	Temperature	°C
UA	Heat Transfer Conductance	W K^{-1}
v	Velocity	m s^{-1}
w	Humidity Ratio	-
W	Width	m

$\dot{W}$	Power Output	W
x	Quality	-
y_n	Mole Fraction	-
Subscripts		
av	Air Vapor Mixture	
a	Air	
c	Compressor, Contraction	
cond	Condenser	
cool	Cooling	
ct	Cooling Tower	
ctc	Cooling Tower Contraction	
cw	Cooling water	
da	Dry Air	
de	Drift Eliminator	
DP	Design Point	
e	electrical	
eco	Economizer	
eqv	Equivalent	
evp	Evaporator	
evap	Evaporated	
fi	Fill Zone	
fie	Effective loss in Fill	

fr	Frontal	
fs	Fill Support	
g	Gas	
gen	Generator	
HEX	Heat Exchanger	
i	In	
il	Inlet Louvers	
ir	Inlet Rounding	
max	Maximum	
min	Minimum	
mix	Mixture	
NG	Natural Gas	
o	out	
ODP	Off Design Point	
p	Polytropic	
pl	Plenum Chamber	
rz	Rain Zone	
s	Saturated, isentropic	
sp	Spray Zone	
sph	Superheater	
t	Turbine	
tot	Total	

up	Upstream	
v	Vapor	
w	Water	
wd	Water Distribution System	
wh	Waste Heat	
Greek Symbols		
ε	Effectiveness	-
η	Efficiency	-
γ	Specific Heat Capacity Ratio	-
μ	Dynamic Viscosity	kg $m^{-1}s^{-1}$
ρ	Density	kg m^{-3}
ϕ	Availability, Equivalence Ratio	-
σ	Surface Tension	N m^{-1}

CHAPTER 1. INTRODUCTION

1.1 Background

The electricity generation sector in the United States (U.S.) is primarily dominated by fossil fuel electricity generation. The U.S. Energy Information Administration (EIA) estimates, in 2016, about 4.08 trillion kWh of electricity were generated at utility-scale facilities in the U.S [5]. About 65% of this generation was from fossil fuels (coal, natural gas, petroleum, and other gases), about 20% was from nuclear energy, and about 15% was from renewable energy sources. Clearly fossil fuel electricity generation has been dominating the industry since the very start, and only recently have renewable energy technologies started to gain significant share in total electricity generation. For example, U.S. renewable energy consumption grew by 6 percent, from 7.600 quadrillion Btu in 2009 to 8.090 quadrillion Btu in 2010. The relative share of renewable energy to total energy consumption has grown to 8 percent in 2010[6]. However, natural gas electricity generation constitutes about 33.8% of the total generation, whereas coal accounts for about 30.4% [5]. As of July 2017, about 54% of the electricity from natural gas-fired capacity came from natural gas combined cycle (NGCC) power plants [7].

Many traditional fossil-fuel fired power plants have efficiencies in the range of 30 to 40 percent, but NGCC power plants are able to meet efficiencies of 50 to 60 percent [8]. Also known as Combined Cycle Gas Turbine (CCGT) power plants, these plants can achieve such high thermal efficiencies through heat recovery steam generation and a bottoming Rankine cycle. Although the efficiencies for NGCC power plants are high compared to other systems, the plants still lose 40 to 50 percent of their energy during the power generation process. The majority of heat losses occur in the condenser, where steam is condensed to resupply boiler feed water of the power plant. The plant also loses energy through the flue gas exhaust because the gas exits to the atmosphere from

the stack at a temperature higher than ambient (~80-150°C). This heat loss also accounts for the total heat losses that occur in the power plant. The efficiency of a typical gas turbine unit is 40%, while the efficiency of the steam cycle operating under a combined cycle is around 30%. For these efficiency numbers, nearly 60% of heat input to the gas turbine cycle is wasted in a simple cycle unit. However, for a combined cycle, nearly 70% of the exhaust heat from the gas turbine cycle is wasted [9]. These losses are form turbomachine performance, heat loss through flue gas, and generator losses. One opportunity to improve power plant efficiency is to use this low-grade waste heat as a heat input for other low-grade heat driven systems. Multiple research studies have been performed in the waste heat recovery (WHR) systems that can potentially increase the overall efficiency of the power plant. One potential use of the low-grade waste heat is to utilize a heat powered cooling system to chill the power plant gas turbine inlet air. Recently, many investigations have focused on enhancing power plant efficiency. Particularly in middle-eastern countries where the ambient temperature is high, gas turbine inlet chilling is practiced widely because increasing ambient temperatures have negative impacts on the performance and the efficiency of the NGCC power plants. Another potential use of waste heat driven systems can be the reduction of dry cooling load for dry cooled power plants because the heat is utilized in a process instead. More discussions are made in the literature review sections.

1.2 Motivation and Objectives

Most NGCC power plants are designed to operate at the International Organization for Standardization (ISO) ambient conditions (15°C dry bulb temperature, 101.325 kPa barometric pressure and 0.6 relative humidity)[10]. However, at higher ambient temperatures, the performance of the power plant and the efficiency degrade such that there is a loss in total MWh produced, and, therefore, revenue generated by the power producers. The increased ambient

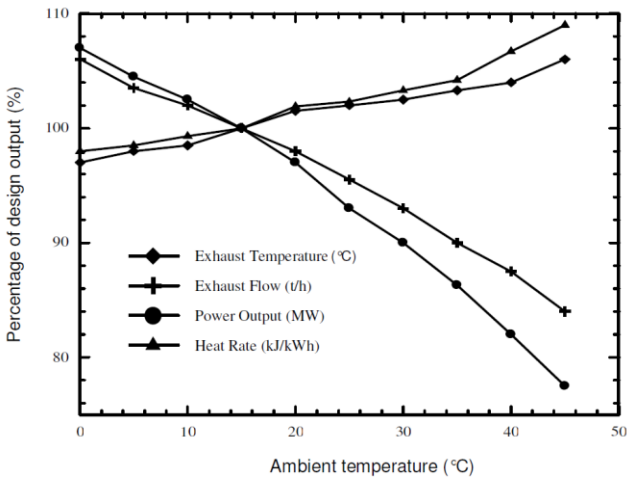

Figure 1-1. Effect of ambient temperature on gas turbine performance [4].

temperatures decrease the plant power output due to the change in air density at the NGCC compressor inlet. The increase in ambient temperature decreases the gas density, so the mass flow rate of air entering the compressor of the gas turbine also decreases. Figure 1-1 shows there is a reduction of nearly 18% in the power output of the gas turbine as the ambient temperature reaches 40°C from the ISO conditions. More details on the gas turbine losses are discussed in section 3.1. Due to the reduced inlet mass flow, the exhaust mass flow from the gas turbine cycle also decreases, causing a subsequent power reduction in the bottoming Rankine cycle. Additionally, for wet cooled power plants, cooling tower performance is highly dependent on ambient temperature and relative humidity. At high ambient temperatures and relative humidity, the inability of the cooling tower to produce cooling water same as that at baseline case will have a negative impact on the condenser operating pressure and temperature. There must be a corresponding increase in the condenser saturation pressure to accommodate any increase in the cooling water temperatures. The increase in saturation pressure is propagated to the low pressure steam turbine connected upstream of the condenser, and results in an increase in the turbine back pressure and a reduction in the turbine power output. The reduction in the power output can be in

the range to 17% to 20% when the ambient temperature is increased to 40°C from 15°C[11]. With all these negative effects, there is a significant amount of power loss from the NGCC power plant at high ambient temperatures and relative humidity conditions. All these effects should be quantified to accurately predict the overall performance of the NGCC power plant at any given ambient conditions. Furthermore, the power plant economics are also affected due to power generation change, which has a direct impact on the revenue generated by the power producers. Hence, this study is primarily motivated to quantify these losses in terms of power plant economics and to analyze the potential benefits of the WHR strategies utilized specifically for chilling the gas turbine inlet air.

The major objective of the present study is to perform a techno-economic study on waste heat recovery strategies used for gas turbine inlet chilling in a wet cooled natural gas combined cycle power plant application. To complete this major objective, several specific objectives are achieved, and are listed as follows:

1. Model a gas turbine cycle and bottoming Rankine cycle of a standard NGCC power plant to predict the performance at any given ambient temperature and pressure.
2. Model a mechanical wet cooling tower to predict the cooling water temperatures at any given ambient temperature and relative humidity conditions and couple it with the NGCC model generated in specific objective 1.
3. Use Typical Meteorological Year 3 (TMY3) data for two representative locations (in this study—Los Angeles, California and Houston, Texas) to predict the hourly performance and efficiency of the plant for a one year period.
4. Generate a financial model to calculate the Levelized cost of Electricity (LCOE) for the power plant based on plant costs and the revenue generated. Use the hourly output and

efficiency of the power plant as predicted in specific objective 3.

5. Modify the NGCC model created in specific objectives 1 and 2 to accommodate three different waste heat recovery schemes (gas turbine exhaust, steam and flue gas) in addition to an electrically driven vapor compression system and calculate the performance output/efficiency for each scenarios.
6. Predict the LCOE for the different WHR schemes and for the electrically driven vapor compression system for two locations. Determine the most optimal system based on investments, tolerable costs and calculated LCOE.

1.3 Thesis Organization

In the following chapters, this thesis describes the motivation, modeling approach, and results for waste heat recovery scenarios in a NGCC power plant application. A detailed literature review is presented in chapter 2 which consists of four subsections. The first subsection discusses the operational characteristics and current state of U.S. NGCC power plants. This also discusses the off-design performance prediction approaches found in the literature. These approaches are used to predict the NGCC power plants performance at different ambient operating conditions. The two subsections after that discuss the extent waste heat recovery options that have been investigated for gas turbine inlet chilling, and the associated economics of the presented options. The final subsection outlines the research needs and motivation for this study. Chapter 3 presents the details of the simplified thermodynamic and heat transfer model developed to predict the performance of the NGCC power plant. Chapter 3 also includes the mechanical wet cooling tower modeling approach and presents the detailed financial modeling approach developed to calculate the LCOE of the power plant. The gas turbine inlet chilling options and WHR scenarios specific to the two given locations are also discussed in this chapter as well. Results of the analysis are

summarized and discussed in chapter 4. Lastly, chapter 5 presents the conclusions of the present study and proposes future recommendations for the best suitable waste heat recovery options and improvements that can be made in future studies.

CHAPTER 2. LITERATURE REVIEW

This chapter is divided into four sections which cover the operation of NGCC power plants, off-design performance, waste heat recovery options for gas turbine inlet chilling and, finally, the need for further research. The first section explores the literature related to NGCC power plants including construction, performance, definitions, and principles of operation. This section also describes the available literature used to predict off-design performance of the NGCC power plants. The second section presents the waste heat recovery technologies in several areas: definition and principles of waste heat, potential waste heat sources, benefits of waste heat recovery systems, and opportunities for research. The third section presents the gas turbine inlet chilling options that are practiced currently. The last section discusses the gaps in the literature that are present in waste heat recovery and inlet air chilling for NGCC power plants, and presents the research needs and the motivations for the present study.

2.1 Natural Gas Combined Cycle Power Plants

NGCC power plants are an electricity producing technology that consume natural gas as a fuel. In this cycle, natural gas is burned in a typical gas turbine unit and the hot exhaust gas is routed through one or more Heat Recovery Steam Generators (HRSG) to produce high pressure steam that passes through a turbine to generate additional work. A combined cycle system can be divided into: a topping Brayton cycle and a bottoming Rankine cycle. The gas turbine unit forms the integral part of the topping Brayton cycle. A boiler/HRSG, steam turbines, condenser and feed water pumps form the bottoming Rankine cycle. Figure 2-1 shows the basic layout of an NGCC power plant. The cycle begins with ambient air being drawn into the compressor at the left of the

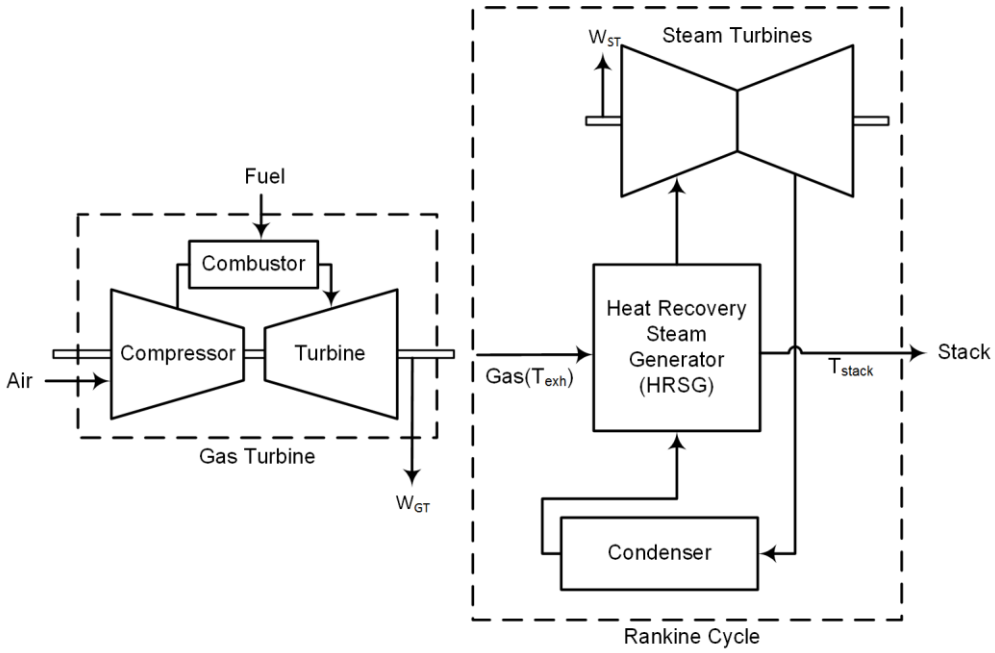

Figure 2-1. A simplified diagram of NGCC cycle containing both Gas Turbine and Rankine Cycle.

figure. The air is compressed to a desired pressure ratio, and then heated to a high temperature (~1300°C - 1500°C) by combusting natural gas. The hot gases are then expanded through a turbine which generates power. Once the heated exhaust leaves the power generation turbine, it is sent to the HRSG that has multiple heat exchangers to generate superheated steam, usually at multiple pressures. This steam is then sent to steam turbines to generate power, and, after exiting, is subsequently condensed and pumped before it returns to the HRSG. Depending on the steam saturation pressure, the HRSG could be a single or multiple pressure type. Modern CCGT power plants have multi-pressure HRSGs which can extract energy from high, medium, and low steam turbines. In this configuration, the exiting steam from the high pressure turbine feeds the medium pressure turbine, which subsequently feeds the low pressure turbine. By utilizing the exiting steam from each turbine, it is possible to generate more power and yield higher thermal efficiencies[12].

Though NGCC power plants came into existence as early as the 1950s, it was not until the 1990s that they gained popularity after the advent of highly efficient gas turbines and HRSGs [13].

Since the start of the 1990s, major companies like General Electric, Siemens, and Alstom have constructed multiple combined cycle operating gas turbine units across the globe. In the U.S. alone, the total number of NGCC power generators built from 2005 to 2015 reached 426 with a total nameplate generation capacity of 73.03 GW_e [14]. Similarly, the average capacity factor of NGCC power plants exceeded that of the coal power plants for the first time in 2015 with NGCC power plants having an average running capacity factor of 56.3%, which is larger than 54.6% for coal fired power plants [7]. The two main reasons that NGCC power plants are gaining more popularity is that natural gas burns cleaner than coal and NGCC power plants have higher thermal efficiency compared to coal power plants. For example, Department of Energy (DOE) analyses indicate that every 10,000 U.S. homes powered with natural gas produced electricity instead of coal produced electricity avoids the annual emissions of 1,900 tons of NOx, 3,900 tons of SO2, and 5,200 tons of particulates [15]. Based on the life cycle assessment performed by National Renewable Energy Laboratory (NREL), the amount of CO_2 produced per kWh of electricity produced for coal and natural gas power plant was 1022 and 499.1 gm-equivalent CO_2 per kWh, respectively [16, 17]. Also, the exhaust from the natural gas turbine can be utilized in a combined cycle that can dramatically increase the thermal efficiency. Compared to the thermal efficiency of coal fired generation systems (~30% - 35%), the combined cycle efficiency can reach higher than 60% due to the utilization of hot exhaust gases from the gas turbine in the bottoming Rankine cycle. In 2017, GE built a CCGT generator unit that achieved a thermal efficiency of 62.22% [18]. Another important reason for NGCC power plants being a more common choice of power producers is the environmental regulations imposed for coal power plants. In the long term, coal-fired generation is anticipated to decline because of environmental regulations such as the U.S. Environmental Protection Agency's (EPA's) implementation of Mercury and Air Toxics Standards (MATS)

which is resulting in some coal plant retirements [7]. The EPA's proposed Clean Power Plan (CPP), which included an implementation schedule starting in 2020, could result in an even more significant decrease in coal-fired generation [7].

The following subsections describe the features and processes related to a typical NGCC power plant. The first subsection discusses the construction and operation of Heat Recovery Steam Generator (HRSG) of an NGCC power plant, which is followed by a subsection that describes the types of cooling systems utilized in the NGCC power plant. Finally, the last subsection discusses the off-design performance of the NGCC plant.

2.1.1 Heat Recovery Steam Generator (HRSG)

The HRSG is a system in which the hot gas turbine exhaust flows over a series of heat exchangers to produce steam. The heat exchanger usually consists of finned tubes with outer diameters averaging 12.7 mm to 120.65 mm [19]. As the hot exhaust gases flow past the heat exchanger tubes in which hot water circulates, heat is absorbed, creating steam in the tubes. The

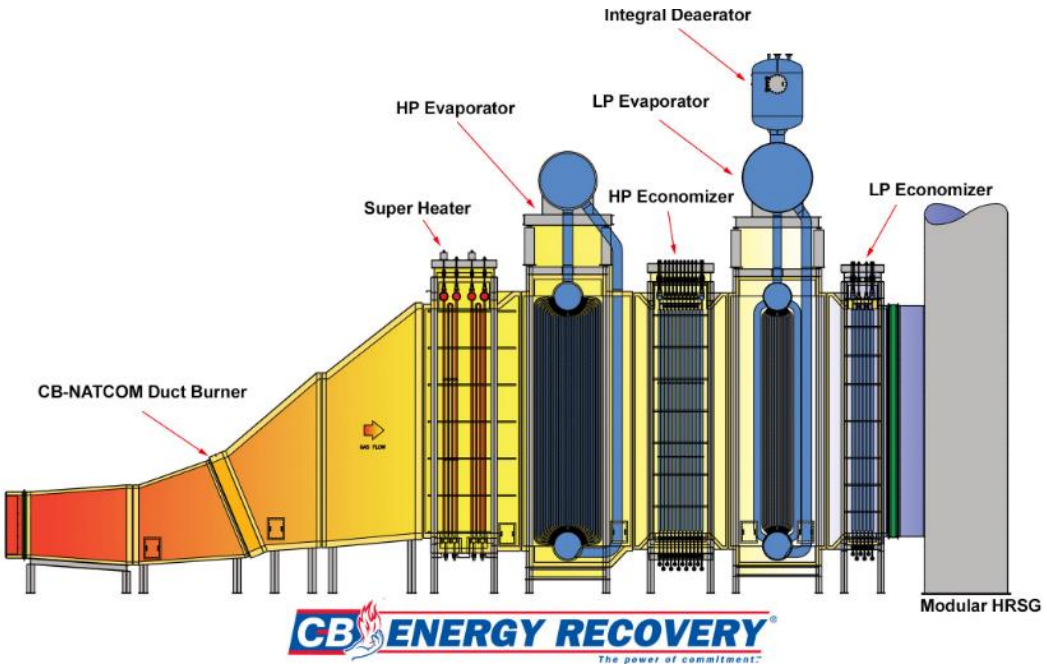

Figure 2-2. A typical heat recovery steam generator [2].

heat exchangers are arranged in sections, or modules, each serving a different function in the production of dry superheated steam. Figure 2-2 shows a typical HRSG with different types of heat exchanger modules. A more descriptive layout of the NGCC plant with a HRSG is shown in Figure 2-3. These modules are referred to as economizers, evaporators, superheaters, reheaters, and preheaters [12]. An economizer is a heat exchanger that preheats the water to nearly the saturation temperature (boiling point). The heated water from the economizer is sent to an evaporator. An evaporator is a heat exchanger where the hot water is boiled and steam is produced. The exhaust gas, after losing a significant amount of heat in the evaporator, leaves the evaporator at a temperature slightly higher than the saturation temperature. The difference between the exhaust gas temperature outlet and the evaporator saturation temperature is called the pinch point temperature difference. The difference between the saturation temperature and water inlet

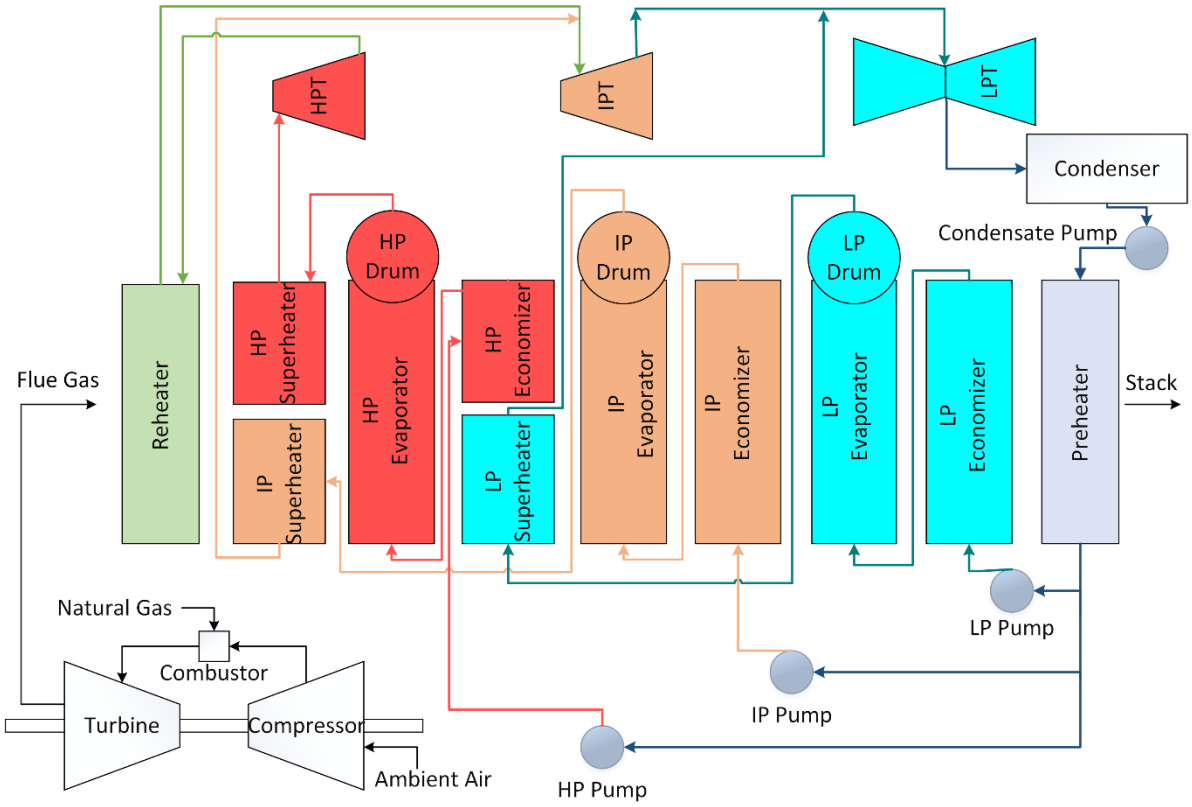

Figure 2-3. Detailed process flow diagram of the modeled NGCC including the steam cycle heat exchangers.

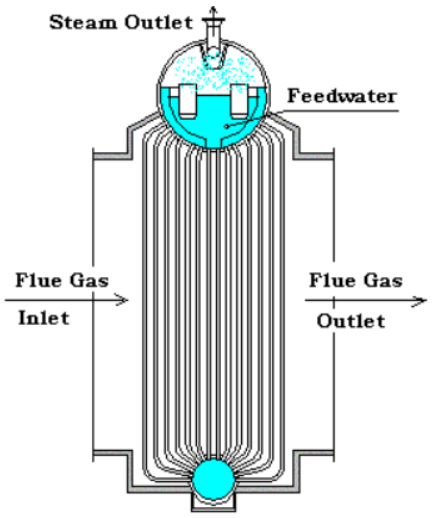

Figure 2-4. HRSG evaporator [2].

temperature to the evaporator is called the approach temperature. Both of these are crucial design parameters for the heat exchangers in the HRSG. Typical average values for the pinch and approach temperature in the design of the HRSG are in the range of 5°C to 15°C and 5°C to 12°C, respectively [12]. Having too low of an approach temperature results in the formation of steam in the economizer. Formation of steam in the economizer should be avoided, because it may result in operational problems such as vibration, water hammer, and possible deposition of salts in the economizer tubes, which result in reduced performance. Also, heat exchanger designs with lower pinch temperatures have higher capital costs, but have better performance due to their higher effectiveness [12].

Evaporators are typically designed with a steam drum located on the top of the finned evaporator tubes to collect the steam. Figure 2-4 shows a typical HRSG evaporator. The steam-water mixture in the tubes enters the steam drum where steam is separated from the hot water using moisture separators and screens. The separated water is recirculated back to the evaporator tubes. Saturated steam from the steam drums is sent to the superheater to produce dry steam, which is required for the steam turbine. The degree of superheat depends on the temperature of the exhaust

gas and the effectiveness of the superheater. Usually the superheat temperatures for modern HRSG with saturation pressure of 16 MPa are in the range of 500°C, while for some systems the temperature can be higher than 600°C [20]. Higher temperatures are rare due to steam turbines and boiler material failure issues, which includes failures in the welding joints and seals and cyclic strength deformation [21]. Higher temperatures can be obtained by the use of nickel based alloys and new ferritic materials [22]. Reheaters are a different kind of superheater that improves the efficiency, and these are standard with large and modern HRSGs (Figure 2-3). The reheater is usually placed near the high pressure superheater in the HRSG and functions to increase the temperature of the returning steam from the first stage of the high-pressure turbine. It does not increase pressure, but the temperature gain improves the efficiency. Usually the superheat temperatures for the reheaters are kept the same as the other superheaters in the HRSG, which is usually in the range of 500°C to 600°C. Like superheaters, reheaters may be placed at various locations within the gas path. Preheaters are located at the coldest end of the HRSG flue gas path, and they absorb energy to preheat water, thus extracting the low temperature waste heat from the exhaust gases. The superheated steam produced by the HRSG is supplied to the steam turbine where it expands through the turbine blades, rotating the turbine shaft. The energy delivered to the generator drive shaft is converted into electricity. After exiting the steam turbine, the steam is sent to a condenser which routes the condensed water back to the HRSG.

2.1.2 Cooling System

Steam exiting from the low-pressure steam turbine must be re-pressurized to higher pressures, reheated to a higher temperature, and sent back to the turbines to keep the cycle running. The re-pressurization of the steam is typically done by condensing the steam and pumping it to a higher pressure. Compressing the steam by using a compressor is very energy consuming operation

and not a feasible solution. Instead, the steam is condensed either in a surface condenser or an air-cooled condenser and then pumped to a higher pressure. The cooling systems can be broadly divided into three categories: a once-through system, a wet (i.e. evaporative) cooled system, and a dry (i.e. air-cooled) system. In a once-through system, the heated water is sent back to a water source and fresh cold water is withdrawn to keep the condensing process running. However, at places where once-through cooling system are not feasible, wet/evaporatively cooled towers are utilized to achieve the range of cooling. Cases where once through cooling are not feasible includes places where large water sources are not readily available, the costs of extracting water are exorbitantly high, or water withdrawal is prohibited by environmental regulations. The evaporatively cooled system (Figure 2-5a) makes use of a surface condenser heat exchanger where the cooling water gets heated by absorbing the heat from the condensing steam. The temperature difference between the cooling water temperature exiting the condenser and the saturation temperature of the steam is termed as Terminal Temperature Difference (TTD). The exiting cooling water at a higher temperature is passed through an evaporative cooling tower. Cooler ambient air gets mixed with the down-coming warm water and by the process of heat and mass

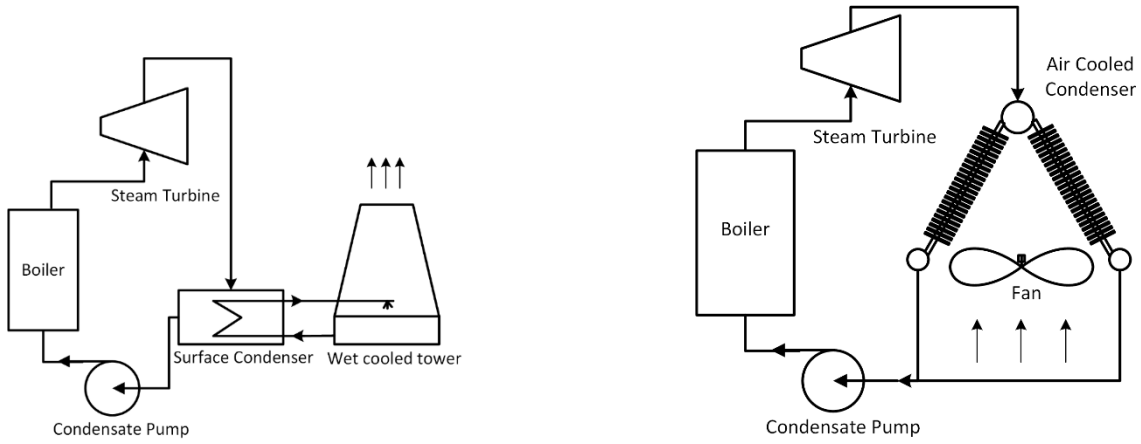

(a) (b)

Figure 2-5. Rankine cycle with cooling system (a) Evaporatively cooled tower (b) Air cooled condenser.

transfer, and the temperature of the water reduces. The colder water is then returned to the surface condenser and to repeat the cycle [11].

On a dry/air-cooled condenser (Figure 2-5b), steam coming out from the steam turbine is passed through a steam header. The header gets divided into multiple rows of finned tubes to form an A-frame. A fan is utilized to force ambient air through the finned tubes. The steam gets condensed while passing down the inclined finned tubes, and the condensate gets collected in the bottom header, which is then pumped back to the HRSG [20]. A wet cooled system has a better performance output compared to a dry cooled system at higher ambient temperatures; however, a wet cooled system needs a continuous supply of make-up water to replenish the evaporated water. A dry cooled system is nearly 2.5 to 5 times more expensive compared to a wet cooled system [23]. Wet cooled systems are expected to remain the economical choice where an adequate supply of make-up water is available at a reasonable cost. However, decreasing water availability, increasing water costs, and more stringent environmental and accessibility regulations could make a dry cooled system a practical and economical choice for more power plants [24].

2.1.3 Off-Design Performance

The off-design performance of the NGCC power plant under consideration in this study is limited to the performance at different ambient conditions. Most of the off-design performance studies found in the literature are based on the effects of ambient temperature on the performance of either the gas turbine cycle or the combined cycle plant as a whole. In one empirical study of gas turbines, for every 1K rise in ambient temperature above ISO conditions, the gas turbine loses 0.1% in terms of thermal efficiency and 1.47 MW of its gross (useful) power output [25]. This study was conducted for specific turbines Siemens SGT 94.2 (160 MW) and Siemens SGT 94.3 (260 MW) installed at the DEWA Power Station located at Al Aweer in Dubai, UAE [25]. In

another similar study [26], the thermal efficiency and power output of the gas turbine was found to decrease linearly with increase of the ambient temperature and air to fuel ratio. However, the specific fuel consumption and heat rate increased linearly with increase of both ambient temperature and air to fuel ratio. Similarly, for smaller gas turbines, in an off-design performance analysis study of a Solar Centaur-40 gas turbine engine (3.5 MW), it was found that as the ambient temperature increases by 10°C (typically from 288 K to 298 K), output power decreased by 11.6%, fuel flow rate decreased by 7.45%, thermal efficiency decreased by 4%, engine pressure ratio decreased by 4.2%, and air flow rate decreased by 4.13% [27].

All of these results discussed above were based on empirical studies, and the results are not consistent for every gas turbine system because they vary in configuration, capacity and manufacturer. As such, there are very few analytical approaches in the literature that can be used to determine the off-design performance of a gas turbine. The power output and efficiency of a gas turbine is highly dependent on compressor pressure ratio, and these parameters are often predicted by using detailed computer generated performance maps that are proprietary [28]. Hence, one focus of this study is to predict the performance of gas turbines by using a standard set of equations that can be applied to any gas turbine system. Although the compressor and turbine performance maps can be predicted with reasonable accuracy using geometric properties of the components (e.g. intake, impeller, diffuser, and casing [29]), to account for these shortcomings without these parameters, a concise formula is needed that could essentially capture the physics inside the gas turbine while also reducing tedious iterative calculations otherwise needed to predict the performance.

There have also been multiple off-design performance studies for combined cycle plants and the results can be found in the literature. In one such empirical study [30], a combined cycle

unit with two Siemens AG 501F gas turbines (174.6 MW each), coupled to a three pressure level HRSG and re-heat cycle with supplementary firing and steam turbines (253.6 MW), was investigated. A thermodynamic modeling software, Gate Cycle [31], was used to predict the off-design results. The results of the analysis show that there is nearly 19.7% power reduction in the gas turbine unit and nearly 17% power reduction in the combined cycle output when the ambient temperature changes from 0°C to 35°C. By utilizing a supplementary firing technique, where extra fuel is combusted after the exit of the gas turbine to increase exhaust flow and temperature, an increase in the exhaust gas temperature from 525°C to 675°C was seen. As a result, there was a gain in nearly 77 MW of power in the steam cycle, which is slightly greater than the power lost (75 MW) in the gas turbine unit due to ambient temperature drop. However, on average, the supplementary firing was estimated to create a drop in thermal efficiency by nearly 1.5% due to burning extra fuel. In another similar study [32], where modeling equations were used to predict the performance of a combined cycle with a single pressure HRSG system, there was a loss of about 0.04% on the combined cycle efficiency for every 1°C rise in ambient temperature. In one example, the gas turbine cycle efficiency decreased in the range of 0.03% to 0.07% for an ambient temperature increase of 1°C. The turbine inlet temperature was also varied in this study. At low turbine inlet temperature, the efficiency decreased more rapidly. Specifically, a decrease in efficiency of 0.07% at a lower turbine inlet temperature (900°C) and 0.03% at higher turbine inlet temperature (1400°C) for every 1°C rise in ambient temperature was reported. Fellah [33] conducted a study on the effects of ambient temperature on combined cycle power plant performance by using a modeling software HYSYS [34]. Two gas turbine units were considered with total power output of 169.8 MW at 15°C ambient and coupled with a dual pressure steam cycle. It was recorded that the output of the combined cycle decreased from 260.58 MW to 208.62

MW when the ambient temperature increased from 15°C to 40°C, which is a reduction in output by nearly 20%. The output reduction in the gas turbine alone was 23.7%.

In the studies discussed so far, commercial software packages were used to predict the off-design performance for the combined cycle plant and very few were done using modeling equations. Of those studies which presented an analytical model, the equations used only involved heat and mass balance approaches and entirely neglected the more complex heat transfer processes. These processes have critical impacts on performance when the operating parameters like temperature, pressure, and phase (water/steam) were changed in the heat exchangers. In particular, when estimating the off-design operation of the HRSG, an estimation of the heat transfer coefficient for each heating surface under different operating conditions is important. As discussed in the previous section, the HRSG is a complex set of heat exchangers including superheaters, evaporators, and economizers where the regime of water/steam and the flue gas temperatures are different for each heat exchanger. Ganapathy [12] presented a modeling approach to predict the heat transfer coefficients by using heat transfer equations for a single pressure HRSG system. Ganapathy considers exhaust parameters such as the temperature, exhaust flow rate, gas composition as well as several physical properties including the thermal conductivity of tube walls, viscosity of the steam, etc. to estimate the overall heat transfer coefficients (U) of different heating surfaces. Ganapathy's research is based on a single pressure system and the geometric parameters of the heat exchangers has to be known for his approach.

There are multiple other approaches in the literature that use analytical methods to predict the performance of the HRSG heat exchangers. Haglind [35] performed a variable geometry analysis for the gas turbine operating in a combined cycle power plant used for ship propulsion. In his study, he presented the mathematical relationship between the overall heat transfer coefficient

and the heat transfer coefficient of the flue gas side for each heating surface of the HRSG. The equations used in the present study are quite similar to Haglind's approach except that a staggered tube arrangement in the HRSG heat exchangers is considered in his study whereas aligned tube arrangements is used in present study. Similarly, in another study [36], to predict the heat transfer coefficient across the heat exchanger tubes in the off-design operation, the overall heat transfer coefficient in the heat exchangers were varied. With the inclusion of the effects of gas-side and water-side convection, tube material conduction, gas side radiation, as well as surface fouling and fin effects (extended surface), the overall heat transfer coefficient was calculated. This calculation method requires numerous geometric parameters and significant computational resources due to the different modes of heat transfer. This approach cannot be used for calculations with minimal information on the heat exchanger's geometry and materials. Hence, by considering all the limitations and discussions in the literature, a simple scaling method for the heat transfer coefficient of the HRSG heat exchangers should be created to predict the performance at off-design operating conditions. More details of the modeling approach are presented in the following chapter. In the following section, the current state-of-the-art waste heat recovery systems, including ongoing research, are presented.

2.2 Waste Heat Recovery

Lawrence Livermore National Laboratory showed that, in 2016, 66.4% of total useful energy is rejected as waste energy [37]. 28.5% of the total energy generation is extracted from natural gas, and 10.3% of the natural gas is used in electricity generation. Enerdata [3] showed that for the base year 2011 that the average efficiency of gas combined cycle power plants in North America (U.S., Canada and Mexico) is nearly 42% with a total penetration of nearly 27%. Figure 2-6 shows the state of combined cycle plants across the globe and the average thermal efficiencies

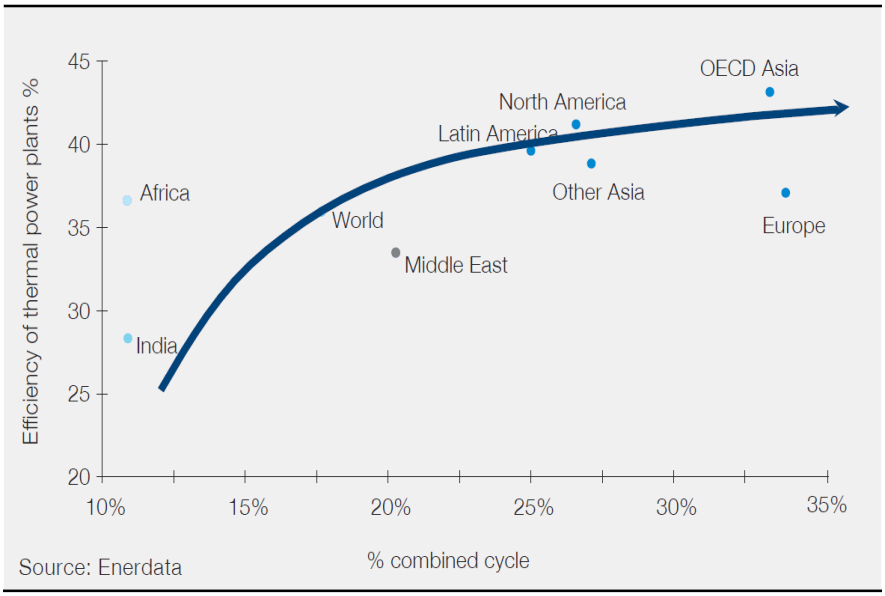

Figure 2-6. Penetration of gas combined cycle technology and efficiency of thermal power generation [3].

of these plants. Compared to the rest of the world, the combined cycle technology is quite mature and efficient in North America; yet, nearly 60% of the total energy is still rejected as waste energy from these power plants. Besides energy losses in power generation, a significant proportion of waste energy rejection also occurs in heavy-duty industrial factories including chemical industries, cement manufacturing, petroleum refineries and mining factories. These heat losses occur in the main processes of the plants that usually involve high temperatures. During these manufacturing processes, as much as 20 to 50% of the energy consumed is ultimately lost via waste heat contained in streams of hot exhaust gases and liquids, as well as through heat conduction, convection, and radiation from hot equipment surfaces and from heated product streams [1]. Waste heat recovery provides an opportunity to increase efficiency, save operational costs, and reduce emissions in these industries.

For waste heat recovery to be a feasible solution, three essential components are required: (1) an accessible source of waste heat, (2) a recovery technology, and (3) a use for the recovered energy [1]. The sources of waste heat include combustion exhaust gases, process exhaust, hot gases

from drying ovens, and cooling tower water. Usually, there are three important parameters used in the description of the waste heat: quantity, quality, and availability [38]. These parameters are

Table 2-1. Temperature classification of waste heat sources and related recovery opportunity [1].

Temperature Range	Example Sources	Advantage/Disadvantage	Typical Recovery Methods/ Technologies
High >650 °C	• Furnaces • Iron cupolas • Coke ovens • Fume incinerators • Hydrogen plants	• High quality energy • High heat transfer rate per unit area • High efficiency power-generation ▪ Chemical corrosion ▪ Thermal stress on materials	• Waste heat boilers and steam generation • Combustion air pre-heating
Medium (230°C – 650°C)	• Steam boiler exhaust • Gas turbine exhaust • Reciprocating engine exhaust • Heat treating furnaces • Drying and baking ovens • Cement kiln	• Medium power generation efficiencies ▪ Chemical and mechanical contaminants	• Waste heat boilers and steam turbines • Organic Rankine Cycle • Pre-heaters • Feed water pre-heating
Low (<230°C)	• Exhaust gas exiting recovery devices in gas-fired boilers, • Ethylene furnaces • Process steam condensate • Cooling water • Low-temperature ovens • Hot process liquids or solids	• Energy contained in numerous small sources ▪ Low-power generation efficiencies ▪ Acid condensate formation if temperature too low	• Organic Rankine Cycle • Heat pump cycles • Space heating • Domestic water heating

better explained by multiplying the Carnot efficiency equation for a power cycle by the amount of waste heat as follows:

$$\phi = Q\left(1 - \frac{T_0}{T}\right) \tag{2.1}$$

In equation (2.1), Q refers to the energy in the waste stream, which is the quantity of heat from the waste stream, T_0 represents the ambient temperature , T represents the waste heat temperature, which can be regarded as the quality of the waste heat, and ϕ represents the availability, which is also known as the maximum amount of waste heat that can be utilized efficiently from a source to produce work.

Depending on temperature, a waste heat source can be categorized into three categories: high grade waste heat which exceeds temperatures of 1,200ºF (649ºC), medium grade which is between 1,200ºF (649ºC) and 450ºF (232ºC), and low grade which has a temperature less than 450ºF (232ºC) [1]. Table 2-1 shows a summary of these three different categories of waste heat sources in industry, their advantages and disadvantages, and the typical recovery methods used to extract the waste heat.

The recovered waste heat can be utilized in three major categorical ways as noted in Table 2-1: heating and cooling, heat engine operation for electricity generation, or as a heat pump for air conditioning/refrigeration purposes. For the heating application, a high to medium temperature waste heat source can be used in a recuperator or a regenerator to exchange heat between working fluids, or in a passive air heater to heat the incoming air or in the waste heat boilers and economizers. Waste heat applications for heat pumps can serve primarily two functions: either the waste heat can be utilized to lift the temperature of another stream, or it can be used as an input to drive an absorption cooling system which is discussed in detail in the following sections. Another potential option is to use the waste heat to drive a heat engine cycle. Table 2-2 presents the

different heat engine cycles and thermal to electrical conversion technologies that can be operated through waste heat utilization. The most popular heat to electricity conversion cycles are the first three presented in Table 2-2. Extensive researches have been done on Organic Rankine Cycle (ORC) and traditional steam cycles to convert waste heat into energy. However, the present study is focused on utilizing waste heat for cooling the inlet air of the gas turbine by using a thermally activated cooling system. In the following section, the practices for gas turbine inlet chilling are discussed.

Table 2-2. Options for waste heat recovery for power generation [1].

Thermal Conversion Technology	Temperature Range	Typical source of waste heat
Traditional Steam Cycle	Medium, High	Exhaust from gas turbines, reciprocating engines, incinerators, and furnaces.
Kalina Cycle	Low, Medium	Gas turbine exhaust, boiler exhaust, cement kilns
Organic Rankine Cycle	Low, Medium	Gas turbine exhaust, boiler exhaust, heated water, cement kilns
Thermoelectric Generation	Medium, High	Not yet demonstrated in industrial applications
Piezoelectric Generation	Low	Not yet demonstrated in industrial applications
Thermal Photovoltaic	Medium, High	Not yet demonstrated in industrial applications

2.3 Gas Turbine Inlet Air Cooling

The power output and efficiency of an NGCC power plant is highly influenced by the gas turbine inlet air temperature. As discussed in previous sections, the performance of the power plant degrades with increasing ambient temperature. One simple strategy to improve the performance of the power plant under high ambient temperature is to employ gas turbine inlet air cooling technologies (GTIAC). GTIAC technologies are extensively used in hot climatic conditions where the average temperature remains high compared to ISO operating conditions throughout the year

[39-41]. Multiple analytical and experimental studies have been carried out to outline the effects of GTIAC technologies in both simple and combined cycle operating power plants. There are several GTIAC technologies which are in practice, including high pressure fogging, wetted media evaporative cooling, absorption cooling, thermal energy storage and using electrically driven vapor compression chiller.

High-pressure fogging is the process of spraying of droplets of demineralized water, 5 to 20 microns in diameter, into air inlet ducts at 1000 to 3000 psi. As the fog droplets evaporate, 100% relative humidity is produced and the air is cooled to the wet-bulb temperature: the lowest possible temperature obtainable without refrigeration [42]. Wetted media evaporative cooling, however, uses the latent heat of vaporization to cool the ambient air temperature from the dry bulb to the wet-bulb temperature. Water in the wetted media vaporizes by taking in heat from ambient air, thus cooling the inlet air to the gas turbine. Both of these cooling techniques are susceptible to lower performance at high ambient relative humidity and cannot cool the incoming air below the wet-bulb temperature [42]. Absorption inlet air cooling is a technique where heat from potential heat sources is recovered in the absorption chiller by use of a binary fluid (e.g., LiBr-H_2O, H_2O-NH_3).

A typical vapor absorption cycle produces a cooling effect in the form of chilled water which is passed through a heat exchanger to cool the ambient air temperature [42]. Similarly, an electrically driven vapor compression chiller can be used in a similar fashion as absorption chiller except the cooling is powered by an electrical compressor compared to heat driven absorption systems. Both absorption and compression systems usually utilize chilled water to cool the turbine inlet air where the temperature can be cooled to a lower temperature irrespective of the wet-bulb temperature. Hence these systems are preferred to fogging or the evaporative cooling when at

places where the relative humidity is high. In the following paragraphs, typical studies conducted by utilizing these cooling systems are presented.

Nasser et. al. [43] noted that by running a single effect LiBr-H_2O absorption chiller and by extracting the gas turbine waste heat, it was possible to enhance the power output by nearly 20% in summer without additional fuel requirements. Al-Bortmany [44] discussed the use of aqua-ammonia absorption chillers powered by heat extracted from gas-turbine exhaust gases. The inlet air of two gas turbines in Oman was cooled to 7°C resulting in power gains of 20% and 14%. Ameri et. al. [45] showed that by installing two steam driven LiBr-H_2O absorption chillers in a 16.6 MW gas turbine unit, a power output enhancement of nearly 11.3% could be achieved. The pay-back period for this retrofit was estimated as 4.2 years. Mohanty et. al. [46] analytically studied a gas turbine power plant (100 MW) in Thailand and demonstrated that electricity generation could increase by nearly 11% by using a double effect absorption chiller. Additionally, they demonstrated that installing a new gas turbine unit to create the same amount of power would cost nearly four times the waste heat driven absorption chiller.

In the previous studies, absorption chillers were used and the major source of energy was the high temperature gas turbine exhaust or process steam. Techniques like evaporative cooling, fogging, and electrical chilling, are also used to chill the gas turbine inlet air and multiple studies have been done. Dawoud et. al [47] compared different gas turbine inlet air cooling techniques for a preinstalled gas turbine (39.62 MW) in Oman. The results of the analysis showed that a fogging technique generated 11.4% more electricity compared to evaporative cooling. For fogging, a 98% approach to wet-bulb temperature was considered, whereas, for evaporative cooling, an 88% approach to wet-bulb temperature was considered. A LiBr-H_2O absorption cooling generated 40% more electricity compared to fogging. Compared to LiBr-H_2O systems, a water-ammonia

absorption system and a vapor compression system generated 39% and 46% more electricity for the same location, respectively. This was because the design inlet temperature of 14°C was assigned to LiBr-H_2O system whereas a design inlet temperature of 8°C was assigned to water-ammonia and vapor compression system.

The study above clearly demonstrated that the vapor compression and vapor absorption cooling technologies are the best suited technologies if a greater amount of power enhancement is required because lower temperatures can be achieved irrespective of the wet-bulb temperature limit. In another such study, Buecker et al [48] demonstrated a technology called Absorption Refrigeration Cycle Turbine Inlet Air Conditioning (ARCTIC). This technology used the combustion turbine exhaust to provide cooling and heating to the gas turbine inlet air depending on the time of the year. On a hot summer day (100°F), it was demonstrated that the plant (~88 MW at 60°F ambient) produced nearly 20 MW and 10 MW more electricity for the ARCTIC system as compared to evaporative chilling and mechanical chilling, respectively. The ARCTIC system was also demonstrated on a combined cycle plant (479 MW_e at 97°F and 43% RH), and generated 532.9 MW_e, which is 4.5 MW_e and 26.5 MW_e higher than the mechanical chilling and evaporative chilling options, respectively.

In another study, Rahim [49] compared evaporative cooling, fogging, absorption cooling and electrical chilling techniques applied to a 96 MW gas turbine plant and found that the most efficient option was to utilize an absorption chiller, which increased the power output by 3.5 MW and the efficiency by 0.05%. The inlet air was cooled to 10°C. Instead of limiting the gas turbine inlet chilling only to a gas turbine power plant, recent studies are being performed for NGCC inlet air chilling as well. In an experimental study performed on a preinstalled 336 MW combined cycle plant, Boonnasa et al [39] found that installing a steam driven (0.6-0.8 MPa) absorption chiller to

cool gas turbine intake air can enhance the annual power production for both the gas turbine and the combined cycle by 10.6% and 6.24%, respectively. For a typical summer month of April, there was a 2.85% reduction in the steam turbine power production due to steam extraction to run these systems. However, there was a 10.16% enhancement in the gas turbine power which explains the increase in overall production. The technology had a pay-back period of 3.81 years. In a particular waste heat to cooling study, Popli et. al [41] analyzed a single effect LiBr-H_2O absorption chiller powered by the gas turbine (8.96 MW) exhaust to cool the gas turbine compressor inlet air. The results showed that by utilizing 17 MW of the exhaust waste heat, the chiller produced 12.3 MW of cooling and decreased the compressor inlet air to 10°C. This approach generated an additional 5263 MWh electricity per year. The payback period for this retrofitting option was estimated in the range of 1.3 to 3.4 years. The major similarities among these studies is that either the gas turbine exhaust or steam from the bottoming Rankine cycle is used to power the thermally activated cooling system (absorption system).

2.4 Research Needs Addressed by Current Investigation

Among the studies discussed above, there are several similarities, including that these studies either compare different cooling systems or describe the performance improvement due to a particular cooling system installed in a gas turbine or combined cycle plant. Some investigations have conducted economic analysis that includes a simple pay-back period calculation. However, those studies that did perform an economic analysis, have not addressed the economic impact that WHR and inlet air chilling have on power plants. Also, most of these studies were based on improving the plant performance during hot summer months while the impact of the ambient temperature over the entire course of the year has not been outlined in any of these studies. In the present study, different absorption cooling systems are compared based on the economic viability

with an electrically driven vapor compression cooling system to cool the compressor inlet air. Three possible heat sources are considered to run the thermally activated cooling systems: high grade heat from the gas turbine discharge (~600-650°C), low pressure steam (~5 bar) from the bottoming Rankine cycle, and low-grade waste heat from the power plant stack (~ 106°C). Utilizing the gas turbine exhaust or the steam from the Rankine cycle would decrease the performance of the bottoming Rankine cycle because of the decreased gas temperature that enters the Heat Recovery Steam Generator (HRSG), or the decreased mass flow rate to the low-pressure steam turbine. However, significant increases in the gas turbine power output can be achieved when care is taken to implement an effective control strategy.

As mentioned earlier, there have been multiple approaches to compare the viability of different turbine inlet chilling systems. However, none of these studies have investigated the impact of these different WHR schemes on the performance of NGCC power plants over the course of an entire year with variable weather conditions at different locations in the US. Furthermore, many of these studies analyze the economic performance of these options using a simple pay-back period analysis. This study aims to perform a more detailed economic impact study for the cost of electricity due to these cooling systems. In the present study, a particular NGGC cycle with performance characteristics given at a single operating condition are simulated to predict the performance at different ambient conditions. This model is then used to investigate a range of possible combinations of heat recovery and turbine inlet chilling scenarios that can minimize the impact of ambient weather on the cost of electricity. This study presents a detailed techno-economic assessment to determine the Levelized Cost of Electricity (LCOE) to assess the profitability of different WHR systems compared to using a commercially available vapor compression system for GTIAC.

CHAPTER 3. MODELING APPROACH

The main objective of the present study is to analyze gas turbine inlet air chilling that is accomplished by utilizing different forms of waste heat within the power plant. Multiple waste heat recovery scenarios are compared using the LCOE as a comparison metric, which is evaluated over the plant's entire life. These WHR systems are compared with mechanical chilling, which is a standard practice in the industry. Because the LCOE is calculated using both thermodynamic and economic performance, the modeling approach described here includes performance-based and economic modeling sections. In sections 3.1 to 3.3, a detailed performance modeling approach for the NGCC power plant gas turbine, steam cycle, and cooling tower are presented. In section 3.4, the details of the WHR systems and turbine inlet air cooling system modeling are presented. Finally, section 3.5 presents the economic modeling approach used to calculate the LCOE for the different combinations of cooling systems.

The baseline performance characteristics for the NGCC power plant investigated in this study are taken from the U.S. Department of Energy (DOE), National Energy Technology Laboratory (NETL) Case 13 (Revision 2a, September 2013) [50]. The performance characteristics used in the present study are summarized in Table 3-1. At ISO operating conditions, this power plant generates 565 MW_e of electrical power of which 362 MW_e is generated in the F-class gas turbine and 203 MW_e is generated by the steam turbines. 10 MW_e is utilized in running the auxiliary systems, resulting in the net power generation of 555 MW_e. This plant also utilizes a triple pressure Heat Recovery Steam Generator (HRSG) in the Rankine cycle and an evaporative cooling tower to reject the heat from the condenser. In the following discussions, the off-design performance prediction methods for these major constituents of the NGCC – gas turbine, steam cycle, and cooling tower – are discussed in detail.

3.1 Gas Turbine Cycle

The gas turbine under consideration in the present study is an advanced F-class gas turbine. These gas turbines were considered advanced technology nearly 20 years ago but have still been a major source of natural gas-fired power generation worldwide [51]. Table 3-2 presents a list of major assumptions used in this study for the gas turbine cycle performance prediction at off design operating conditions. For the compressor, a constant volumetric air flow rate is assumed because compressors are constant volume machines. At high ambient temperatures, the density of the

Table 3-1. Baseline performance characteristics of the NGCC power plant at 15ºC [50].

Parameter(Unit)	**Value**
Ambient Temperature (ºC)	15
Atmospheric Pressure (kPa)	101.32
Net Total Electric Power (MW_e)	555
Fuel	
Natural Gas, LHV (kJ/kg)	47454
Supply Condition (MPa/ºC,kg s^{-1})	3.1 / 37.8/21.08
Gas Turbine Parameters	
Net output (MW_e)	362
Compressor Isentropic Efficiency (%)	80.2
Turbine Isentropic Efficiency (%)	91.5
Turbine Pressure Ratio	18.5
Turbine Inlet/Outlet Temperature (ºC)	1371, 628.6
Turbine Outlet Pressure (kPa)	104.8
Steam Turbine Cycle	
Net Output (MW_e)	203
High-Pressure Steam (MPa/ºC/kg s^{-1})	16.5/525/104
Intermediate Pressure Steam (MPa/ºC/kg s^{-1})	2.5/510/13
Reheat Pressure Steam (MPa/ºC/kg s^{-1})	2.5/570/104
Low Pressure Steam (MPa/ºC/kg s^{-1})	0.51/330/27
Approach Temperature (HP,IP,LP) ºC	10,10,5
Stack Flue Gas Temperature (°C)	106
Steam Turbines and Pumps	
HP, IP, LP Turbine Isentropic Efficiency (%)	85, 93, 93.1
Condenser Inlet Steam Quality	0.93
Pump Isentropic Efficiency (%)	71
Condenser	
Condenser Temperature/Pressure (°C/MPa)	38.71/6.89
Condenser Heat Duty (MW_{th})	324.97

incoming air to the compressor decreases, thus reducing the mass flow of air entering the compressor. Similarly, the pressure ratio of the compressor is varied by using an equation which is presented in the compressor section below. A constant polytropic efficiency for the compressor is assumed [52]. For the combustor, a pressure loss of 5% is assumed in the combustion process, while a lean and complete combustion is assumed. Furthermore, adiabatic combustion is assumed in the compressor. More details are presented in the combustor section below. For the turbine, a constant isentropic efficiency is assumed. This assumption is based on a gas turbine model used in the Gate Cycle software and produces accurate results at varying operating conditions. A

Table 3-2. List of major assumption for gas turbine cycle to predict off design performance.

Component	**Major Assumptions**
Compressor	Constant air volumetric flow rate Pressure ratio dependence on speed and intake mass flow Mechanical efficiency: 95 % Constant polytropic efficiency
Combustor	Combustor pressure loss: 5 % Lean and complete combustion Adiabatic combustion: Negligible heat loss
Turbine	Constant isentropic efficiency Constant firing temperature: 1371 ºC Constant discharge pressure: 104.8 kPa Mechanical efficiency: 95 % Generator electrical efficiency: 97.7%

constant turbine inlet temperature of 1371°C (baseline) for the combustion products is assumed. This method of fixing the inlet temperature is due to material performance issues in the turbine which is explained in detail later. A constant turbine discharge pressure of 104.8 kPa is assumed to be consistent with the NETL Case 13. For both compressor and turbine, a mechanical efficiency of 95% and a generator electrical efficiency of 97.7% is assumed to match the NETL Case 13 gas

turbine power output values. The following sections presents the modeling approach for each of the components of the gas turbine: compressor, combustor, and turbine sections.

3.1.1 Compressor

F-class gas turbines usually have multi-stage axial flow compressors. In these compressors, the pressure ratio is a function of non-dimensional mass flow parameter and non-dimensional rotational speed [52]. At off-design and part load conditions, the compressor is operated on what is called a working line to achieve maximum possible efficiency. A decrease in the mass flow rate would essentially decrease the operational speed and the pressure ratio on the working line, which can be predicted by using equation (3.1) as follows [52]:

$$\frac{\dot{m}\sqrt{C_{\mathrm{p}}T_{01}}}{D^2 p_{01}} = C\left(\frac{p_{0\mathrm{e}}}{p_{01}}\right)^{1-\left(\frac{\gamma-1}{2\gamma\eta_{\mathrm{p}}}\right)} \tag{3.1}$$

On the left side of equation (3.1), C_{p} and D are held constant for each separate operating condition in the analysis. The C_{p} value for air is assumed constant within the operating ambient temperature range and D represents the diameter at the compressor exit. The constant C on the right side of equation (3.1) is the product of the compressor non-dimensional mass flow at the exit during a choked flow condition and the exit area ratio:

$$C = \frac{\dot{m}\sqrt{C_{\mathrm{p}}T_{0\mathrm{e}}}}{D^2 p_{0\mathrm{e}}} \tag{3.2}$$

For these types of axial flow compressors, a small range of fluctuation of the incoming mass flow of air would generate a minimal change in the polytropic efficiency [52]. Hence, by assuming a constant polytropic efficiency, the effect of changing ambient temperature is simply the ratio of the design point (i.e., NETL Case 13) to the off-design point. By eliminating equal terms, the ratio can be simplified to a relation between the inlet temperature, air mass flow, and pressure ratio

given by equation (3.3) as follows:

$$\frac{\left(\dot{m}\sqrt{T_{01}}\right)_{\mathrm{DP}}\left(p_{01}\right)_{ODP}}{\left(\dot{m}\sqrt{T_{01}}\right)_{\mathrm{ODP}}\left(p_{01}\right)_{DP}}=\left(\frac{PR_{\mathrm{DP}}}{PR_{\mathrm{ODP}}}\right)^{1-\left(\frac{(\gamma-1)}{2\gamma\eta_{\mathrm{p}}}\right)} \tag{3.3}$$

By assuming a constant volumetric flow rate, the changing air mass flow rate across the compressor at off-design conditions is determined. The pressure ratio across the compressor and the corresponding isentropic efficiency of the compressor are evaluated at different operating conditions by using equation (3.3). Equation (3.4) is used to convert polytropic efficiency to isentropic efficiency of the compressor:

$$\eta_c=\frac{PR^{\left[\frac{\gamma-1}{\gamma}\right]}-1}{PR^{\left[\frac{\gamma-1}{\eta_{poly,c}\gamma}\right]}-1} \tag{3.4}$$

3.1.2 Combustor

In combustor, heat is added to the incoming hot air from the compressor by burning fuel. In this study, a lean and complete adiabatic combustion is assumed in the combustor. This is because the combustor in modern gas turbines have low NOx type of combustion chambers, which are nearly 100% efficient at converting almost all fuel energy into heat energy with minimum losses [53]. For the present analysis, complete and adiabatic combustion is assumed and the turbine inlet temperature is assumed to be constant at 1371°C. Equation (3.5) is used to model the combustion reaction in the gas turbine combustor:

$$C_nH_{2n+2}+\frac{a_s}{\Phi}\left(O_2+3.76\times N_2\right)\rightarrow nCO_2+(n+1)H_2O+a_s\left(\frac{1}{\Phi}-1\right)O_2+\left(3.76\times\frac{a_s}{\Phi}\right)N_2 \tag{3.5}$$

In equation (3.5), a_s represents the stoichiometric coefficient for a given hydrocarbon to burn completely in 100% theoretical air (stoichiometric combustion). The representative values of a_s

for Methane and Ethane are 2 and 3.5 respectively. During this analysis in equation (3.5), the volumetric composition of air is taken as 79% Nitrogen and 21% Oxygen. The fuel air equivalence ratio (Φ) is defined as the actual fuel-air mass ratio (*FA*) divided by the stoichiometric fuel-air mass ratio, (FA_s) as given by equation (3.6):

$$\Phi = \frac{FA}{FA_s} \tag{3.6}$$

For fuel rich combustion, the value of Φ is greater than 1, while for lean combustion, the value of Φ is less than 1. In this study, the natural gas is assumed to be composed of several constituent gases as shown in Table 3-3. To account for the different volumetric compositions of the constituent gases, a stoichiometric coefficient (a_s = 2.035) is calculated with individual combustion equations for the various hydrocarbons. This coefficient is then used in equation (3.7) to determine the equivalence ratio based on the mass flow rates of air and natural gas as specified in the NETL Case-13:

$$\Phi = \frac{4.76 a_s \dot{m}_{NG} MW_{air}}{\dot{m}_{air} MW_{NG}} \tag{3.7}$$

The equivalent molecular weights of air and natural gas are calculated by the equation (3.8):

$$MW_{eqv} = \sum y_n \times MW_n \tag{3.8}$$

Table 3-3. Composition of natural gas.

Component	**Formula**	**Volume Percentage**
Methane	CH_4	93.1
Ethane	C_2H_6	3.2
Propane	C_3H_8	0.7
n-Butane	C_4H_{10}	0.4
Carbon Dioxide	CO_2	1.0
Nitrogen	N_2	1.6

The molar flow of air and natural gas is computed using equation (3.9):

$$\dot{n}_{\text{mix}} = \frac{\dot{m}_{\text{mix}}}{MW_{\text{mix}}} \tag{3.9}$$

Equation (3.10) is used to calculate the enthalpy of the reacting and product mixtures:

$$I_{\text{mix}} = \dot{n}_{\text{mix}} \sum y_{\text{n}} \times i_{\text{n}} \tag{3.10}$$

An adiabatic combustion is assumed in the gas turbine combustor. By fixing the temperature of the gas that enters the turbine, the temperature of the reacting mixtures is determined for the design case by utilizing the equation below:

$$I_{\text{reactants}} = I_{\text{products}} \tag{3.11}$$

For the off-design cases, the mass flow rate of natural gas is adjusted so the turbine inlet temperature remains constant. At high temperatures, the turbine blades are exposed to significant thermal stress, so keeping the inlet temperature constant keeps the blades from becoming damaged [54]. To account for the pressure loss that occurs in the combustion chamber, a fractional pressure drop of 5% is assumed in the combustor.

3.1.3 Overall Performance

As discussed in subsection 3.1.2, the turbine inlet temperature in this study is kept constant to the value at the baseline case (1371°C). The turbine isentropic efficiency and the turbine discharge pressure are held constant at all operating conditions. Figure 3-1 shows the flowchart for the performance prediction of the overall gas turbine cycle based on characteristic data points from the NETL Case-13 and the assumptions made in this study. Subscripts 1, 2, 3 and 4 represent compressor inlet, combustor inlet, turbine inlet and turbine outlet stations, respectively, while variables *T* and *P* represent temperature and pressure respectively (Figure 3-2). As can be seen in

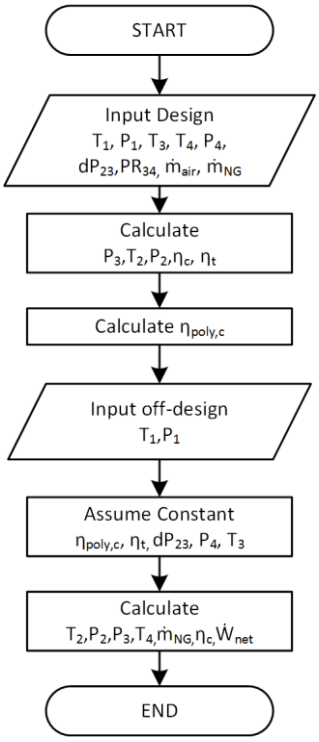

Figure 3-1. Flow chart for gas turbine performance prediction.

Figure 3-1, the state points from NETL Case 13 are T_1, P_1, T_3, T_4, P_4, turbine pressure ratio (PR_{turb}), and mass flow rates of air and natural gas ($\dot{m}_{air}$ and $\dot{m}_{NG}$). With these input values known, and by assuming a constant pressure drop (dP_{23}) of 5% across the combustor, the following values for P_3, P_2, T_2, turbine efficiency (η_t), and compressor isentropic (η_c) and polytropic efficiencies ($\eta_{poly,c}$) can be determined by using equation (3.4) and equations (3.12) through (3.17):

$$PR_{comp} = \frac{P_2}{P_1} \tag{3.12}$$

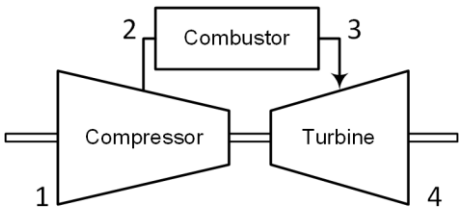

Figure 3-2. State points for gas turbine simulation.

$$PR_{\text{turb}} = \frac{P_3}{P_4} \tag{3.13}$$

$$\eta_{\text{c}} = \frac{i_{2s} - i_1}{i_2 - i_1} \tag{3.14}$$

$$\eta_{\text{t}} = \frac{i_4 - i_3}{i_{4s} - i_3} \tag{3.15}$$

$$T = f(i, P) \tag{3.16}$$

$$\dot{m}_{\text{gas}} = \dot{m}_{\text{air}} + \dot{m}_{\text{NG}} \tag{3.17}$$

The respective power for the compressor and turbine can also be determined by using equations (3.18) and (3.19) respectively:

$$\dot{W}_{\text{c}} = \dot{m}_{\text{air}}(i_2 - i_1) \tag{3.18}$$

$$\dot{W}_{\text{t}} = \dot{m}_{\text{gas}}(i_3 - i_4) \tag{3.19}$$

The net output ($\dot{W}_{\text{net}}$) from the gas turbine is the difference between the turbine work generated and the compressor work consumed. This work ($\dot{W}_{\text{net}}$) when multiplied with the generator efficiency and mechanical efficiency gives the final output in MW_e generated from the gas turbine by using equation (3.20):

$$\dot{W}_{\text{e}} = \eta_{\text{gen}}\eta_{\text{mech}}\dot{W}_{\text{net}} = \eta_{\text{gen}}\eta_{\text{mech}}(\dot{W}_{\text{t}} - \dot{W}_{\text{c}}) \tag{3.20}$$

In off-design conditions, (i.e., new T_1 and P_1), the values for dP_{23}, P_4, T_3, $\eta_{\text{poly,c}}$ and η_{t} remain constant, and the new values for unknown variables T_2, P_2, P_3, T_4, $\dot{m}_{\text{NG}}$, η_{c} and $\dot{W}_{\text{net}}$ can be determined by solving equations (3.12) through (3.20) respectively. The different outputs of this off-design solution ensures the exhaust gas temperature and flow rate changes as there is change in the ambient air temperature and pressure. The changing gas turbine exhaust conditions have a

significant impact on the performance of the bottoming Rankine cycle, which is outlined in the following section.

3.2 Steam Cycle

In off-design conditions, there are significant changes in the gas turbine exhaust temperature and flow rates, which has effects on the performance of the bottoming Rankine cycle. In this section, the detailed methods used to predict the baseline and off-design performance of the Rankine cycle are presented. One component in NETL Case-13 NGCC is a triple pressure HRSG. Figure 3-3 shows a process flow diagram for a NGCC power plant with a triple pressure HRSG. Hot turbine exhaust gas passes through a series of heat exchangers from left to the right. The heat exchangers for a triple pressure HRSG typically include economizers, evaporators, super-heaters,

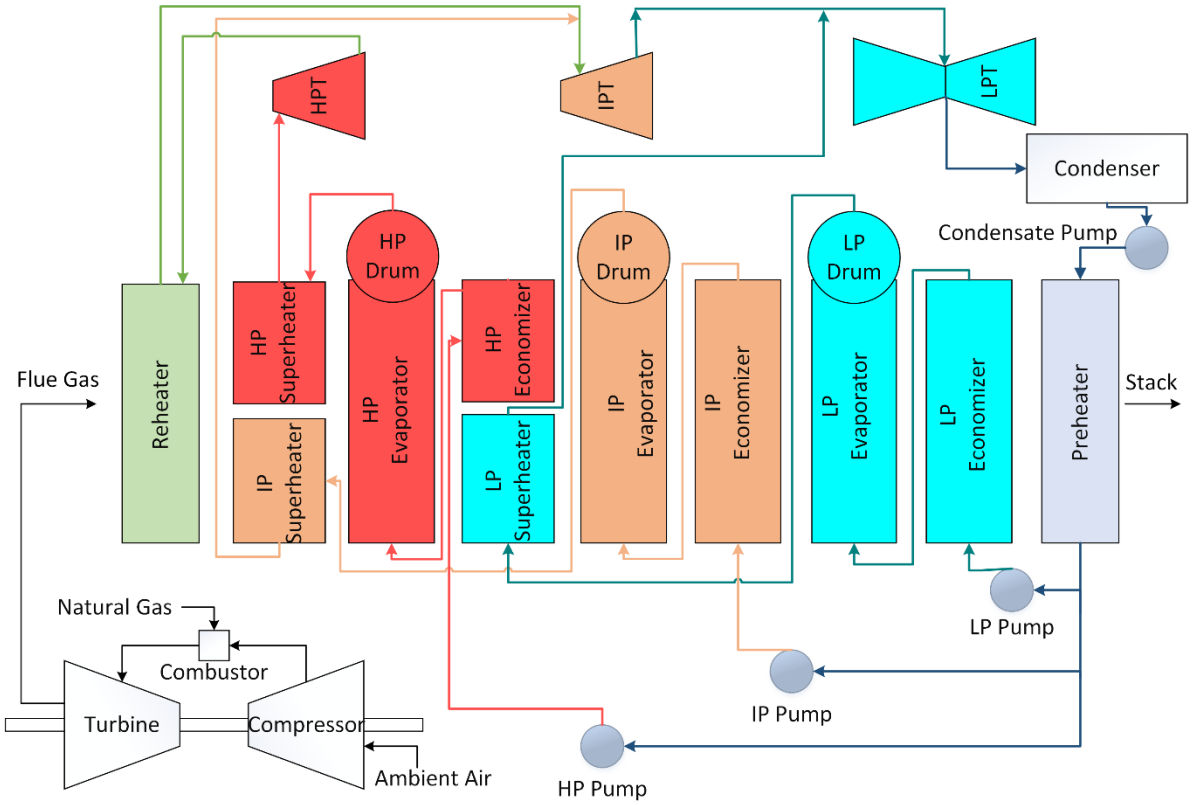

Figure 3-3. Detailed process flow diagram of the modeled NGCC including the steam cycle heat exchangers.

re-heaters, and preheaters, each divided into high pressure (HP), intermediate pressure (IP) and low pressure (LP) systems. The order of these heat exchangers is selected to maximize the extraction of energy from the waste heat stream. A reheater is kept in front of these superheaters to match the NETL Case-13 state points. The superheaters are kept on the side of the HRSG where the exhaust gas is hottest because a high degree of superheat is desired before the steam enters the steam turbines. In Figure 3-3, HP and IP superheaters are kept in parallel so a high degree of superheat can be achieved in both heat exchangers. A similar configuration is made with the HP economizer and LP superheater (outlet temperature of LP steam is 330°C for the baseline case). For both parallel configurations, the exhaust gas is assumed to be equally divided to these heat exchangers and the resulting gas mixture temperature downstream of the heat exchangers is solved by performing an energy balance. A preheater is installed last to extract the last remaining portion of heat from the flue gas after which the flue gas is sent to the atmosphere through the stack. In practice, a NOx removal selective catalytic reduction (SCR) module is used in the HRSG. The SCR operates by injecting ammonia (NH_3) into the flue gas to form N_2 and H_2O. The SCR module is located in the HRSG where the temperature is between 250°C and 380°C, and has a minimal pressure and temperature drop in the overall system [55]. For this reason, the SCR module is not shown in Figure 3-3 and is not considered in this analysis.

The Rankine cycle operation at the baseline case (ISO ambient conditions) starts with superheated steam (525°C/16.5 MPa) that is generated in the HP superheater. This superheated steam is sent to the HP steam turbine where shaft power is generated as the steam expands to the exit pressure of 2.5 MPa. The exiting steam from the HP steam turbine is sent to the reheater where its temperature increases to 570°C by heat exchange with the hot exhaust gases. Most modern power plants consist of a reheat cycle because this take advantages of the increased efficiency that

results with higher boiler pressures and yet avoid low-quality steam at the turbine exhaust [56]. This reheat steam is at the same pressure as the IP superheated steam (510°C/2.5 MPa) generated in the IP superheater. These two streams are mixed which results in a temperature of 563°C, at the IP steam turbine inlet. After expansion in the IP steam turbine, the exiting steam (at 333°C/517 kPa) is mixed with the LP superheated steam (330°C/517 kPa) from LP superheater and sent to the LP steam turbine. In each mixing process, the steam pressure is equal for both streams and the mixture temperature is found by performing an energy balance as shown in equation (3.21) and (3.22):

$$\dot{m}_{\text{gas},1} i_1 + \dot{m}_{\text{gas},2} i_2 = \dot{m}_{\text{gas}} i \tag{3.21}$$

$$\dot{m}_{gas} = \dot{m}_{gas,1} + \dot{m}_{gas,2} \tag{3.22}$$

In equation (3.21) and (3.22), the streams 1 and 2 are the mixing gas streams that results in the final stream. The outlet steam from the LP steam turbine is two-phase (quality = 0.929, pressure = 6.89 kPa). The quality of this exiting wet steam should be kept higher than 88% at all times to prevent any erosion to the steam turbine blades [20]. In the condenser, the steam is condensed at a condensing pressure of 6.89 kPa (1 psi). Cooling water is circulated in the condenser for the condensation of the steam. The entering and exiting cooling water temperatures at the baseline case are 16°C and 27°C, respectively. The warm cooling water at 27°C exiting the condenser is sent through an evaporative cooling tower where it is cooled by cold ambient air. More details of the cooling process in the cooling towers are presented in section 3.3. After cooling, the cooled water at 16°C is returned to the condenser. The amount of water that is evaporated during this mixing process is resupplied in the form of make-up water which is nominally 2% of the total mass flow rate of cooling water [20]. After condensation, the Rankine cycle process water is pumped to a preheater where it increases temperature while exchanging heat with the remaining portion of

the flue gas. The flue gas exits the preheater at 106°C and is sent to the atmosphere through the stack while the heated process water is pumped to the economizers by the respective feed water pumps (HP, IP, and LP). The cycle then gets repeated. In the following section, a detailed approach to determine the steam cycle performance characteristics at the baseline case is presented.

3.2.1 Baseline Performance

In this section, a detailed approach to calculate the baseline operating characteristics for the Rankine cycle is presented. The characteristic state points from the NETL Case-13 are taken as reference during this calculation process. These characteristic state points are shown in Table 3-1. Among these characteristic state points are the flue gas stack temperature, condenser pressure, HP, IP and LP operating pressures, isentropic efficiencies of the steam turbines and pumps, HP, IP and LP steam mass flow rates, and the respective superheat temperatures. Slight modifications are made to the mass flow rates (HP, IP, and LP) including the respective superheat temperatures from the NETL Case-13 values to match the NGCC layout presented in Figure 3-3 and to ensure all heat exchangers were less than 85% effective at the baseline case such that these effectiveness reflect those in real practices. The detailed flowchart of the simulation process used to calculate the parameters in this study is shown in Figure 3-4.

Initially, the mass flow rates and the superheated steam temperatures across the HP, IP and LP systems are assumed equal to NETL Case-13. With the supplied mass flow rates and the superheated temperatures, the heat duties for all the superheaters were determined by using equation (3.23):

$$\dot{Q}_{\mathrm{HEX}} = \dot{m}_{\mathrm{stm}}(i_{\mathrm{out}} - i_{\mathrm{in}}) \tag{3.23}$$

In equation (3.23), the mass flow rate of steam represents either HP, IP or LP steam mass flow rates across these respective HP,IP or LP superheaters. For the evaporators, the process is slightly

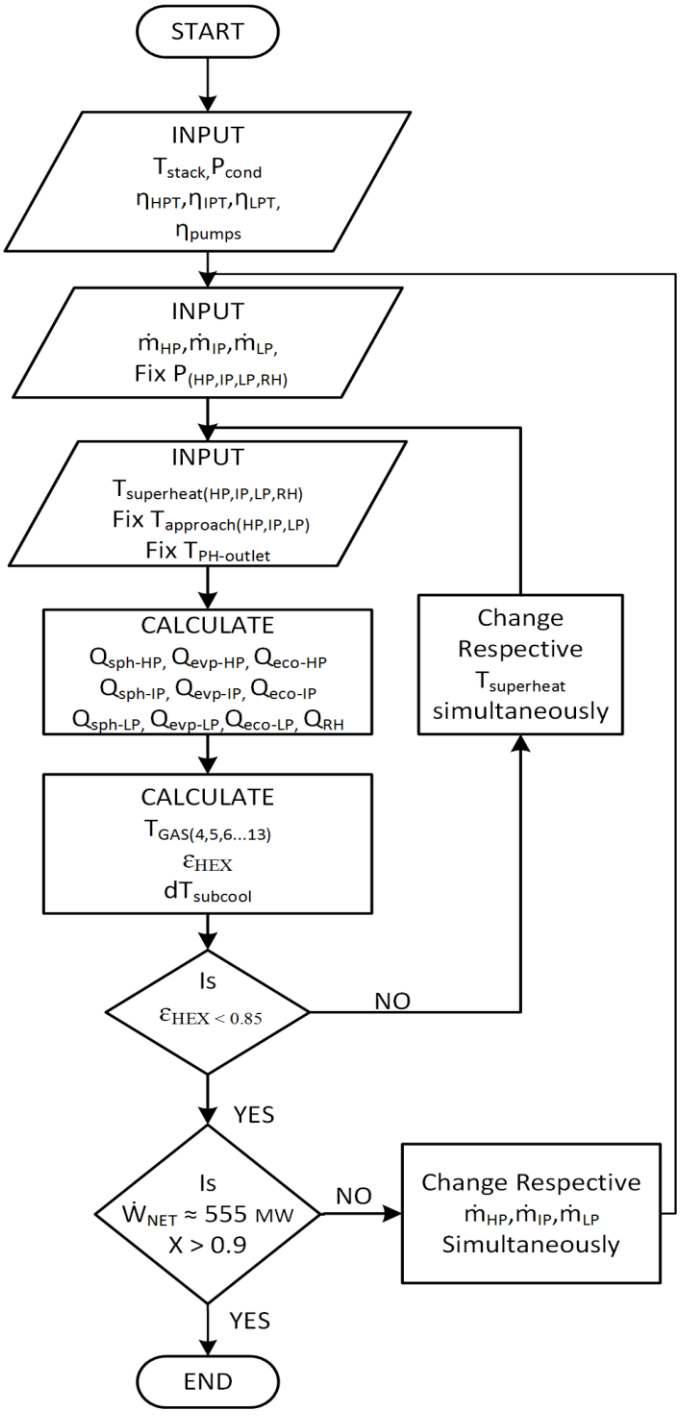

Figure 3-4. Flow chart of steam cycle design point performance prediction.

different. The temperature at which the hot water enters the evaporator is less than the saturation temperature. This temperature difference between the saturation temperature and the evaporator

inlet (or economizer outlet) temperature is known as the approach temperature. It is important to maintain this temperature difference to prevent any boiling that might occur in the economizers [12]. For conventional NGCC power plants with gas temperatures below 1200°F (648.9°C), the suggested approach temperature difference is in the range of 10-40°F (5.5-22.2°C) [12]. In the present study, the value for the HP and IP evaporators is assumed as 10°C, and 5°C for the LP evaporator to be consistent with NETL Case-13. With these temperatures known, the heat duties of the respective HP, IP and LP evaporators can be calculated based on the mass flow rates of steam by using the same equation (3.23). To calculate the heat duties of the economizers, the inlet water temperatures must be determined. An iterative process is used to calculate the inlet conditions of the respective economizers by initially assuming the preheater outlet temperature. After determining the steady state operation of all the heat exchangers, steam turbines, pumps and condensers, the assumed preheater outlet temperature is replaced with the calculated temperature. At this point, with all the heat duties of the HRSG heat exchangers known, the gas temperatures at respective heat exchanger outlet as well as the effectiveness of the heat exchangers can be determined by equating the gas and steam side heat duties of heat exchangers as given by equation (3.24):

$$\dot{m}_{\text{stm}}(i_{\text{out}} - i_{\text{in}})_{\text{stm}} = \dot{m}_{\text{gas}}(i_{\text{in}} - i_{\text{out}})_{\text{gas}} \tag{3.24}$$

During this phase of simulation, a trial and error process was adopted to adjust the maximum superheat temperatures in the superheaters so that the effectiveness of each heat exchanger was equal to or below 85%. Furthermore, the mass flow rates across the HP, IP and LP systems were adjusted to match the total power output generated from the steam turbines with the specified NETL Case 13 values. The quality of the outlet steam from the LP steam turbine was checked to ensure that it remained above minimum limit at all times. The final outcome of this exercise is an

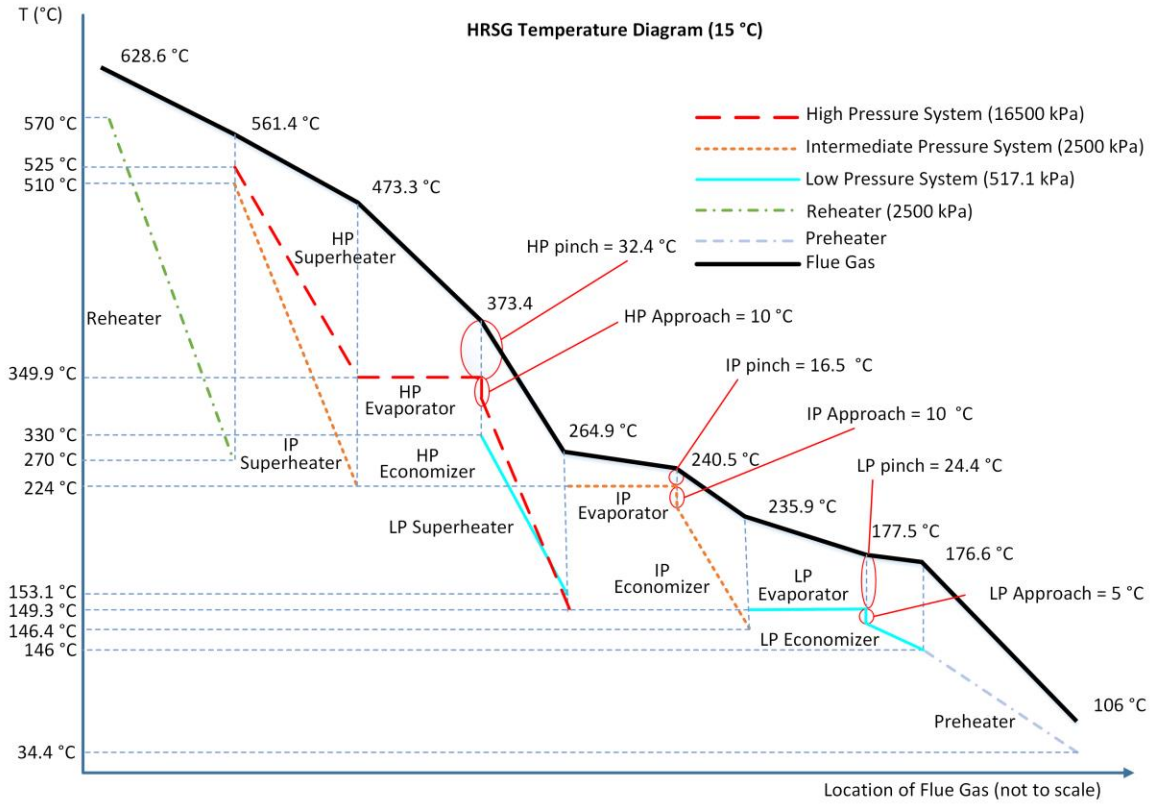

Figure 3-5. Temperature profile across the HRSG heat exchangers at the 15˚C baseline condition.

operating baseline case with state points and operating variables that match well with NETL Case-13. For the baseline operating case, Figure 3-5 presents the temperature state points for all the heat xchangers in the HRSG. This figure is in conjunction with the HRSG layout shown in Figure 3-3. In Figure 3-5, the temperature of the incoming exhaust gas from gas turbine decreases as it passes through the heat exchangers and finally leaves the stack at 106°C. The pinch temperature (i.e., temperature difference between exiting gas temperature and saturation temperature of each evaporator) is important in HRSG design, and, for a conventional NGCC power plant, it is suggested to be greater than 10°F [12]. For all HP, IP and LP evaporators, the pinch point is greater than the suggested value at the baseline operating case. After the temperatures and mass flow rates across each heat exchanger is known and plotted at the design case (as in Figure 3-5), the heat

exchanger effectiveness (ε) and heat transfer conductance (UA) can be calculated for each heat exchanger by using the ε-NTU relationship. The effectiveness of the heat exchangers is calculated by using equation (3.25):

$$\varepsilon = \frac{C_{\mathrm{c}}(T_{\mathrm{c,out}} - T_{\mathrm{c,in}})}{C_{\min}(T_{\mathrm{h,in}} - T_{\mathrm{c,in}})} = \frac{C_{\mathrm{h}}(T_{\mathrm{h,in}} - T_{\mathrm{h,out}})}{C_{\min}(T_{\mathrm{h,in}} - T_{\mathrm{c,in}})} \tag{3.25}$$

For most heat exchangers in the HRSG, a crossflow heat exchanger ε-NTU relationship as given in Equation (3.26) is used to predict the NTU:

$$NTU = -\ln\left[1 + \frac{1}{C_{\mathrm{r}}}\ln\left(1 - \varepsilon C_{\mathrm{r}}\right)\right] \tag{3.26}$$

In equation (3.26), C_{r} is defined as the ratio of $C_{\min}$ and $C_{\max}$ and given by equation (3.27). $C_{\min}$ and $C_{\max}$ represent the heat capacity rate of the heat exchange fluids, either steam or exhaust gas, as follows:

$$C_{\mathrm{r}} = \frac{C_{\min}}{C_{\max}} \tag{3.27}$$

There are several heat exchangers (i.e., HP superheater, HP economizer and preheater) with high effectiveness for which the cross-flow relationship does not yield a feasible solution for NTU, so a counter-flow relationship is used:

$$NTU = \frac{1}{C_{\mathrm{r}} - 1}\ln\left(\frac{\varepsilon - 1}{\varepsilon C_{\mathrm{r}} - 1}\right) \tag{3.28}$$

The evaporators have both single phase and two-phase regions, so the UA and NTU are determined for both fluid regimes. Equation (3.28) is used to calculate the NTU for the single phase regions and equation (3.29) is used to calculate the NTU for the two phase regions:

$$NTU = -\ln(1 - \varepsilon) \tag{3.29}$$

After calculating the respective NTU's for all the heat exchangers, the heat exchanger UAs are

calculated using the relationship in equation (3.30). For the HP, IP and LP evaporators where there are two separate *UA*s for single and two phase regions, the equivalent *UA* is calculated by summing the two *UA*s, which is given by equation (3.31):

$$NTU = \frac{UA}{C_{\min}} \tag{3.30}$$

$$UA_{\text{evp}} = UA_{1\text{P}} + UA_{2\text{P}} \tag{3.31}$$

The main reason for calculating baseline heat exchanger *UA*s is to predict the performance of these heat exchangers at different operating conditions. In off-design cases, the *UA*s can be scaled to a different value by using a scaling technique discussed in subsection 3.2.2.

3.2.2 Off-design Performance

After the baseline performance characteristics of the bottoming Rankine cycle are determined at ISO operating conditions, the performance at different operating conditions can be predicted. Multiple assumptions are made for this process which are listed in Table 3-4.

For the HRSG, a negligible pressure loss on the gas stream is assumed. Similarly, a negligible heat loss from the HRSG to the surroundings is assumed. This ensures all the heat energy from the exhaust gases is utilized to generate steam, thus simplifying the calculation. As

Table 3-4. List of major assumptions to predict Rankine cycle performance.

Component	Major Assumptions
HRSG	Negligible pressure loss on gas stream Negligible heat loss in heat exchangers Maximum heat exchangers effectiveness ≈ 85%
Steam Turbines	Constant isentropic efficiency (85.8%,93.0%,93.0%: HP,IP,LP) Outlet steam quality LP turbine > 90%
Feed Water Pumps	Negligible pressure loss in piping- feed lines Constant pump isentropic efficiency: 71%
Condenser	Constant cooling water flow rate: 7062.2 kg/s Constant degree of sub-cooling: 4.4 ºC Constant Terminal Temperature Difference (*TTD*): 11.7°C
Heat Exchangers	UA scaling

mentioned in subsection 3.2.1, the heat exchanger effectiveness at the baseline case is limited to 85%. At different operating conditions, the effectiveness of each heat exchanger is calculated based on the inlet and outlet temperatures of steam and gas streams.

The isentropic efficiencies of HP, IP, and LP steam turbine calculated for the baseline case are 85.8%, 93.0% and 93.0%, respectively, which are held constant at all times during the off-design case simulation. Similarly, the isentropic efficiencies of the HP, IP, and LP feed water pumps and condensate pump are held constant at the baseline value of 71% based on NETL Case-13. A constant mass flow of cooling water is maintained to the condenser at all operating conditions. This required mass flow rate is calculated by accounting for the cooling water temperatures (16°C/27°C) and the condenser heat duty.

As briefly discussed in subsection 3.2.1, in the off-design model, the heat exchanger *UA*s at the baseline case are scaled to a different value based on the off-design operating conditions. The *UA* of these heat exchangers are scaled based on a simple heat transfer modeling approach. A typical heat exchanger in a HRSG consists of an array of bare or finned tubes arranged in an aligned or staggered configuration to form heat exchanger modules known as harps [57]. These modules are placed either in horizontal or vertical orientations depending on the gas flow path. The overall heat transfer conductance (*UA*) from the gas to the steam in these heat exchangers consists of the heat transfer resistances from the gas-side convection, tube conduction, and the steam-side convection. For this modeling approach, it was assumed the wall thermal resistance is negligible due to tubes material and thickness. In this study, it is assumed that the majority of the thermal resistance exists on the gas exhaust side and a very small portion is accounted for by the tube and the steam side. This assumption allows the heat exchanger *UA* to be approximated as only a function of gas side heat transfer coefficient as follows:

$$UA \approx h_{gas} A_o \tag{3.32}$$

As a result, any significant change to the flue gas mass flow rate and temperature will yield a significant change in the heat exchanger *UA*. For the exhaust, the heat transfer coefficient is assumed to have the following functional relationship with constants a, b and c:

$$h = aRe^{b} Pr^{c} \tag{3.33}$$

In the present study, Zakauskas correlation for aligned tube banks has been adopted where the constant b in equation (3.33) takes the value of 0.63 [58]. Furthermore, the Prandtl number does not change significantly for the given exhaust gas temperature from the inlet to outlet of the heat exchanger. Hence the effects of Prandtl number can be neglected. The Reynolds number is given by equation (3.34):

$$Re = \frac{\left(\frac{\dot{m}}{A}\right) d}{\mu} \tag{3.34}$$

Also, assuming the change in the mass flow rate of the flue gases has a dominant share compared to the viscosity for any changes on the Reynolds number, it can be approximated that the Reynolds number is solely a function of the exhaust mass flow rate. Owing to this, the ratio of *UA*s between the design and off-design points can be calculated using equation (3.35) as follows:

$$\frac{(UA)_{DP}}{(UA)_{ODP}} = \left(\frac{\dot{m}_{g,DP}}{\dot{m}_{g,ODP}} \right)^{0.63} \tag{3.35}$$

At different gas mass flow rates, the calculated *UA*s at the baseline case are scaled using this equation. These new *UA* values are then used to solve for changed effectiveness of the HRSG heat exchangers. This is done by applying same sets of ε-*NTU* relationships discussed in subsection 3.2.1. With the new values of effectiveness, the new superheat temperatures and the steam mass flow rates for the HP, IP, and LP systems are solved using equation (3.23) to equation (3.31). For

an exercise, the representative *UA*s at 15°C are calculated and scaled to 40°C ambient temperature as listed in Table 3-5. It can be seen that the representative *UA*s at 40°C are smaller than at 15°C ambient temperature due to the reduction in exhaust gas flow rate.

Table 3-5. Representative HRSG heat exchanger UA at 15°C and 40°C ambient temperature.

Heat Exchanger	***UA* at 15°C ambient [kW K^{-1}]**	***UA* at 40°C ambient [kW K^{-1}]**
Reheater	599.15	568.09
HP Superheater	1169.43	1108.81
IP Superheater	60.03	56.92
LP Superheater	103.83	98.44
HP Evaporator	1514.24	1435.74
IP Evaporator	918.07	870.48
LP Evaporator	1210.58	1147.83
HP Economizer	2623.58	2487.58
IP Economizer	76.63	72.66
LP Economizer	8.30	7.87
Preheater	1396.60	1324.26

At higher operating ambient temperatures, due to the inability of the cooling towers to produce chilled water at the same temperature as during the baseline case, the condensing pressure of the steam increases, which also increases the LP steam turbine back pressure. The back pressure increase is accompanied by a significant loss in power output from the LP steam turbine, which is a loss of 26.4% when the ambient temperature changes from 15°C to 40°C when the initial temperature difference is kept constant [11]. This loss is due to the steam being extracted at earlier stages of turbine blades [59]. The condenser saturation temperature has to be varied with regards to the operating ambient conditions; in this study the saturation temperature is selected by maintaining a constant terminal temperature difference (TTD) of 11.7°C (i.e., the temperature difference between the condenser saturation temperature and cooling water outlet temperature). The value of 11.7°C for TTD is the same as that during the baseline operating condition. Hence,

with the increasing ambient temperature, the same TTD will yield a different condenser saturation pressure (higher for ambient temperatures greater than 15°C and lower for ambient temperatures less than 15°C). Also, the temperature at which the cooling water returns to the condenser is solely dependent on the performance of the cooling tower. To accurately assess the changing temperatures and to account for the effects of the changing relative humidity, an evaporative cooling tower model is developed and coupled to the NGCC model. Section 3.3 outlines this detailed modeling approach. With this cooling tower model, the cooling water temperatures and the evaporative loss due to cooling can be accurately assessed.

3.3 Cooling Tower

Cooling towers are an integral part of nuclear, coal, and natural gas combined cycle power plants where they supply the cooling water to the condenser. The condensing steam in the condenser rejects heat to the cooling water, after which the cooling water is sent to the cooling tower. The ambient air comes into contact with the cooling water and cools down the water by an evaporative process. The ambient conditions (temperature and relative humidity) are crucial in determining the performance and the temperature of the exiting cooling water from the cooling tower. The following section presents a detailed modeling approach to predict these temperatures.

3.3.1 Heat Transfer Modeling

Wet cooling towers in combined cycle power plants can be of two types: natural draft and mechanical draft. In natural draft cooling towers, air is drawn into the cooling tower by buoyancy forces, while in a mechanical draft tower, an induced draft fan is utilized to draw in the air. Most conventional power plants utilize natural draft cooling towers; however, modern power plants are equipped with mechanical cooling towers equipped with induced draft fans. It is easier to control the air flow rate with the fans, which is why most modern plants consists of mechanical wet cooled

towers instead of natural draft towers. In this study, a mechanical draft cooling tower is considered to be consistent with most power plant operation.

The entering and exiting cooling water temperatures at the cooling tower for the baseline operating case are 27°C and 16°C, respectively. These temperature values along with the condenser heat duty are used to calculate the required cooling water mass flow by using equation (3.36):

$$\dot{Q}_{\text{cond}} = \dot{m}_{\text{cw}} C_{\text{p}} (T_{\text{out}} - T_{\text{in}}) \tag{3.36}$$

The cooling water mass flow rate is kept constant in this study because, although there will be an evaporation loss of water in the cooling tower (nominally 1-3%)[24], there will also be make-up water to compensate for the evaporative deficit.

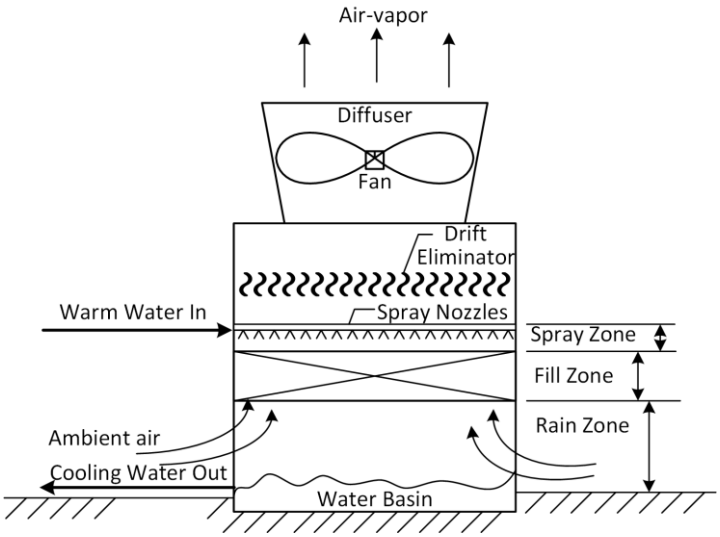

Figure 3-6. Wet cooled mechanical tower.

Figure 3-6 shows a typical mechanical cooling tower equipped with an induced draft fan. Warm water from the condenser is sprayed downward through the nozzles. The area below the spray nozzles up to the fill zone is known as spray zone. Up to ~15% of heat transfer occurs in the spray zone [24]. The water from the spray nozzles falls through a series of differently shaped and sized packed materials called fill. The major function of the fill zone is to break-up the falling

water so a greater surface can be maintained between the cooling air and water. Often, the fills induce a film that increases the water surface area, allowing the water to spread in a thin layer over a large area instead of forming droplets. The major portion of the heat and mass transfer occurs in the fill zone, the quantity of which depends on the type of the fill. The area just below the fill zone is the rain zone where the water drops fall into the collecting basin. Approximately 10-20% of the total heat is rejected in the rain zone [24].

The widely adopted Merkel's theory is used to design the wet cooled tower [24]. Equation (3.37) gives the functional relationship between dimensionless Merkel number (Me) and the temperature distribution across the different points in the cooling tower:

$$Me = \frac{h_{\mathrm{d}} A}{\dot{m}_{\mathrm{w}}} = \int_{T_{\mathrm{wo}}}^{T_{\mathrm{wi}}} \frac{c_{\mathrm{pw}} dT_{\mathrm{w}}}{(i_{\mathrm{masw}} - i_{\mathrm{ma}})} \tag{3.37}$$

Merkel assumes the air leaving the wet cooled tower is saturated with water vapor. For many practical cases, this assumption yields reasonable results [24]. Based on this assumption, the relative humidity at the outlet of the cooling tower is set at unity at all times in this study. Equation (3.37) can be extended for the ease of calculation by applying a four point Chebyshev integral as given by equation (3.38):

$$Me = \frac{h_{\mathrm{d}} A}{\dot{m}_{\mathrm{w}}} = \int_{T_{\mathrm{wo}}}^{T_{\mathrm{wi}}} \frac{c_{\mathrm{pw}} dT_{\mathrm{w}}}{(i_{\mathrm{masw}} - i_{\mathrm{ma}})} \approx \frac{c_{\mathrm{pw}} (T_{\mathrm{wi}} - T_{\mathrm{wo}})}{4} \left(\frac{1}{\Delta i_{(1)}} + \frac{1}{\Delta i_{(2)}} + \frac{1}{\Delta i_{(3)}} + \frac{1}{\Delta i_{(4)}} \right) \tag{3.38}$$

Given that the temperature of inlet and outlet cooling water is known, the Merkel number is calculated by dividing the cooling tower into four points and calculating the respective temperatures and enthalpy differentials at those four points [24]. The enthalpy differentials are defined as the difference in the enthalpy of saturated air at a given temperature to that of the enthalpy of dry air at same temperature and calculated by the equation (3.39):

$$\Delta i_{(1)} = (i_{\text{masw}_{(1)}} - i_{\text{ma}_{(1)}}) \tag{3.39}$$

To determine the enthalpies as stated above, the four temperatures at the intermediate zones are calculated by equation (3.40) through (3.43) for the Chebyshev approach:

$$T_{\text{w(1)}} = T_{\text{wo}} + 0.1(T_{\text{wi}} - T_{\text{wo}}) \tag{3.40}$$

$$T_{\text{w(2)}} = T_{\text{wo}} + 0.4(T_{\text{wi}} - T_{\text{wo}}) \tag{3.41}$$

$$T_{\text{w(3)}} = T_{\text{wo}} + 0.6(T_{\text{wi}} - T_{\text{wo}}) \tag{3.42}$$

$$T_{\text{w(4)}} = T_{\text{wo}} + 0.9(T_{\text{wi}} - T_{\text{wo}}) \tag{3.43}$$

With the four enthalpy differentials and the cooling water temperature known, the Merkel number can be estimated using equation (3.38). Table 3-6 shows the dimensions of the cooling tower used in the present study. Figure 3-7 shows the corresponding labels on the wet cooling tower. The Merkel number for the cooling tower can also be estimated by using characteristic correlations.

Table 3-6. Dimensions of the cooling tower [24].

S.N.	Description	Value (m)
1	Tower Height (H_9)	13.5
2	Fan Height (H_6)	10.5
3	Tower Inlet Height (H_3)	4
4	Tower inlet width (W_i)	16
5	Tower Breadth/ Length (B_i)	16
6	Fill Height (L_{fi})	2.878
7	Height of Spray Zone (L_{sp})	0.5
8	Plenum Chamber Height (H_{pl})	2.4
9	Inlet Rounding (r_i)	$0.025W_i$

In addition to the approach discussed above, the spray zone, fill zone, and rain zone, can be modeled with their respective individual Merkel number based on their geometry and heat and mass transfer characteristics. The overall Merkel number in the cooling tower is the sum of these individual Merkel numbers.

$$Me_{tot} = Me_{sp} + Me_{fi} + Me_{rz} \tag{3.44}$$

The Merkel number specific to the fill zone used in the present study is taken for an Ecodyne Shape 10 type fill and can be approximated by equation (3.45) [24]. This fill was chosen because it generated less pressure drop while increasing the heat and mass transfer performance compared to other types of fills.

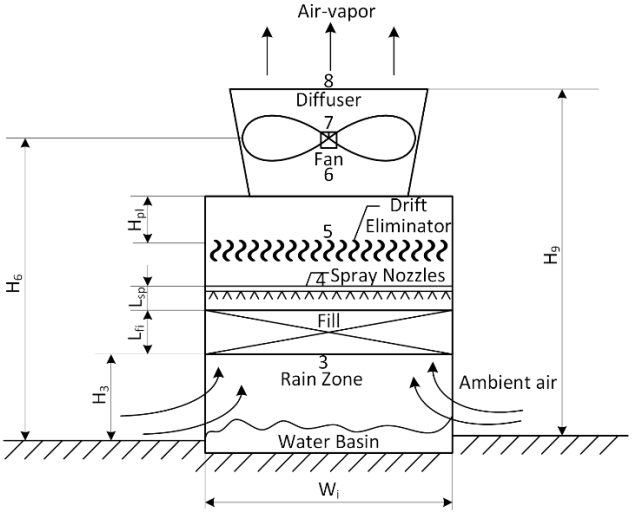

Figure 3-7. Wet cooling tower with numbered location.

$$Me_{fi} = 0.605 L_{fi} G_w^{-0.35} G_a^{0.35} \tag{3.45}$$

For example, by choosing a different type (American Tower), the pressure loss in the tower was calculated as 265 Pa; however, the pressure drop for the Ecodyne Shape 10 type of fill is 253 Pa (baseline case), which is the lowest pressure drops among the types of fills [24].

The Merkel number specific to the spray zone is taken from a study by Lowe and Christie and is given by equation (3.46) [24]:

$$Me_{sp} = 0.2 L_{sp} \left(\frac{G_a}{G_w} \right)^{0.5} \tag{3.46}$$

G represent the mass flux in equations (3.45) and (3.46), and calculated using equation (3.47):

$$G = \frac{\dot{m}}{A_{fr}} \tag{3.47}$$

The frontal area (A_{fr}) is the product of the breadth and width of the cooling tower basin. Similarly, to calculate the Merkel number specific to the rain zone, the following empirical relation is used [24]:

$$Me_{rz} = 3.6\left(\frac{D}{v_{av,o}d_d}\right)\left(\frac{H_i}{d_d}\right)\left(\frac{p_{a1}}{\rho_{w,o}R_vT_{av}}\right)Sc^{0.33}\left[\ln\left(\frac{w_s+0.622}{w+0.622}\right)/\left(w_s-w\right)\right]\times$$
$$\left[\begin{array}{l} 4.68851a_\rho\rho_{av} - 187128.7a_\mu\mu_{av} - 2.29322 + 22.4121\left\{0.350396\left(a_v v_{av,o}\right)^{1.38046}+0.09\right\} \\ \left\{1.60934\left(a_L H_i\right)^{-1.12083}+0.66\right\} \\ \times\left\{34.6765\left(a_L d_d\right)^{0.732448}+0.45\right\} \\ \exp\left\{7.7389\exp\left(-0.399827a_L H_i\right)\ln\left(0.087498\exp\left(0.026619a_L W_i\right)+0.85\right)\right\} \end{array}\right] \tag{3.48}$$

The '*a*' coefficients in equation (3.48) are given by equations (3.49) through (3.52) respectively:

$$a_\mu = 3.061\times10^{-6}\left(\frac{\rho_{w,o}^4 g^9}{\sigma_{w,o}}\right)^{0.25} \tag{3.49}$$

$$a_\rho = \frac{998}{\rho_{w,o}} \tag{3.50}$$

$$a_v = 73.298\left(\frac{g^5\sigma_{w,o}^3}{\rho_{w,o}^3}\right)^{0.25} \tag{3.51}$$

$$a_L = 6.122\left(\frac{g\sigma_{w,o}}{\rho_{w,o}}\right)^{0.25} \tag{3.52}$$

The Schmidt number in equation (3.48) is given by equation (3.53):

$$Sc = \frac{\mu}{\rho D} \tag{3.53}$$

In equation (3.53) and equation (3.48), *D* is the diffusion coefficient at a given state point (evaluated at averaged inlet and exit conditions of rain zone). The air velocity before the fill is

given by equation (3.54) where the subscript 1 represents the cooling tower inlet air position:

$$v_{\text{av3}} = \frac{\dot{m}_{\text{av1}}}{\rho_{\text{av1}} A_{\text{fr}}} \tag{3.54}$$

The Merkel number can now be calculated using equation (3.44) and must equal the Merkel number calculated from equation (3.38). This approach of equating the Merkel numbers enables the calculation of the total air mass flow rate required to cool the water to specified temperatures depending on the heat and mass transfer properties.

The air-vapor outlet temperature can be solved by calculating the air-vapor enthalpy which can be calculated by equating the total heat transfer on the water and air-vapor side by using equation (3.55):

$$\dot{m}_w c_p (T_{w,in} - T_{w,out}) = \dot{m}_a (i_{a,5} - i_{a,1}) \tag{3.55}$$

$i_{a,5}$ in equation (3.55) is given by equation (3.56):

$$i_{a,5} = c_{pa} T + w[i_{fg} + c_{pv} T] \tag{3.56}$$

In equation (3.56), c_{pa}, c_{pv} and T refers to the specific heat of dry air, specific heat of vapor and the outlet temperature respectively. Similarly, ω and i_{fg} refers to humidity ratio and enthalpy of vaporization at temperature T respectively.

The total mass of water lost due to evaporation from cooling tower is given by equation (3.57):

$$\dot{m}_{\text{evap}} = \left(\dot{m}_{\text{av5}} - \dot{m}_{\text{av1}}\right) \tag{3.57}$$

Point 1 and point 5 in equation (3.55) and (3.57) refer to the start of the rain zone and the end of the spray zone and do not represent the four Chebyshev points as stated by equations (3.40) through (3.43). The Chebyshev integral points are specific to the zones where water is being cooled and represents the intermediate points between entering and leaving water temperatures of the cooling tower used for solving the Chebyshev integral. The mass flow rate of the air-vapor mixture at the

cooling tower inlet and exit is calculated from the humidity ratio and dry air mass flow rate at those positions. Equation (3.58) and equation (3.59) give the mass flow rates at inlet and exit respectively:

$$\dot{m}_{av1} = \dot{m}_a \left(1 + w_1\right) \tag{3.58}$$

$$m_{av5} = m_a \left(1 + w_5\right) \tag{3.59}$$

The averaged mass flow of air-vapor mixture from the inlet of the tower to the exit of the tower is given by equation (3.60):

$$\dot{m}_{av15} = \frac{\left[\dot{m}_a \left(1 + w_1\right) + \dot{m}_a \left(1 + w_5\right)\right]}{2} \tag{3.60}$$

The mass flow rates calculated in the above equations are used to calculate the mass fluxes in equations (3.45) and (3.46). Figure 3-8 shows a flowchart that shows the calculation and iteration process used for determining performance of the cooling tower. By using the NETL Case-13 parameters for inlet and outlet cooling water temperatures and the condenser heat duty, the cooling water mass flow rate can be calculated by using equation (3.36). The total condenser heat duty is divided into ten cooling tower cells and the calculations are done for individual cells. The average air-vapor mass flow rate in the cooling tower and the air-vapor outlet temperature are initially assumed to calculate the total Merkel's number. This is done by using the respective correlations for Merkel's number given in equations (3.45), (3.46) and (3.48). This Merkel's number is again calculated by using an integral equation (3.38). When the total Merkel's number calculated by these two different ways are equal, the average air-vapor mass flow rate is determined. Similarly, by equating the heat transferred from water to the cooling air, the outlet air temperature at the cooling tower exit is solved using equations (3.55) and (3.56). For the off-design case, a fixed

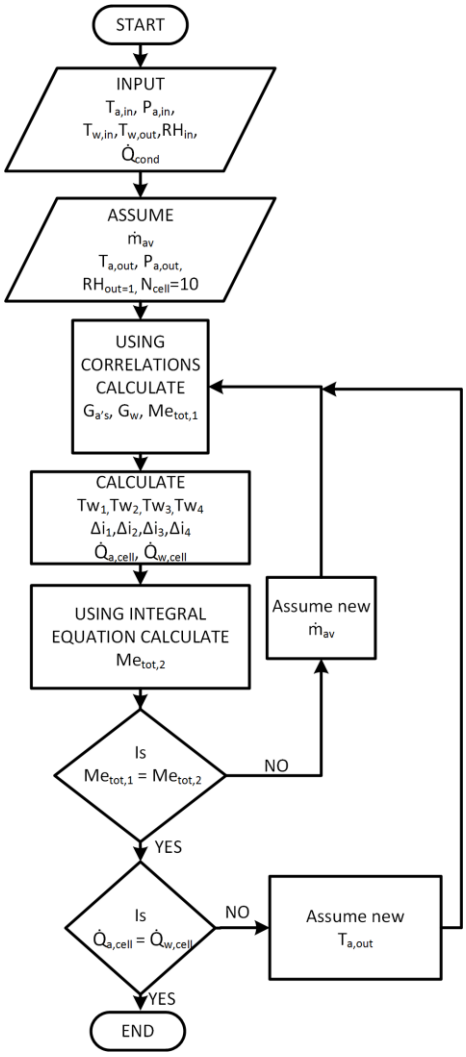

Figure 3-8. Flowchart for cooling tower design point calculation

volumetric air-vapor flow rate at the cooling tower exit is assumed while keeping the cooling water mass flow rate as constant. This enables the calculation of new water temperatures at cooling tower inlet and exit. A representative EES and hand calculation is presented in the Appendix B to better understand the calculations for the cooling tower. In the following section, a detailed approach to calculate the pressure drop across the cooling tower and the fan size required for the cooling tower is presented.

3.3.2 Pressure Drop and Fan Size

The pressure drop across the cooling tower, which determines the fan power requirements, are estimated by calculating the flow losses in the cooling tower. Estimating the fan power is necessary because it adds up to the auxiliary power consumption in the power plants. Equation (3.61) is used to calculate the pressure drop in the cooling tower:

$$dP = \left(K_{il,fi} + K_{rz,fi} + K_{fs,fi} + K_{fi} + K_{sp,fi} + K_{wd,fi} + K_{de,fi} + K_{ct,fi} + K_{up,fi} \right) \left[\frac{\left\{ \frac{\dot{m}_{av15}}{A_{fr}} \right\}^2}{2\rho_{av15}} \right] \quad (3.61)$$

The different loss coefficients in the above equation that occurs in the cooling tower are listed in Table 3-7. The loss coefficient across the inlet louvers, K_{il}, is estimated as 2.5 for the cooling tower dimensions which are presented in Figure 3-7. Other losses like fill support loss and contraction loss (K_{fs} and K_{ctc} respectively) are estimated as 0.5. The water distribution loss (K_{wd}) and upstream

Table 3-7. Different loss coefficients in cooling tower [24].

Loss Coefficient	Description	Value (Baseline)
$K_{il,fi}$	Loss due to inlet louvers specified to mean conditions through fill	4.88
$K_{rz,fi}$	Loss due to rain zone specified to mean conditions through fill	1.79
$K_{fs,fi}$	Loss due to fill support specified to mean conditions through fill	0.49
K_{fi}	Loss due to fill zone	1.81
$K_{sp,fi}$	Loss due to spray zone specified to mean conditions through fill	0.61
$K_{wd,fi}$	Loss due to water distribution specified to mean conditions through fill	0.50
$K_{de,fi}$	Loss due to drift eliminator specified to mean conditions through fill	4.62
$K_{ct,fi}$	Loss due to inlet specified to mean conditions through fill	7.38
$K_{up,fi}$	Upstream loss specified to mean conditions through fill	5.49

losses (K_{up}) are estimated as 0.5 and 0.52, respectively. These losses values are estimated on the basis of specified loss coefficients for a tower with similar dimensions [24]. All these specified loss coefficients need to be expressed and calculated based on the mean temperature conditions through the fill zone which includes the properties of water-vapor mixture in the fill zone. The specified loss coefficient due to the inlet louvers should be expressed based on the mean conditions through the fill and is given by equation (3.62):

$$K_{\mathrm{il,fi}} = K_{\mathrm{il}} \left(\frac{\rho_{\mathrm{av15}}}{\rho_{\mathrm{av1}}} \right) \left(\frac{W_{\mathrm{i}} B_{\mathrm{i}}}{2 H_3 W_{\mathrm{i}}} \right) \left(\frac{\dot{m}_{\mathrm{av1}}}{\dot{m}_{\mathrm{av15}}} \right)^2 \tag{3.62}$$

In equation (3.62), W_{i} and B_{i} refers to the width and breadth of the cooling tower whereas H_3 represents the height of the rain zone as shown in Figure 3-7. The loss coefficient for the rain zone is calculated based on equation (3.63):

$$\begin{aligned} K_{\mathrm{rz}} &= 1.5 a_{\mathrm{v}} v_{\mathrm{w,i}} \left(\frac{H_3}{d_{\mathrm{d}}} \right) \times \\ &\left[\begin{array}{l} 0.219164 - 0.30487 a_{\rho} \rho_{\mathrm{av1}} + 8278.7 a_{\mu} \mu_{\mathrm{av1}} \\ +0.954153 \left\{ 0.328467 \exp\left(135.7638 a_{\mathrm{L}} d_{\mathrm{d}} \right) + 0.47 \right\} \\ \times \left\{ 26.28482 \left(a_{\mathrm{L}} H_{\mathrm{i}} \right)^{-2.95729} \right) + 0.56 \right\} \times m \end{array} \right] \end{aligned} \tag{3.63}$$

In equation (3.63), the value of m is calculated based on equation (3.64):

$$\begin{aligned} m &= \left\{ 2.177546 \left(a_{\mathrm{v}} v_{\mathrm{av3}} \right)^{-1.46541} + 0.21 \right\} \times \\ &\exp \left\{ \begin{array}{l} \ln\left(0.204814 \exp\left(0.066518 a_{\mathrm{L}} w_{\mathrm{i}} \right) + 0.21 \right) \\ \times \left(3.9186 \exp\left(-0.3 a_{\mathrm{L}} H_{\mathrm{i}} \right) \right) \times \\ \left(0.31095 \ln\left(a_{\mathrm{L}} d_{\mathrm{d}} \right) + 2.63745 \right) \end{array} \right\} \end{aligned} \tag{3.64}$$

The a coefficients in equation (3.63) are given in equations (3.49) through (3.52). The water velocity is given by equation:

$$v_{\mathrm{w,i}} = \frac{G_{\mathrm{w}}}{\rho_{\mathrm{w,o}}} \tag{3.65}$$

The rain zone loss coefficient referred to the mean fill condition is given by equation (3.66):

$$K_{\mathrm{rz,fi}} = K_{\mathrm{rz}} \left(\frac{\rho_{\mathrm{av15}}}{\rho_{\mathrm{av1}}} \right) \left(\frac{\dot{m}_{\mathrm{av1}}}{\dot{m}_{\mathrm{av15}}} \right)^2 \tag{3.66}$$

Similarly, the specified loss coefficient of the support structure of the fill referred to the mean conditions through the fill is given by equation (3.67):

$$K_{\mathrm{fs,fi}} = K_{\mathrm{fs}} \left(\frac{\rho_{\mathrm{av15}}}{\rho_{\mathrm{av1}}} \right) \left(\frac{\dot{m}_{\mathrm{av1}}}{\dot{m}_{\mathrm{av15}}} \right)^2 \tag{3.67}$$

Similarly, the losses in the spray zone referred to the mean conditions through the fill is given by equation (3.68), which is based on the data of Cale [60]:

$$K_{\mathrm{sp,fi}} = L_{\mathrm{sp}} \left[0.4 \left(\frac{G_{\mathrm{w}}}{G_{\mathrm{a}}} \right) + 1 \right] \left(\frac{\rho_{\mathrm{av15}}}{\rho_{\mathrm{av5}}} \right) \left(\frac{\dot{m}_{\mathrm{av5}}}{\dot{m}_{\mathrm{av15}}} \right)^2 \tag{3.68}$$

Similarly the loss coefficient due to the water distribution system referred to the mean conditions through the fill is given by equation (3.69):

$$K_{\mathrm{wd,fi}} = K_{\mathrm{wd}} \left(\frac{\rho_{\mathrm{av15}}}{\rho_{\mathrm{av5}}} \right) \left(\frac{\dot{m}_{\mathrm{av5}}}{\dot{m}_{\mathrm{av15}}} \right)^2 \tag{3.69}$$

The loss coefficient for the C type drift eliminator considered for this study is given by equation (3.70) [24]:

$$K_{\mathrm{de,fi}} = 27.4829 Ry^{-0.14247} \left(\frac{\rho_{\mathrm{av15}}}{\rho_{\mathrm{av5}}} \right) \left(\frac{\dot{m}_{\mathrm{av5}}}{\dot{m}_{\mathrm{av15}}} \right)^2 \tag{3.70}$$

In equation (3.70), *Ry* refers to the characteristic flow parameter and is defined as the ratio of mass flux (G_{fr}) to viscosity (μ) given by equation:

$$Ry = \frac{G_{\mathrm{fr}}}{\mu} \tag{3.71}$$

The cooling tower in the present study is equipped with an induced draft fan and the fill zone is

considered isotropically packed (e.g., splash or trickle type fill). The inlet loss coefficient for isotropically-packed, induced draft, rectangular towers is given by equation (3.72):

$$K_{ct} = 0.2339 + \left(3.919\times10^{-3}K_{fie}^{2} - 6.84\times10^{-2}K_{fie} + 2.5267\right) \times \exp\left[\frac{W_i}{H_i}\left\{0.5143 - 0.1803\exp\left(0.0163K_{fi}\right)\right\}\right] - \sinh^{-1}\left[\begin{array}{l} 2.77\exp\left(0.958\dfrac{W_i}{H_i}\right)\exp\left\{10^{-2}K_{fi}\left(2.457 - 1.015\dfrac{W_i}{H_i}\right)\right\} \\ \times\left(\dfrac{r_{ir}}{W_i} - 0.013028\right)\end{array}\right] \quad (3.72)$$

In equation (3.72) r_{ir} refers to the inlet rounding (rectangular inlet fillet). By introducing the inlet rounding, the overall inlet losses can be minimized [24]. The specified fill loss coefficient for the Ecodyne Shape 10 type of fill is given by equation (3.73)[24]:

$$K_{fdm} = 1.103L_{fi}^{\ 0.32}G_{w}^{\ 1.1}G_{a}^{\ -0.640} \quad (3.73)$$

By using the specified fill loss coefficient the actual fill loss coefficient applicable to the cooling tower can be calculated by using equation (3.74):

$$K_{fi} = K_{fdm} + \frac{\left(\dfrac{G_{av5}^{2}}{\rho_{av5}} - \dfrac{G_{av1}^{2}}{\rho_{av5}}\right)}{\left(\dfrac{G_{av15}^{2}}{\rho_{av15}}\right)} \quad (3.74)$$

The effective loss coefficient in the vicinity of the fill (K_{fie}) is given by the sum of different loss coefficients:

$$K_{fie} = K_{fs,fi} + K_{fi} + K_{sp,fi} + K_{wd,fi} + K_{de,fi} \quad (3.75)$$

The inlet loss coefficient (K_{ct}) referred to the mean conditions through the fill is given by equation (3.76):

$$K_{ct,fi} = K_{ct}\left(\frac{\rho_{av15}}{\rho_{av1}}\right)\left(\frac{\dot{m}_{av5}}{\dot{m}_{av15}}\right)^2 \tag{3.76}$$

Similarly, the specified fan upstream loss coefficient referred to the mean conditions through the fill is given by equation (3.77):

$$K_{up,fi} = K_{up}\left(\frac{\rho_{av15}}{\rho_{av5}}\right)\left(\frac{\dot{m}_{av5}}{\dot{m}_{av15}}\right)\left(\frac{A_{fr}}{A_c}\right)^2 \tag{3.77}$$

With all these loss coefficients determined, the pressure drop across the cooling tower is calculated using the equation (3.61). The local pressure along the height of the cooling tower is evaluated for baseline case and presented in Figure 3-9. The initial pressure drop zone 1 as shown in Figure 3-9

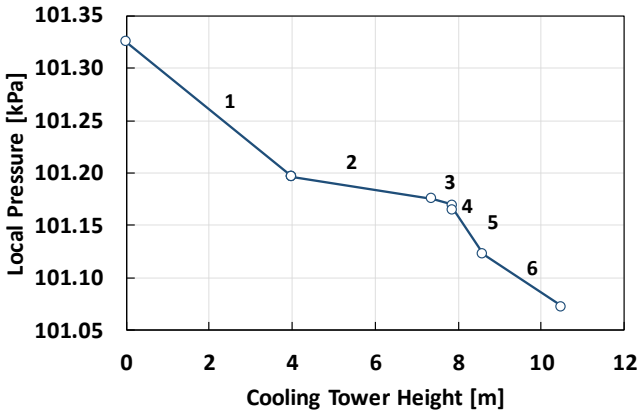

Figure 3-9. Local pressure in the cooling tower at baseline case

is 128.7 Pa which includes the losses due to the inlet, inlet louvers and rain zone, which have respective values of 67.6, 44.7 and 16.4 Pa. After the rain zone, significant pressure loss occurs in the fill zone (zone 2 in Figure 3-9), which equals 21.1 Pa. The loss due to spray zone (zone 3) and water distribution (zone 4) are 5.6 and 4.5 Pa respectively. The drift eliminator (zone 5) and upstream pressure losses (zone 6) dominates rest of the pressure losses that occurs in the tower which equals 42.4 Pa and 50.3 Pa respectively. With the pressure drop calculations across the cooling tower, the fan power requirements now can be calculated by applying equation (3.78):

$$P = \frac{m_{av5}}{\rho_{av5}}\left(\frac{dp}{\eta}\right) \tag{3.78}$$

The fan power calculated in the above equation is treated as the power plant auxiliary power and is subtracted from the total power plant output. In the following section, the waste heat recovery scenarios for the NGCC plant is identified and discussed in detail.

3.4 Waste Heat Recovery Scenarios

A number of waste heat recovery scenarios are considered for the current study to provide gas turbine inlet chilling. Table 3-8 lists the options for the present study. Three important heat sources have been identified to operate these thermally activated cooling systems: high temperature gas turbine exhaust (~628°C), low pressure steam (~5 bar, 330 °C), and low temperature flue gas (~106°C). For the first system, the high temperature turbine exhaust gas is utilized at the desorber of the absorption cooling system (Figure 3-10). The outgoing flue gas is then sent to the HRSG at a decreased temperature (~600 °C). For the present study, the pressure drop in the system is assumed to be negligible. In the second option, a fraction of the low pressure steam is routed to a heat exchanger to power the cooling system which, after being utilized, is mixed with the major portion of steam into the surface condenser. In so doing, only a portion (~6%) of the generated steam is utilized for running the WHR system. For the third option, the

Table 3-8. WHR scenarios.

Energy Source	System	Resulting Effect
Gas Turbine Exhaust (High Grade)	Absorption	Turbine Inlet Chilling
Low Pressure Steam	Absorption	
Flue Gases (Low Grade)	Absorption	
Electricity	Vapor Compression	

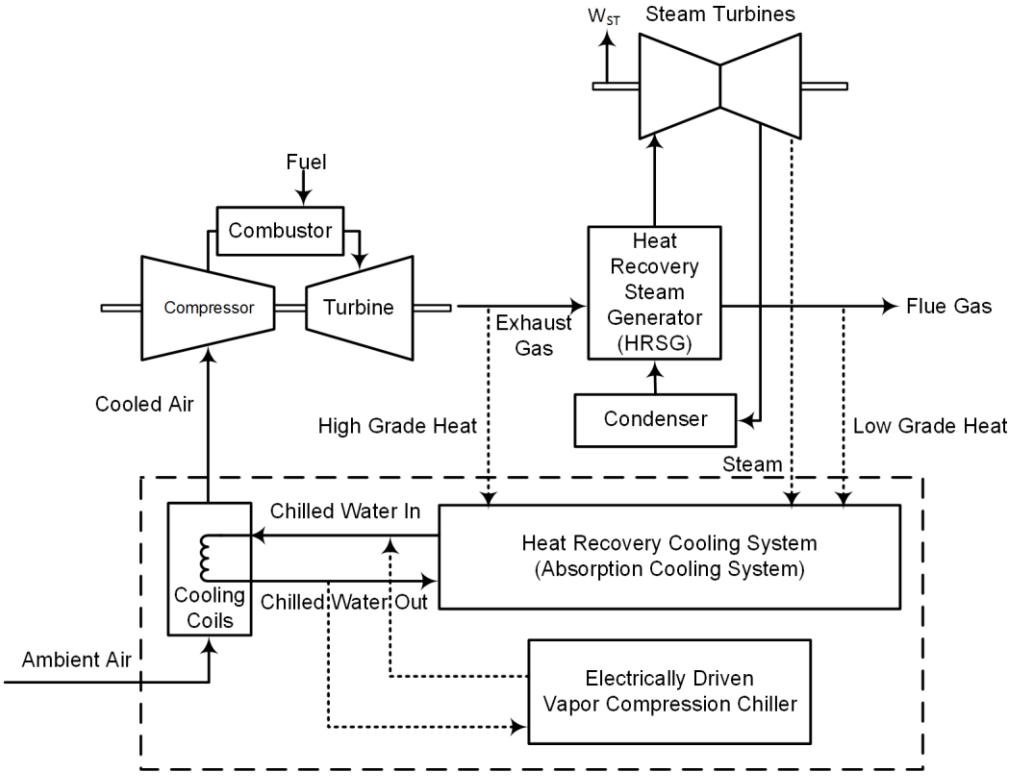

Figure 3-10. Evaluated schemes for waste heat recovery and mechanically driven gas turbine inlet chilling systems.

low temperature flue gas exiting the HRSG is utilized. After utilization, the flue gas is sent into the atmosphere through the stack. The operation of these thermally activated cooling systems is compared to a vapor compression chiller which is powered from the power plant output. The cooling capacity of the electrically driven vapor compression chiller is considered the same as that of the absorption chiller for efficient comparison.

3.4.1 Cooling Load Calculation

As the ambient temperature increases, the gas turbine inlet air cooling load changes because the air requires more chilling. The chilled water outlet temperatures that will be considered for this study from absorption and vapor compression chillers is ~3°C. This temperature can be lowered if the absorption chillers use brines instead of water as a cooling fluid. As a result, the

present study assumes the incoming air can be effectively cooled to 7°C. This minimum cooled temperature is kept constant. It is not effective to extract steam or use the gas turbine exhaust to operate the inlet air cooling system in a combined cycle power plant at low ambient temperatures (~8-10°C) because the performance of the bottoming Rankine cycle would decrease. This approach is effective only if the reduction in Rankine cycle power output can be offset by the power augmentation generated by employing inlet air cooling. Conversely, this would not be the case when the heat source to run the thermally activated cooling system is low grade heat from the power plant stack which is otherwise wasted. Hence, in the present study, the incoming air is cooled only if the ambient temperature is above ISO operating conditions (i.e., 15°C). The hourly cooling load for a given location is calculated by using equation (3.79). The cooling load here represents the heat duty required to drop the temperature from the current ambient temperature down to 7°C:

$$\dot{Q}_{\text{cool}} = \dot{m}_{\text{da}} \left[(i_{\text{a1}} - i_{\text{a2}}) + w_1 i_{\text{g1}} - w_2 i_{\text{g2}} + (w_2 - w_1) i_{\text{w}} \right] \tag{3.79}$$

In equation (3.79), state 1 represents the incoming ambient air and state 2 represents the air after inlet chilling just before it enters the compressor. To calculate the maximum cooling load at a given location, state 2 is set at 7°C. Typical Meteorological Year (TMY3) data has been used for two locations to extract the ambient weather conditions (temperature, pressure and relative humidity). With the aid of equation (3.79), the maximum cooling load at a particular hour for locations Houston and Los Angeles are estimated as 53.80 MW_{th} and 34.06 MW_{th}, respectively. The reason that Houston has a higher maximum cooling load compared to Los Angeles is that the maximum temperature is 39.4 °C while for Los Angeles is 32.2°C. The major reason for taking these two locations for the present analysis is also due to the reason that the weather in Houston is more extreme with hot and humid summers and cold winters. In contrast, the weather at Los

Angeles is milder and nearly constant throughout the year. To assess the effectiveness of the gas turbine inlet air chilling, these two weather patterns serve well and capture the overall climactic variation. The total number of hours that cooling is required (hours the ambient temperature is greater than 15°C) for these locations are calculated as 6467 and 5954 hours, respectively. The relative humidity and temperature of the incoming air is highly important to estimate the outgoing conditions from the inlet air chiller. If the relative humidity at any given hour is high, the outgoing air from the chiller could be saturated by a slight amount of cooling and water droplets might be formed. If continuous cooling is provided, the temperature of the air-water mixture decreases and more vapor from the air is condensed. The water droplets which are formed during this cooling process have to be separated by utilizing a filtration system immediately before the compressor inlet. Trace water droplets entering the compressor might damage the compressor blades. The mass flow of condensed water is subtracted from the total air mass flow and the mass flow of air that goes into the compressor is calculated using equation (3.80):

$$\dot{m}_{av,2} = \dot{m}_{av,1} - \dot{m}_{w} \tag{3.80}$$

In equation (3.80), states 1 and 2 represents the incoming and outgoing air to the process heat exchanger used to cool the gas turbine inlet air. $\dot{m}_{\mathrm{w}}$ represents the mass flow rate of the condensed water during the inlet air chilling process. In the following section, the basis for the selection of the size of the thermally activated cooling system is discussed.

3.4.2 WHR System Sizing

The WHR system size selection is based on the amount of waste heat that is extractable from the power plant stack flue gases. If the temperature of the flue gas is dropped beyond certain threshold, which depends on the composition of flue gas, the corrosive acid SO_2 can form in the flue gas path. This minimum temperature of the exiting flue gas to prevent acid condensates in the

stack depends on the volume fraction of sulfur-dioxide and water in the flue gas [61]. For most combined cycle power plants, the lower temperature limit to prevent acid condensates is 80°C [62]. Hence, in the present study, the maximum waste heat that can be extracted from the flue gas is based on this temperature limit. The instantaneous extractable waste heat at any given time is calculated by using equation (3.81) below:

$$\dot{Q}_{wh} = \dot{m}_g (i_T - i_{80}) \tag{3.81}$$

In equation (3.81), i_T refers to the enthalpy of flue gas at the preheater exit in the HRSG and i_{80} refers to the enthalpy of the same flue gas composition dropped to a temperature of 80°C. The minimum amount of waste heat that can be extracted from the flue gas occurs at the combination of lowest gas flow rate and lowest preheater exit temperature. Over the yearly simulation, this minimum waste heat value is calculated as 22.646 MW_{th} and 22.763 MW_{th} for locations Los Angeles and Houston, respectively. Hence, if a WHR cooling system with these minimum waste heats and COP of 1 is installed at these two locations, the minimum amount of cooling generated will be 22.646 MW_{th} and 22.763 MW_{th}, respectively. Instantaneous cooling generated will be higher than the minimum value. If systems with different COPs are installed, the amount of cooling generated will be different for the same waste heat. A typical single effect LiBr-H_2O absorption chiller has a COP in the range of 0.7- 0.9, whereas for a double effect absorption chiller, COP values are as high as 1.2 -1.5 [63]. Double effect systems, however, have a higher capital cost compared to the single effect systems. Triple effect systems have been commercialized recently

Table 3-9. Minimum cooling generated (MWth) based on location and COP.

Location	**COP**									
	0.2	0.4	0.6	0.8	1.0	1.2	1.4	1.6	1.8	2.0
Los Angeles	4.53	9.05	13.59	18.12	22.65	27.18	31.70	36.23	-	-
Houston	4.55	9.11	13.66	18.21	22.76	27.32	31.87	36.42	40.97	45.53

and have the highest COP compared to single and double effect systems and are the most expensive systems [64]. Also, the heat source required to run the double or triple effect absorption system is high compared to a single effect absorption system. To account for the range of waste heat temperatures considered in this study, the COP range for the absorption chillers was varied from 0.2 to 2.0 at an increment of 0.2. Hence, with the available minimum waste heat, a particular system operating in Houston with a COP of 0.2 will provide 4.552 MW_{th} of cooling, whereas a system with a COP of 2.0 will provide 45.526 MW_{th} of cooling. A similar calculation can be made for the location of Los Angeles. The amount of cooling that can be generated for a range of different COPs based on the minimum flue gas waste heat are listed in Table 3-9. In this study, the cooling capacity of the absorption system is set to these minimum values. In other words, in order to install a WHR system with the cooling sizes listed in Table 3-9, the system requires the corresponding minimum COP in the table to prevent the temperature in the stack from dropping below the 80°C threshold. For Los Angeles, a system with COP greater than 1.6 (cooling of 36.233 MW_{th}) is not considered in this study because the cooling generated at higher COPs exceeds the maximum cooling load (34.06 MW_{th}).

The cooling system size and the minimum cooled air temperature are of crucial importance in this modeling approach. The cooling system size limits how low the gas turbine inlet temperature can reach. For example, if the maximum cooling size under consideration is 4 MW, but it requires 7 MW to cool the ambient air to 7°C, the ambient air is cooled to that temperature which is possible by employing only 4 MW of cooling, resulting in an inlet temperature higher than 7°C. Also, for example, if cooling to 7°C only requires 2 MW of cooling at any instant but the chiller size under consideration is higher than 2 MW, the air is only cooled to a temperature limit of 7°C.

To compare the different potential heat sources presented in this study, including the gas turbine exhaust as well as steam from the Rankine cycle, it is assumed that the same amount of waste heat is extracted from all of these sources. For example, at Los Angeles, setting the minimum exiting flue gas temperature to 80°C is equivalent to extracting 22.65 MW_{th} of waste heat from flue gas stream. The same amount of heat is extracted from the gas turbine exhaust or steam as a heat source for running an absorption chiller. This is done to ensure that the comparison between these systems is based on same amount of heat extracted.

In addition to analyzing thermally activated absorption cooling systems, a comparison with an electrically operated vapor compression chiller is performed. For this comparison, the vapor compression chiller is compared to other thermally activated cooling system assuming that all of these systems provided an equal amount of cooling to the incoming gas turbine air. Depending operational percentage of total cooling capacity and the type of the compressor used, the COP of an electrically driven vapor compression chiller might vary in the range of 3 to 6 [62]. The COP of the vapor compression chiller is fixed at 5 throughout the year and the cooling provided by the chiller is selected on the basis of Table 3-9 for both locations Los Angeles and Houston whenever it is compared to other thermally activated cooling systems. The weather dependence of the COP of the chillers is not taken into consideration in the present study because a more rigorous modeling is required in order to predict the instantaneous COP for thermally activated cooling systems and vapor compression cooling system which is beyond the scope of present study. The electricity required by the vapor compression chiller is calculated by using the COP equation (3.82):

$$MW_e = \frac{\dot{Q}_{\text{cool}}}{COP} \tag{3.82}$$

For example, an absorption chiller with COP of 0.2 provides a cooling of 4.53 MW_{th} by extracting a waste heat of 22.65 MW_{th}. In comparison, a vapor compression chiller with the same cooling

requires 0.9 MW_e of electricity from the power plant for a COP of 5. This approach provides an opportunity to compare the vapor compression cooling system with the waste heat powered absorption systems either based on heat extracted or electricity required to operate these chillers. In the following section, a detailed economic modeling approach for the calculation of LCOE is presented.

3.5 Economic Modeling

As discussed in chapter 2, most of the techno-economic analysis done in previous studies focused merely on the calculation of pay-back period for different WHR options. The impact of installing these WHR systems on the overall cost of electricity has not been outlined in the literature. In this section, the change in LCOE by considering the entire life of the power plant is investigated for these cooling options. NETL's Cost Estimation Methodology for Power Plant Performance [65] is used to estimate the global economic parameters and procedures to calculate the LCOE for the NGCC power-plant and for the different turbine inlet chilling scenarios. In the following paragraphs, a detailed description and methods to calculate the LCOE is presented.

3.5.1 COE, LCOE and IRR

The Cost of Electricity (*COE*) is the revenue received by the power producer per net megawatt-hour during the first year of operation of the power plant. The *COE* over the life of the plant increases annually at an annual rate equal to the general inflation rate [65]. Equation (3.83) gives the functional relationship of *COE* based on the first year's operation costs (*OC*- variable and fixed), Total Overnight Capital (*TOC*), Capital Charge Factor (*CCF*), Capacity Factor (*CF*), and the *MWH* generated at 100% *CF*.

$$COE = \frac{CCF \times TOC + OC_{\text{FIX}} + CF \times OC_{\text{VAR}}}{CF \times MWH} \tag{3.83}$$

In equation (3.83), *TOC* includes the owner's costs and other costs related to the power plant total capital. More details and the calculation of the *TOC* is based on the approach presented by NETL [65]. The *CCF* is the rate of return required on the invested capital and is calculated based on the global economic parameters presented in Table 3-10. This value requires a complicated iteration and calculation technique, however, for a number to be estimated as a combination of economic parameters and plant life [65]. The *CF* is the percentage of total output generated by the power plant throughout the year compared to the total nameplate generation capacity. It is anticipated that the weather at certain times of the year are extreme (eg. Extreme snowfall, rain or high temperature) while because of some externalities (eg. flood, disaster etc.), the power plants needs to partially or completely shut off. To take into account these extreme weather patterns, in real practices, the *CF* usually is set between 80 and 90% depending on the scheduled complete shutoff or maintenances required in the power plant. In the present study, the *CF* is taken as 100% for analytical purposes.

Table 3-10. Global economic assumptions.

Parameter	Value
Income Tax Rate	38 %
Capital Depreciation	20 years, 150% DB
Repayment term of Debt	15 years
Capital Expenditure Period	3 years
Plant Operational Period	30 years
Economic Analysis Period	33 years
Capital Costs Escalation During Capital Expenditure	3.6%
Distribution of Capital over construction years	10%,60%,30%
Interest/Discount Rate	5.5%
Annual Inflation Rate	3%
Escalation of COE, O&M costs and Fuel costs	3%
Desired Internal Rate of Return (IRR)	12%
Finance Structure	45% Debt,55% Equity

The *LCOE* is different from the *COE* in that it is the revenue received by the power producer while assuming a nominal annual inflation rate of 0 percent. In other words, the *LCOE*

includes the inflation effects on the cost of electricity over the entire course of power plant's life. Equation (3.84) can be used to calculate the *LCOE* based on *COE* and a Levelization Factor (*LF*).

$$LCOE = COE \times LF \tag{3.84}$$

The corresponding *LF* value which is a function of project's operating life, discount rate, and inflation rate can be calculated by the equation (3.85):

$$LF = \frac{A(1 - K^{LPn})}{(D - N)} \tag{3.85}$$

In equation (3.85) the variables *D*, *N* and *LPn* are the discount rate (i.e., internal rate of return used in this case), nominal escalation rate (i.e., general inflation rate), and Levelization period (active period of the project life - 30 years), respectively. The internal rate of return (IRR) is the discount rate at which the net present worth of the project is zero [66]. The values *K* and *A* in equation (3.85) are calculated based on the two equations below:

$$K = \frac{1 + N}{1 + D} \tag{3.86}$$

$$A = \frac{D(1 + D)^{LPn}}{(1 + D)^{LPn} - 1} \tag{3.87}$$

In this study, the *COE* value is initially assumed to be in the range of $50 per MWh and is then varied until a fixed IRR of 12% is achieved on the investment. In other words, the *COE* is calculated to achieve an IRR of 12% which is typical of what most power producers desire for their return on their investment [65]. This approach allows power producers to decide if a project is worth investing and would generate profitable returns on their investment [65]. IRR values for first of a kind investments projects are higher because of the risks associated with immature failure, however technologies like combined cycle plants are quite mature because of which the required IRR are set low and uncertainties can be predicted near accurately. Hence, in this study, the

baseline *COE* for the power plant is first calculated at a corresponding IRR of 12%. The *COE* value that yields an IRR of 12% is then used in equation (3.84) to calculate the corresponding *LCOE*. The *IRR* is a function of the revenue generated and the expenses of the power plant. In other words, *IRR* is calculated based on the yearly net cash flows throughout the power plant's life. The yearly revenue generated by the power plant depends on the MWh produced from the power plant and is given by the equation (3.88):

$$Rev = MW_{\text{avg}} \times COE \times 8760 \times CF \tag{3.88}$$

In equation (3.88), *Rev* is the yearly revenue in dollars, MW_{avg} is the average annual MW generated from the power plant, *COE* is the yearly costs of electricity. This *COE* escalates each year throughout the power plants life with rate equal to the general inflation rate. The net profit that the power producers make each year depends on the revenue generated, operation and maintenance expenses, interest expenses, depreciation and taxes and is given by equations (3.89) and (3.90):

$$NI = (1\text{-}x)\,TI \tag{3.89}$$

$$TI = Rev - O\&M - Dep - FE \tag{3.90}$$

In equation (3.89) *NI*, *x* and *TI* stands for net income, tax percentage and taxable income respectively. Similarly, *O&M*, *Dep* and *FE* in equation (3.90) refers to operation and maintenance expenses (both variable and fixed), depreciation and finance expenses. The *LCOE* values change at various locations due to the different MWh of power generated based on the variation in weather. Similarly, for the different WHR cooling system scenarios, the change in the MWh generated by the system from the baseline case would produce a change in the *LCOE* of the plant. As such, the WHR cooling system that produces the lowest *LCOE* but highest power output is most economical choice. To better understand the process used in calculating the *LCOE* the major spreadsheets including the income and costs statements are presented in Appendix C.

3.5.2 Capital and Operation and Maintenance Cost Estimation

The capital costs and operation and maintenance costs associated with the wet-cooled NGCC power plant are taken from the U.S. (DOE), NETL Case 13 (Revision 2a, September 2013) [67]. These costs are presented for the base year 2007. A general inflation rate of 3% is used to convert these costs to the base year 2017. The variable costs including the natural gas costs and water costs are estimated on the basis of plant hourly data and the capacity factor (CF), which for the present study is taken as 100%. The major expenses for the power plants are the sum of variable and fixed operating expenses. The fixed operating expenses includes the operating labor and maintenance costs, taxes and insurances and administrative expenses.

A parametric analysis is performed by varying the capital costs of the WHR unit between \$10 per kW_{th} to \$10,000 per kW_{th} of cooling provided. This approach is followed because these systems can be effectively compared based on economic impact they have on the overall *LCOE* of the power plant. For estimating the installation costs, more detailed analysis on the costs of the heat exchangers and other flow movement devices and their dependence on the chilled water flow rate, chiller heat duty and water temperatures is required. This requires rigorous heat exchanger calculations and quote requests from multiple vendors, which is beyond the scope of the present study. Hence an approximation is done by estimating the heat exchanger and installation costs as 25% of the WHR unit capital cost. This approximation produces near accurate results [68]. The annual operation and maintenance costs for the absorption chiller is the sum of the annual costs of both the electricity and water required by the absorption chiller. In the present study, these costs are taken as 10% of the installed costs (WHR unit cost plus 25 % installation costs) of the cooling system. Similarly, the annual operation and maintenance costs for the vapor compression chiller other than electricity requirements can be estimated as 2.5% of the initial installation costs of the

cooling unit [68]. The operational costs of the electricity required to operate the vapor compression chiller is not considered because the chiller power required is subtracted from the total power plant output.

3.6 Model Validation

The gas turbine cycle, steam cycle and the wet cooled tower modeling approach presented in this chapter are validated by comparing the results with a similar model that is generated by using a GE's Gate Cycle modeling suite [31]. The GE's Gate Cycle suite however has computational limitations requiring the user to input weather data manually each time the model is solved. Hence, a limited number of off-design weather data is used to validate the model. Figure 3-11 shows the Gate cycle model process flow diagram equivalent to the NGCC power plant model generated for this study. In the following sub-sections, the model validation approach for the individual cycle: Gas turbine cycle, steam turbine cycle and cooling tower for both methods are presented.

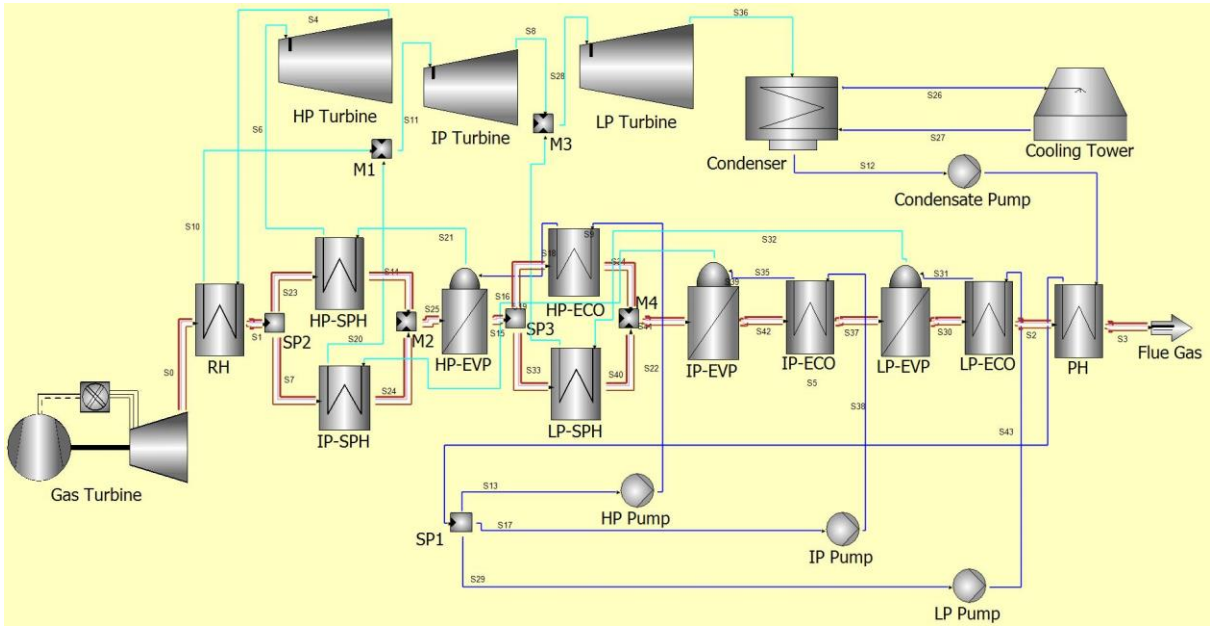

Figure 3-11. NGCC model generated by using Gate Cycle Software

3.6.1 Gas Turbine Cycle

The gas turbine type chosen for the Gate Cycle model is Mitsubishi M701DA SC (GTW 2009). Some of the parameters for this gas turbine were modified so that the baseline case matched well with the NETL Case-13. The gas turbine performance characteristics that are analyzed in this

Table 3-11. Model validation results for gas turbine cycle

	Ambient Temperature (°C)							
Ambient Pressure 101.32 kPa	**5**		**20**		**30**			
Parameter	**CM**	**GCM**	**CM**	**GCM**	**CM**	**GCM**	**Units**	**Deviation (%)**
Gas Turbine Net Power	389.00	384.34	349.58	352.19	325.78	333.97	MWe	-2.45
Compressor Pressure Ratio	20.57	20.81	19.93	19.87	19.54	19.32	-	-1.15
Exhaust Mass Flow Rate	930.14	926.68	881.85	883.51	852.32	857.22	kg/s	-0.57
Exhaust Temperature	625.21	624.8	630.3	632.02	633.57	639.19	C	-0.88
Compressor Efficiency	80.15	79.59	80.22	80.40	80.27	81.00	%	-0.90
Turbine Efficiency	91.52	91.53	91.52	91.53	91.52	91.53	%	-0.01
Ambient Pressure 98 kPa	**5**		**20**		**30**			
Parameters	**CM**	**GCM**	**CM**	**GCM**	**CM**	**GCM**	**Units**	**Deviation (%)**
Gas Turbine Net Power	370.43	371.65	332.57	340.65	309.7	323.11	MW_e	-4.15
Compressor Pressure Ratio	20.57	20.81	19.93	19.87	19.54	19.32	-	-1.15
Exhaust Mass Flow Rate	899.61	896.08	852.91	854.39	824.35	828.97	kg/s	-0.56
Exhaust Temperature	631.43	621.86	636.57	632.1	639.86	639.31	C	1.54
Compressor Efficiency	80.15	79.59	80.22	80.46	80.27	81.00	%	-0.90
Turbine Efficiency	91.52	91.53	91.52	91.53	91.52	91.53	%	-0.01

validation process include gas turbine net electric power output, compressor pressure ratio, compressor efficiency, turbine efficiency, turbine exhaust temperature and turbine exhaust mass flow rates evaluated at multiple off-design ambient temperatures and pressures respectively. These parameters are evaluated at off-design ambient temperatures of 5°C, 20°C and 30°C while the ambient pressure is kept fixed at 101.32 kPa (baseline) and 98 kPa respectively. The effect of relative humidity is minimal for the gas turbine performance hence the effect of relative humidity variation is only considered for cooling tower. Table 3-11 compares the values for these specified parameters for both modeling approaches and also presents the maximum deviation percentage evaluated for one ambient pressure under consideration. CM and GCM refers to the values predicted by "Current Model" and "Gate Cycle Model" respectively.

From Table 3-11, it can be inferred that the deviation for nearly all gas turbine operating parameters lies in the ±2% margin except for the gas turbine net power output which has a higher deviation at a lower operating ambient pressure. One reason for this is because the Gate cycle utilizes a standard equation to predict the performance based on the geometric properties (eg. vane angle, compressor outlet diameter, nozzle area etc.). However, in the present study the geometric parameters for the specified F-class gas turbine is unknown. Hence, given that the deviation is below 5%, the gas turbine modeling approach used in the present study still captures the essential performance characteristics and fits well with other models with greater than 95% certainty.

3.6.2 Steam Cycle

The steam cycle under consideration here consists of high, intermediate and low pressure systems. Each pressure system consists of individual steam turbines, economizer, evaporator, superheater and feed water pumps. In addition, the steam cycle also consists of a condenser, reheater and a preheater. Since there are multiple performance parameters involved with these

components of the steam cycle, the model validation is performed only on the major parameters that can alter the LCOE of the overall plant. These parameters are identified as the steam turbines power output, pumps auxiliary power, stack gas temperature and condenser heat duty.

Table 3-12 presents the validation results for the parameters of the steam cycle for both the modeling approaches. The maximum deviation for the parameters evaluated is for the auxiliary power consumption of the pumps which is 8.8% at 5°C ambient temperature, however, the auxiliary power consumption only shares nearly 0.4% of the total baseline net power output (555

Table 3-12. Model validation results for steam cycle

Ambient Temperature (°C)								
Ambient Pressure 101.32 kPa	**5**		**20**		**30**		**Units**	**Deviation (%)**
Parameter	**CM**	**GCM**	**CM**	**GCM**	**CM**	**GCM**		
Total Steam Turbine Output	215.56	206.68	199.83	198.29	189.41	192.34	MW	4.29
Pump auxiliary power	2759	2643	2652	2569	2587	2543	kWe	4.35
Stack Gas Temperature	104.1	105.10	107.06	107.01	109.50	109.29	°C	-0.91
Condenser Heat Duty	332.38	327.24	321.50	321.76	315.05	320.43	MWth	-1.68
Ambient Temperature (°C)								
Ambient Pressure 98 kPa	**5**		**20**		**30**		**Units**	**Deviation (%)**
Parameter	**CM**	**GCM**	**CM**	**GCM**	**CM**	**GCM**		
Total Steam Turbine Output	212.63	200.75	195.27	197.20	192.55	187.26	MW	5.92
Pump auxiliary power	2710	2490	2610	2419	2567	2396	kW_e	8.82
Stack Gas Temperature	103.00	104.48	105.95	106.44	108.35	108.72	°C	-1.42
Condenser Heat Duty	325.11	316.19	314.41	311.03	307.89	309.84	MW_{th}	2.82

MW_e). Due to this, very little or no effects in the final results is produced due to this deviation. For the steam turbines power output, the maximum deviation between the results of these two modeling approaches is ~6%.

3.6.3 Cooling Tower

For the cooling tower model validation, the major parameters that are compared are the cooling water inlet and outlet temperatures. These parameters are evaluated at relative humidity of 0.4, 0.6 and 0.8 while the ambient temperature is fixed to 20°C and 30°C respectively. The results for the cooling tower model validation are presented in Table 3-13.

The maximum deviation between the cooling water temperatures as predicted by two different models is below ±3%. This value is less than 5% which shows that the modeling approach adopted for the cooling tower design predicts the performance near accurately.

Table 3-13. Model validation results for cooling tower

Ambient Temperature 20°C	**Ambient Relative Humidity**							
	0.4		**0.6**		**0.8**			
Parameter	**CM**	**GCM**	**CM**	**GCM**	**CM**	**GCM**	**Units**	**Deviation %**
Water Inlet Temperature	27.88	27.85	29.95	29.79	31.9	31.64	°C	0.82
Water Outlet Temperature	17.02	17.41	19.07	19.32	20.99	21.14	°C	-2.24
Ambient Temperature 30°C	**Ambient Relative Humidity**							
	0.4		**0.6**		**0.8**			
Parameter	**CM**	**GCM**	**CM**	**GCM**	**CM**	**GCM**	**Units**	**Deviation %**
Water Inlet Temperature	33.33	33.04	36.4	36.01	39.19	38.75	°C	1.14
Water Outlet Temperature	22.7	22.81	25.73	25.72	28.49	28.4	°C	-0.48

CHAPTER 4. RESULTS AND DISCUSSIONS

In the previous chapter, a detailed modeling approach for calculating the techno-economic performance of the NGCC power plant was presented. In this chapter, a summary of the major results is separated into two different sections: performance based results and economic results. The major effects of ambient weather in the performance of the power plant is presented in the performance section. This section consists of two subsections: gas turbine and steam cycle results. Followed by that, the modeling results specific to two locations, and the results for the WHR cooling systems are presented. Lastly, the economic results for different WHR systems for two locations are presented and discussed.

4.1 Performance

4.1.1 Gas Turbine Cycle

The increasing ambient temperature has a serious impact on the power output and the efficiency of the gas turbine. The increasing ambient temperature reduces the density of the incoming air to the gas turbine compressor causing a reduction in the overall inlet air mass flow rate. As discussed in subsection 3.1.1 and shown in equation (3.1), there is also a decrease in the compressor pressure ratio and the operational speed. Table 4-1 shows the comparison of major gas turbine characteristics at ambient temperature of 15°C to 40°C ambient temperature. Figure 4-1

Table 4-1. Comparison of gas turbine characteristics at 15°C and 40°C ambient temperature.

Ambient Temperature (°C)	Net Output (MW_e)	Compressor Pressure Ratio	Natural Gas Flow (kg/s)	Gas Cycle Efficiency (LHV)	Exhaust Flow Rate (kg/s)	Exhaust Temperature (°C)
15°C	362.20	20.14	21.08	36.21%	897.40	628.6
20°C	359.62	19.93	20.49	35.95%	881.85	630.3
30°C	335.14	19.54	19.37	35.43%	852.32	633.6
40°C	303.73	19.16	18.33	34.91%	824.68	636.7

shows trends of some of these gas turbine parameters while changing the ambient temperature. The overall output and the efficiency decrease by nearly 16% and 4%, respectively, from the baseline operating conditions (15°C) if the ambient air temperature reaches 40°C. The corresponding decrease in the pressure ratio of the compressor is nearly 5%. At these higher temperatures, the compression work reduces due to the reduced mass flow rate and exit pressure. The corresponding decrease in the exhaust gas flow is nearly 8%. This reduction in the exhaust gas flow accounts for the mass flow reduction of the air and the natural gas required to achieve the constant turbine inlet temperature of 1371°C. Since the compressor polytropic efficiency and the turbine isentropic efficiency were held constant, a limited sensitivity analysis is performed by varying these efficiencies and noting the gas turbine performance. Figure 4-2 shows the effects of varying the compressor polytropic efficiency from 84% to 87% in an increment of 0.5%. Two representative operating ambient temperatures: 15°C and 35°C are taken to assess the effects of the changing compressor efficiency. With the increasing compressor efficiency, there is a decrease

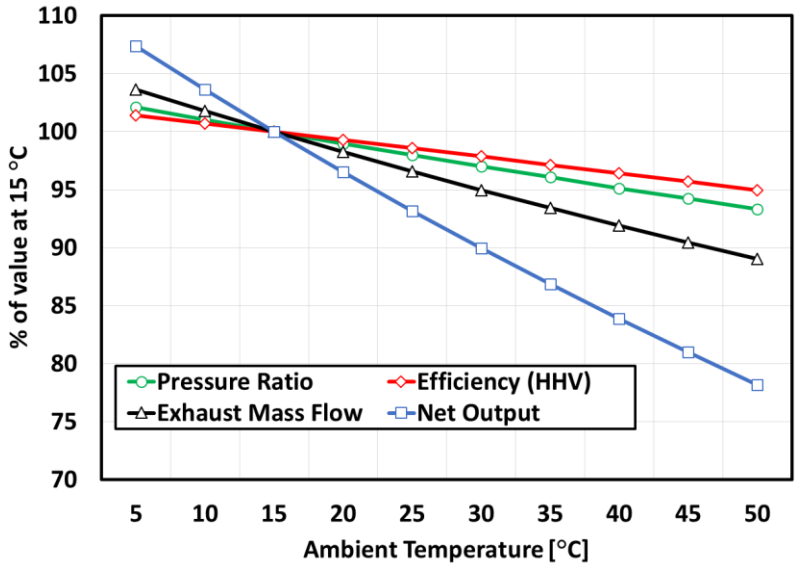

Figure 4-1. Gas turbine performance at varying ambient temperature.

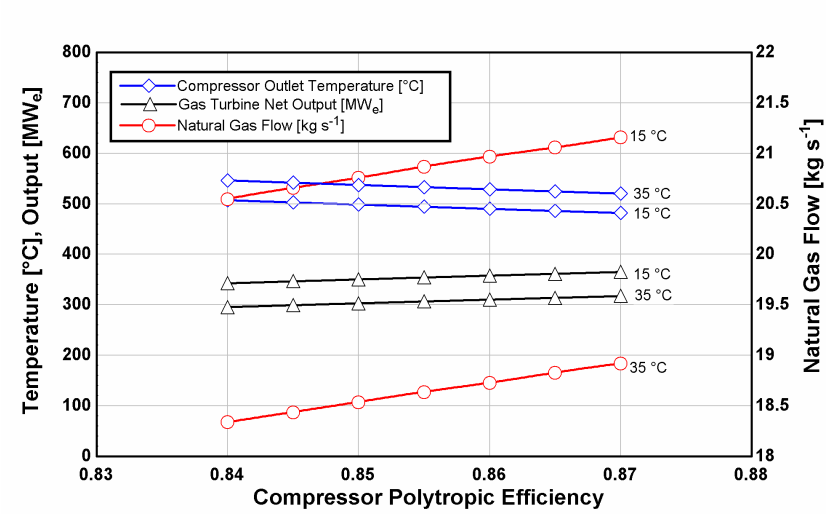

Figure 4-2. Sensitivity analysis on compressor polytropic efficiency.

in the compressor outlet temperature. For example, at 15°C ambient, the compressor outlet temperature is 507.4°C at a polytropic efficiency of 84%, and at 35°C the outlet temperature decreases to 482°C at compressor polytropic efficiency of 87%. This is obvious because with increased efficiency there is a reduction in frictional and other irreversible losses. These loses generally contribute to increasing the temperature, so increasing the efficiency decreases the compressor outlet temperature. The results of this temperature decrease are propagated in the corresponding mass flow rate of natural gas. To achieve a constant turbine inlet temperature, there is a concomitant increase in the natural gas flow rate. For example, at 15°C ambient, the natural gas flow rate is 20.55 kg/s at compressor polytropic efficiency of 84%. This increases to 21.16 kg s^{-1} at polytropic efficiency of 87%. Similarly, the net output from the gas turbine tends to increase slightly because with a better compressor efficiency, the work required for compression decreases resulting in an increased net output. For example, the net gas turbine output at 87% compressor polytropic efficiency is 365 MW_e whereas at 84% polytropic efficiency, the new gas turbine output is 342.7 MW_e. Based on the ambient temperature analysis, the natural gas flow rate is higher for lower ambient temperatures, because more air is drawn into the compressor requiring more natural

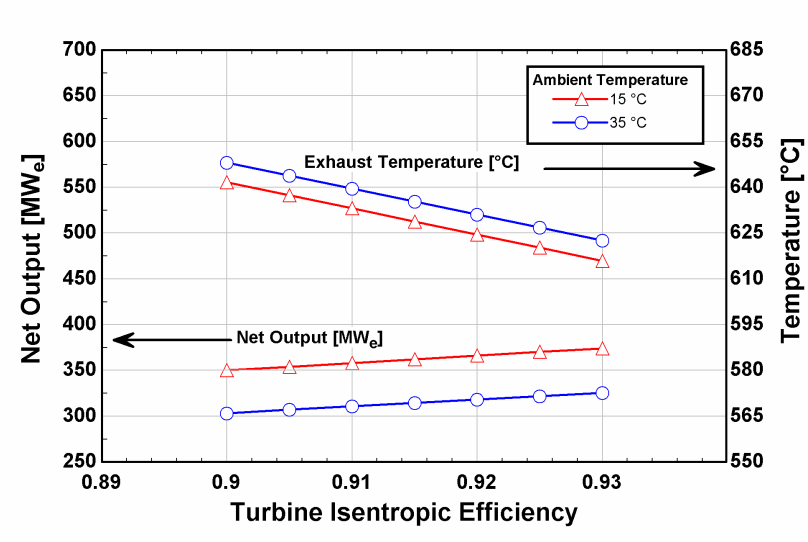

Figure 4-3. Sensitivity analysis on turbine isentropic efficiency.

gas. The same increasing trend is true with the gas turbine net output because higher outputs occur at low ambient temperatures compared to higher ambient temperatures.

Figure 4-3 shows the sensitivity analysis performed on the isentropic efficiency of the turbine. The efficiency was varied from 90% to 93% in an increment of 0.5%. It is noticed that with the increasing efficiency, the net output from the gas turbine increases and the exhaust temperature decreases. The output of the turbine increases due to the reduction in frictional and irreversible losses that naturally occur in the turbine blades. At high ambient temperatures though the net output is lower than output at lower ambient temperatures. For example, the net output at 90% turbine efficiency and 15°C ambient temperature is 350 MW_e. This output is 303.2 MW_e at 35°C ambient temperature. This output reduction is due to the decrease in mass flow rate of the combustion products at high ambient temperatures (i.e. from 897.4 kg/s at 15°C to 838.2 kg/s at 35°C). Similarly, the turbine exhaust temperature increases at high ambient temperatures (i.e. 641.7°C to 648.1°C when ambient temperature changes from 15°C to 35°C at a 90% turbine efficiency). With the reduced gas flow and decreased pressure ratio across the turbine, there is an increase in the exhaust gas temperature because the turbine inlet temperature is kept fixed. This is

because for an isentropic efficiency relation, if the turbine pressure ratio decreases at a fixed efficiency and inlet temperature, then the exhaust temperature has to increase. In the following section, the performance characteristics of the Rankine cycle is discussed.

4.1.2 Steam Cycle

This section discusses the detailed performance results for the Rankine cycle. As discussed in section 3.2, any changes in the gas turbine exhaust temperature and gas flow rate will have a direct impact on the temperatures and mass flows of steam in the bottoming Rankine cycle. In addition to this, as discussed in section 3.3, the cooling tower operational characteristics will also change at different ambient temperatures which will have a significant impact in the condenser pressure. Figure 4-4 shows the temperature profile across the HRSG heat exchangers at an ambient temperature of 40°C. Compared to Figure 3-5, which shows the temperature profile at a 15°C ambient temperature, there is a significant change in the HRSG operational temperatures. Table 4-

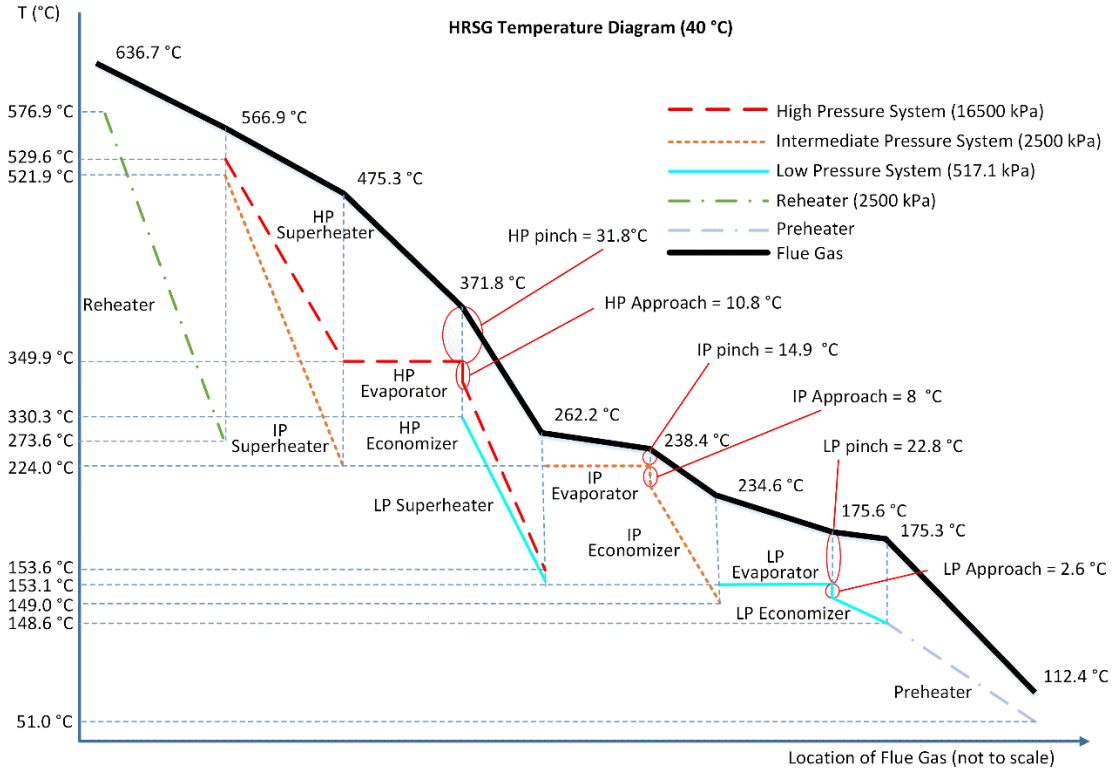

Figure 4-4. Temperature profile across HRSG at an ambient temperature of 40°C.

2 shows the inlet and outlet gas temperatures across each HRSG heat exchangers at ambient temperature of 15°C and 40°C.

Table 4-2. Inlet and outlet gas temperatures for HRSG heat exchangers at 15°C and 40°C ambient temperature.

Heat Exchanger	15 °C Ambient Temperature		40°C Ambient Temperature	
	Inlet Temperature (°C)	Outlet Temperature (°C)	Inlet Temperature (°C)	Outlet Temperature (°C)
Reheater	628.6	561.4	636.7	566.9
HP Superheater	561.4	473.3	566.9	475.3
IP Superheater	561.4	473.3	566.9	475.3
HP Evaporator	473.3	373.4	475.3	371.8
HP Economizer	373.4	264.9	371.8	262.2
LP Superheater	373.4	264.9	371.8	262.2
IP Evaporator	264.9	240.5	262.2	238.4
IP Economizer	240.5	235.9	238.4	234.6
LP Evaporator	235.9	177.5	234.6	175.6
LP Economizer	177.5	176.6	175.6	175.3
Preheater	176.6	106	175.3	112.4

Since the heat exchanger *UA*s are scaled at the off-design operating temperatures, the heat exchangers have different inlet and outlet temperatures depending on their changed effectiveness shown in Table 4-3. The inlet gas temperature for all heat exchangers changes slightly depending

Table 4-3. Heat exchanger effectiveness at 40°C and 15°C ambient temperature.

Component	40°C	15°C
Reheater	0.83	0.83
HP Superheater	0.83	0.82
IP Superheater	0.86	0.84
LP Superheater	0.81	0.80
HP Evaporator (1p,2p)	0.25,0.75	0.23,0.73
IP Evaporator (1p,2p)	0.35,0.60	0.37,0.59
LP Evaporator (1p,2p)	0.10,0.72	0.17,0.70
HP Economizer	0.85	0.85
IP Economizer	0.75	0.72
LP Economizer	0.07	0.06
Preheater	0.78	0.78

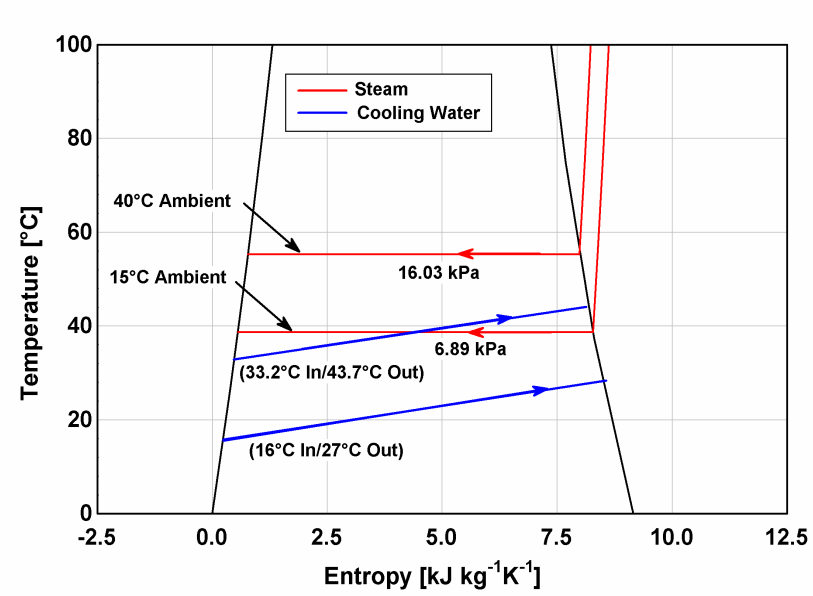

Figure 4-5. Temperature-entropy diagram for steam and condenser pressure variation.

on the scaled *UA*s compared to that at ISO operating conditions. As presented earlier, a representative case for ambient temperature of 40°C in shown in Figure 4-4. Figure 4-5 shows the condenser pressure based on the change in the ambient temperatures from 15°C to 40°C. As discussed in section 3.3, the cooling water temperature supplied by the cooling tower is highly dependent on the ambient air temperature and the relative humidity. At an ambient temperature of 15°C (baseline), the inlet and exit cooling water temperatures for the condenser are 16°C and 27°C, respectively. At an ambient temperature of 40°C, however, these temperatures change to 33.2°C and 43.7°C, respectively. This increase in temperature of cooling water is caused due to the inability of the cooling tower to reject the cooling load when the air temperature is high. Based on the assumption of maintaining a constant TTD, the condenser saturation pressure increases to 16.03 kPa compared to 6.89 kPa at the baseline case. Maintaining a constant TTD is important to prevent the condensing temperature and the cooling water temperature from crossing. The condenser pressure increase also increased the turbine back pressure, which causes a nearly 20% decrease in the LP steam turbine power output (105.14 MW to 84.4 MW). The preheater inlet

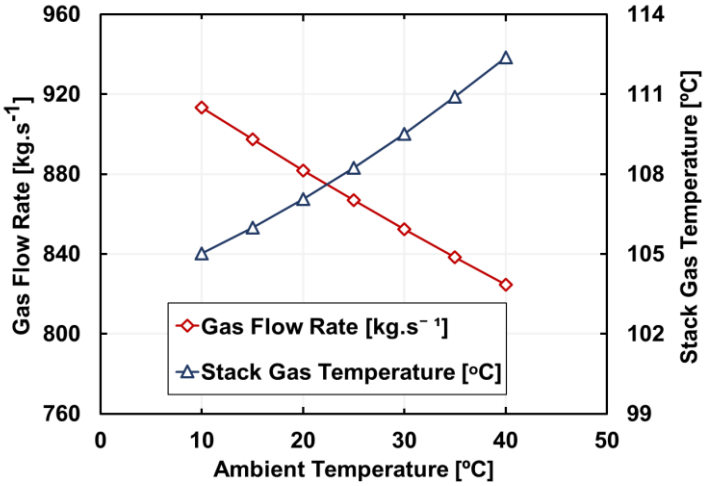

Figure 4-6. Flue gas flow rate and temperature variation with ambient temperature.

temperature (51.0°C) and the gas temperature at the stack (112.4°C) in Figure 4-4 reflect the change in the condenser pressure at different operating ambient temperatures.

Figure 4-6 shows how the flue gas flow rate and the gas temperature at the power plant stack change with increasing ambient temperature. There is an approximately 8.2% reduction in the flue gas mass flow rate (Table 4-1) at the ambient temperature of 40°C compared to at 15°C. The gas temperature that leaves the stack increases almost linearly, i.e., nearly 1°C for every 4°C

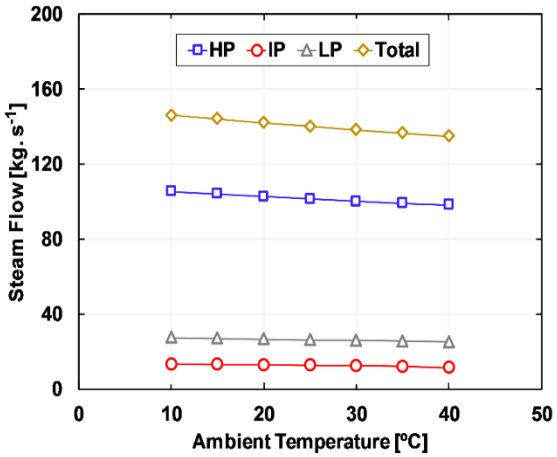

Figure 4-8. Steam flow rates through different pressure systems.

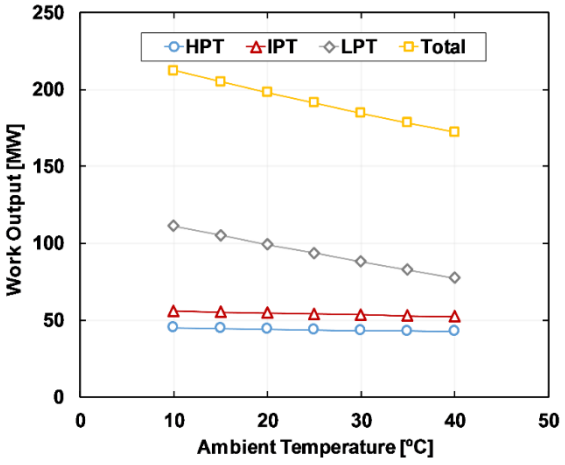

Figure 4-7. Steam turbine output at varying ambient temperatures.

rise in the ambient temperature. The temperature of gas leaving the preheater is important for a flue gas driven absorption cooling system because a higher temperature increases the performance (COP) of an absorption chiller. The dependence of the WHR system COPs with temperature however, are not considered in this study.

The changing temperatures also cause the steam mass flow rates and the respective steam turbine power outputs to change. Figure 4-8 and Figure 4-7 show the steam mass flow rates for the 3 different pressure systems and the power output from the three steam turbines, respectively. The steam turbine mass flow rates for the HP, IP, and LP system at baseline case are calculated as 104, 13, and 27 kg s^{-1} respectively. The steam flow that enters the HP turbine is entirely comprised of the HP flow but that is not the case for the IP and LP steam turbines. The steam flow that enters the IP turbine is the sum of the HP and IP steam flows. Similarly, the steam flow that goes into the LP turbine is the sum of HP, IP and LP steam flows. This is shown in the process flow diagram of the NGCC system in Figure 3-3. In Figure 4-8, it can be noticed that the mass flow of the respective HP, IP and LP systems is reduced with the increasing ambient temperature. At 40°C, these mass flow rates are 98.1, 11.4, and 24.9 kg s^{-1}, respectively. This corresponds to a decrease of 5.6%, 12.4%, and 7.8%, respectively. The total mass flow rate at this temperature is 134.40 kg s^{-1}, a total reduction of 6.6%. The decreased mass flow rates in the HP, IP, and LP systems (5.9, 1.6, 2.1 kg s^{-1} respectively) are due to the changing temperatures and available heat in the exhaust stream which has a direct impact on the heat exchanger *UA*s.

Figure 4-7 shows the power outputs from the HP, IP and LP steam turbines. At baseline operating conditions, these outputs are 44.6 MW, 55.2 MW, and 105.1 MW, respectively. At the 40ºC ambient temperature, these outputs are 42.5 MW, 52.2 MW, and 84.4 MW, respectively, which corresponds to a decrease of 4.7%, 5.4% and 19.7%. The major portion of the output

reduction for the HP and IP steam turbines is due to the reduction in the mass flow rates of the steam. However, for the LP steam turbine, the major reduction is due to the increase in the turbine back pressure rather than the reduction in the total steam mass flow rate. The total output of the LP steam turbine without the change in condenser pressure would be 99.5 MW. This is equivalent to a reduction of 5.3%. The additional loss of nearly 15 MW (14.4%) is solely due to the increased condenser pressure. For each steam turbine, the power output decreases linearly with ambient temperature.

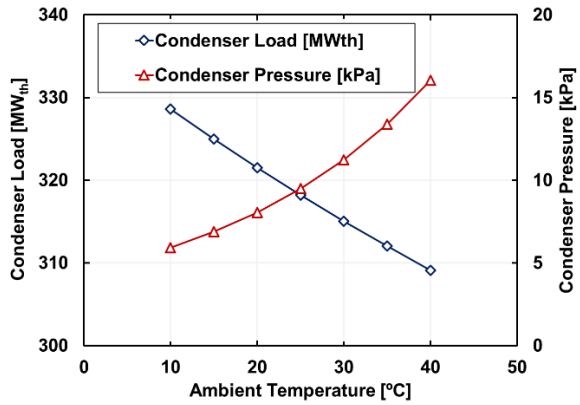

Figure 4-9. Condenser load and pressure variation with ambient

Figure 4-9 shows the variation of the condenser pressure and condenser cooling load at different ambient temperatures. The condenser cooling load decreases as the ambient temperature increases. At 40°C, the condenser load decreases to 309.9 MW_{th} compared to 324.9 MW_{th} at 15°C. One of the major reasons for this trend is the overall steam mass flow decrease (Figure 4-8). This reduction in the steam mass flow is induced by the change in the amount of heat added into the Rankine cycle, thereby reducing the condenser load. For example, at 15°C ambient temperature, the heat added in the Rankine cycle is 527.3 MW_{th}. At 40°C, the heat added to the HRSG is 485.7 MW_{th}. Another reason is that the condensing pressure increases with the condensing temperature. On a temperature-entropy (T-s) diagram of steam, at higher pressures the heat rejected in the two-

phase region is smaller than at lower pressures. The corresponding dry fraction (steam quality) due to this increase in condenser pressure is 0.963 (0.929 at baseline operating case). Hence, both of these factors play significant role in determining the condenser load.

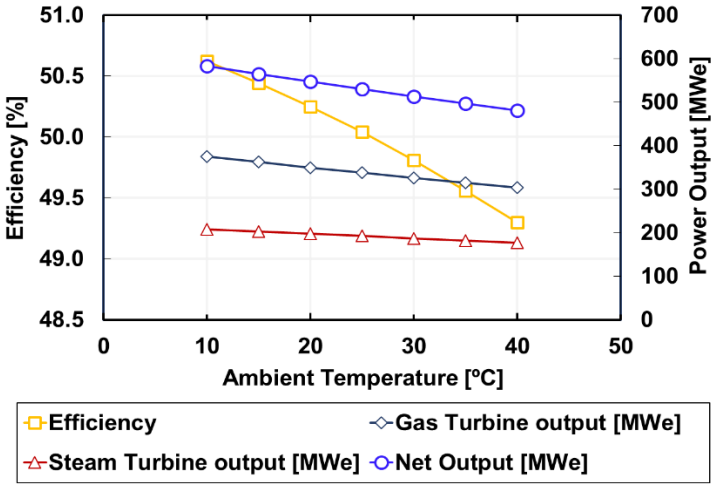

Figure 4-10. Efficiency and power output for NGCC power plant.

Figure 4-10 shows the overall efficiency and the output for the gas turbine and the steam turbine. The net output of the power plant decreases by almost 15% at the 40°C ambient temperature. The gas turbine has a larger reduction (16.1%) compared to the steam turbine (12.6%). The overall plant efficiency reduces from 50.4% to 49.3%. In the following section, the location based performance is presented for the two locations chosen in this study: Los Angeles, CA and Houston, TX.

4.1.3 WHR System Performance

By using the modeling approach discussed earlier, the yearly power generation for the two locations (Los Angeles, CA and Houston, TX) is predicted. To complete this analysis, the yearly temperature, pressure, and relative humidity data was taken from TMY3 weather data. Figure 4-11

shows the average monthly temperature and average power plant power output for the two locations at the baseline operation without any gas turbine inlet chilling.

The highest average temperature for Los Angeles is 20°C during August, while the highest average temperature for Houston is 28°C in July. For both locations, the average yearly relative humidity is 0.73. The averaged power output for these locations during these hottest months (i.e. July, August and September) are 534.3 MW_e and 509 MW_e, respectively, at a 100% capacity factor. The elevated average temperature during these months causes a 3.73% and 8.29% power

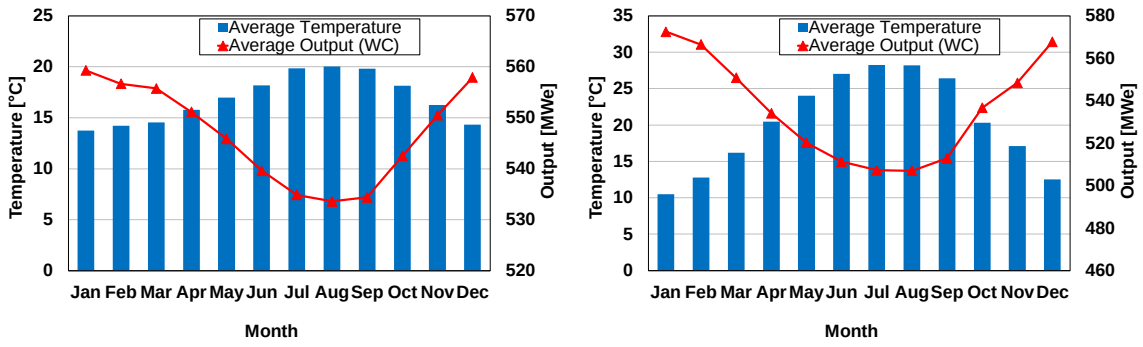

(a) (b)

Figure 4-11. Average temperature and power output a) Los Angeles b) Houston.

output decrease compared to the baseline power output (555 MW_e at 15°C). During the winter, the average temperature for Los Angeles and Houston for the month of January are 13.7°C and 10.5°C, respectively. The average power output for these two locations increases to 559.3 MW_e and 572.5 MW_e, respectively. Over the entire year, the average NGCC output for these two locations are 546.79 MW_e and 536.18 MW_e, respectively, which is a 1.48% and 3.39% decrease in power output from the baseline. Los Angeles represents a milder climate, with the ambient temperature ranging between 10°C and 20°C for ~60% of the year and an average relative humidity of 73%. In contrast, Houston has a more extreme climate, with temperatures reaching as high as 40°C during the summer, and as low as -7°C during the winter with the average relative humidity of 73%. Therefore, gas turbine inlet air chilling to increase the power output of the plant is more promising

for locations with similar temperature profiles as Houston during the summer months, than for milder climates like Los Angeles. In the following sections, the economic results of applying the gas turbine inlet chilling for four different possible scenarios are presented: flue gas, steam, gas turbine exhaust gas, and vapor compression system.

4.2 Economic Results

In this section, the economic results for the two locations are presented. The LCOE of the two power plants at Los Angeles and Houston, by accounting for the yearly weather data, without gas turbine inlet chilling are calculated as $62.50 and $63.05 per MWh, respectively. Without accounting for weather effects (i.e., 15°C the entire year), the LCOE for a 555 MW_e power plant with the baseline overall efficiency of 50.1% would be $62.05 per MWh. The difference between the baseline LCOE and the LCOE's of these two locations with weather effects is $0.45 and $1.0 per MWh, respectively. Similarly, besides the weather affects, LCOE is also function of major plant inputs that includes different plant costs and performance factors. Figure 4-12 shows the dependence of LCOE on multiple factors. These cost factors are changed within ±10% of the

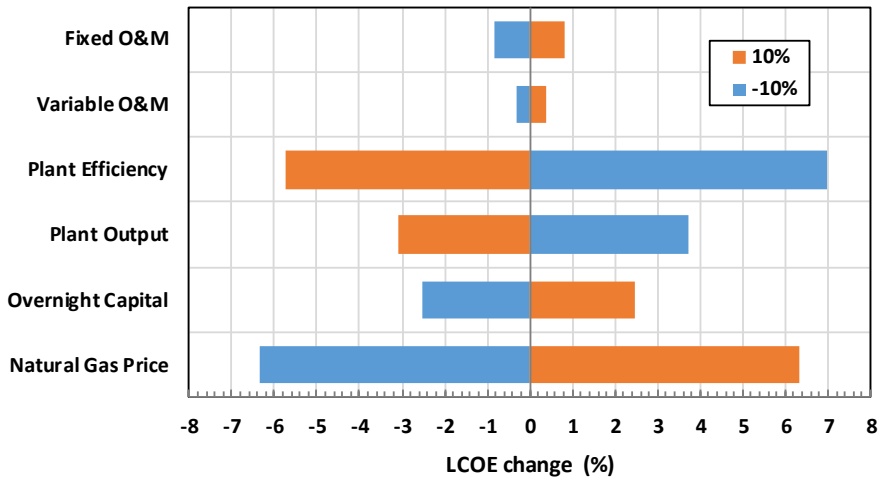

Figure 4-12. LCOE sensitivity analysis

values at baseline case and the change in the LCOE of the plant is plotted in x-axis. From Figure 4-12, it can be inferred that the plants LCOE is highly dependent on natural gas price, plant output and efficiency. At 10% increase in natural gas price, the LCOE of the plant increases by nearly 6.5%. A higher plant efficiency combined with a lower natural gas price is desirable to yield lower LCOE. The uncertainties in the operation and maintenance costs (both variable and fixed) have lesser impact compared to natural gas costs and efficiency. To account for the uncertainties, most financial analysis are performed by taking a fixed annual percentage increase in these costs. In this study, the natural gas price and the operation and maintenance costs are escalated by 3% annually.

The total power generation per year for these two locations are calculated as 4790 GWh and 4357 GWh, respectively. This power generation is calculated for 8760 hours of yearly operation (i.e., a 100% capacity factor). The LCOE values for a different capacity factor will be less compared to the one at 100% CF. By installing a gas turbine inlet air chiller powered by the waste heat, significant changes in the power output and the LCOE can be noticed. Figure 4-13 shows the power output for the NGCC plant with a WHR cooling system used for gas turbine inlet

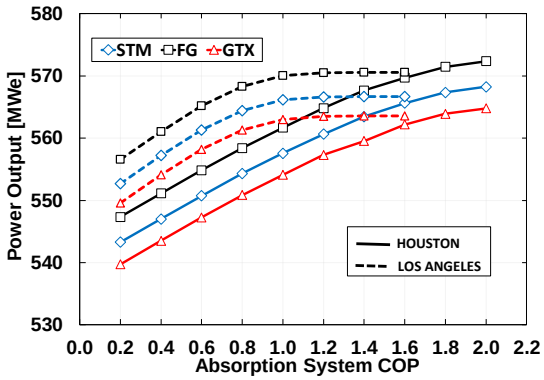

Figure 4-13. Average output vs. COP of the absorption system for Houston and Los Angeles. The absorption system heat source options are compared: turbine exhaust (GTX), steam (STM), and flue gas (FG).

chilling. From Figure 4-13, it can be noticed that the output for the location of Los Angeles is higher compared to the location of Houston for all the WHR scenarios. This is because, for Los Angeles, the hourly ambient air temperature is low compared to that of Houston as seen in Figure 4-11. For Houston, however, installing an absorption chiller with a high COP has a significant impact. For example, increasing the COP from 0.2 to 2.0 increases the power output by 25.1, 25.0, and 26.0 MW_e for gas turbine exhaust (GTX), steam (STM), and flue gas (FG), respectively. These increases result in an additional electricity generation of 219.5, 218.8, and 227.9 GWh per year, respectively. Compared to Los Angeles, this increase is significant because no further gain beyond a COP of 1.6 is achieved. Additionally, the WHR system powered by the flue gas generates the highest power output. This is because GTX or STM systems have negative impacts on the power generated by the bottoming Rankine cycle. For example, the average Rankine cycle output for a WHR cooling system with COP of 1.0 in Houston are 192.4 MW_e, 196.0 MW_e, and 200.1 MW_e for GTX, STM, and FG systems, respectively. Clearly for the GTX and the STM system, the net Rankine cycle output is less compared to the FG system because useful heat is extracted to run these systems compared to the flue gases heat that is normally wasted.

For all these WHR systems, the power output for Los Angeles increases until the COP reaches 1.2, after which the output increases minimally. The primary reason for this trend is that the maximum cooling load is met with a COP of 1.6 for the moderate climate conditions in Los Angeles. When limiting the gas turbine inlet temperature to 7°C, the maximum cooling load at any particular hour in Los Angeles is 34.06 MW_{th}. For a WHR cooling system driven by flue gas, with a COP of 1.6, the maximum extracted waste heat (limited by a 80°C exhaust temperature), generates 36.23 MW_{th} of cooling, which exceeds the maximum cooling needs for Los Angeles. A flue gas driven absorption chiller with a COP of 1.2 generates 27.18 MW_{th} of cooling, which meets

the cooling requirement for 96.7% of the total cooling hours for Los Angeles. Therefore, installing a WHR system with a COP greater than 1.2 generates minimal gas turbine inlet chilling and has minimal impact on average yearly power output. For Houston, a similar trend begins at a COP of 2.0 where the slope of the power output curve starts decreasing.

Figure 4-14 shows the relationship between the cooling system cost, COP, and LCOE for the three waste heat recovery options and the electrically driven vapor compression chiller (VC). In these figures, the costs for each WHR and VC unit is expressed in terms of $ per kW_{th} of cooling to estimate the LCOE. It must be noted that the $ per kW_{th} only represents the costs of the cooling unit and does not include the installation costs that includes piping and other flow movement

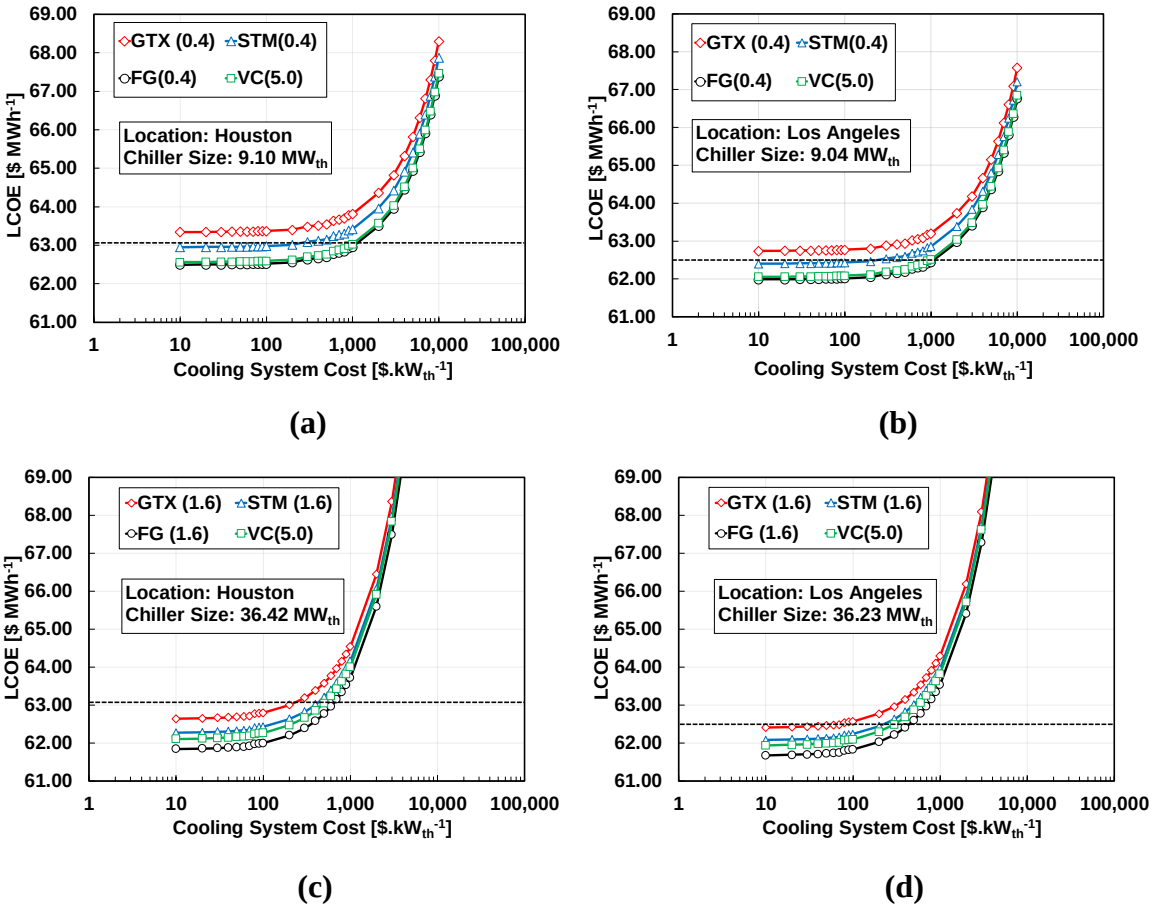

Figure 4-14. LCOE variation with cooling system costs for Houston and Los Angeles at chiller sized of approximately 9 MW and 36 MW.

devices. However, the LCOE accounts for the installation costs as 25% percent of the cooling unit cost. For comparison, the LCOE of the power plants in Los Angeles and Houston without gas turbine inlet chilling are shown in a dotted line in each graph of Figure 4-14. These values for Los Angeles and Houston are $62.50 and $63.05 per MWh, respectively.

At a WHR system cooling load of 9.10 MW_{th} (COP = 0.4) for Houston (Figure 4-14 a), the vapor compression chiller has a lower LCOE than an absorption chiller powered with turbine exhaust gases or steam if the cost for all these systems is nominally the same $ per kW_{th} of cooling provided. For example, at $100 per kW_{th}, the LCOE of the GTX system and STM system LCOE are $63.37 and $62.97 per MWh respectively. This value for VC system is $62.59 per MWh. Los Angeles has a similar trend (Figure 4-14 b), except that the LCOEs are slightly lower than in Houston because the average yearly output is higher in Los Angeles (543.5 MW_e and 554.1 MW_e for GTX system respectively).

At larger cooling system loads (Figure 4-14 c and d), similar patterns emerge for the LCOE, with the GTX system yielding the highest LCOE at a given cooling system cost. In addition, at both cooling loads, an absorption system powered by flue gas yields the lowest LCOE at a fixed cooling system cost, and even outperforms vapor-compression at the higher cooling load conditions. For example, in Houston, at a system cooling cost of $200 per kW_{th}, the FG and VC systems yield LCOEs of $62.55 per MWh and $62.62 per MWh, respectively, at a maximum cooling load of 9.1 MW_{th}. At a cooling load of 36.4 MW_{th}, however, the LCOEs are $62.20 and $62.47 per MWh, respectively. Moreover, the difference between the LCOEs of the steam-powered chiller and the electrically driven vapor compression chiller also decreases as the cooling increases. For example, in Los Angeles, at a system cooling cost of $200 per kW_{th}, the STM and VC systems yield LCOEs of $62.46 and $62.11 per MWh, respectively, at a maximum cooling of

9.04 MW_{th}. At the higher cooling duty of 36.23 MW_{th}, the LCOEs are $62.44 and $62.30 per MWh, respectively.

Clearly, the cost effectiveness of each system is controlled by the size of the cooling provided and the cost of the system in $ per kW_{th}. Furthermore, the decision to select a particular gas turbine chilling system is dependent on the system cost which might be different for different WHR systems. For example, in Houston at a cooling load of 9.10 MW_{th}, the LCOE of a STM system at a cost of $1000 per kW_{th} ($63.42 per MWh) is less than the LCOE of a FG system with a cooling cost of $2000 per kW_{th} ($63.49 per MWh). A similar result can be seen for STM and VC systems at these costs as well. Therefore, to understand which system yields a lower LCOE, a better understanding of the costs of each system is required.

One possible method for understanding the impact of system cost is to determine the "tolerable cost" of implementing a particular system, which is the cooling system cost that yields an LCOE that is less than or equal to the baseline LCOE. Cooling system costs less than the tolerable cost yield a lower LCOE than the baseline, and, as a result, are more likely to be implemented. Figure 4-15 (a and b) shows the tolerable cost for the different cooling systems as

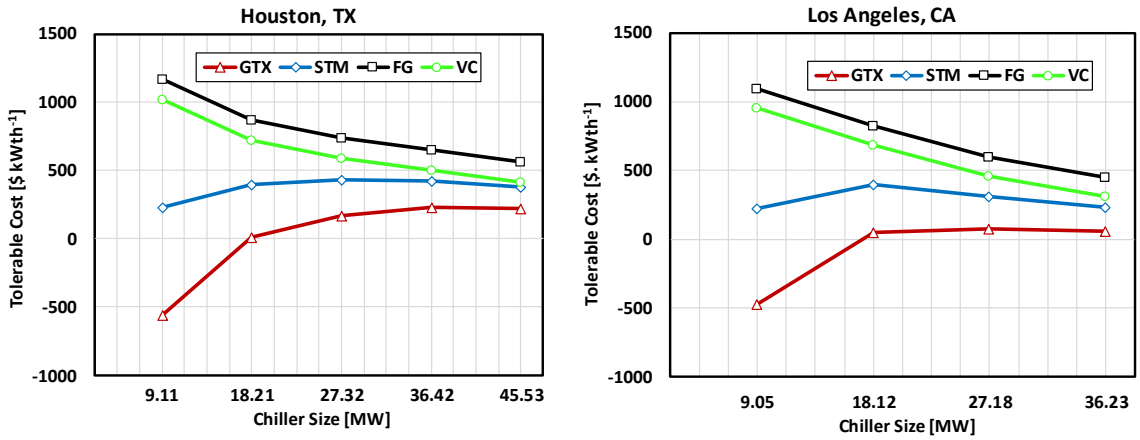

(a) **(b)**

Figure 4-15. Tolerable costs for the cooling systems a) Houston-TX b) Los Angeles-CA

a function of cooling provided for Houston and Los Angeles. These figures show that the tolerable costs for the FG system is highest at all cooling sizes, followed by VC, STM, and GTX systems, respectively. At lower cooling sizes, this limiting cost for the GTX system is negative until the size is nearly 18 MW_{th} and 16.3 MW_{th} for Houston and Los Angeles, respectively. The negative tolerable costs mean that installing a GTX system with a low COP and cooling size below 18.21 MW (Houston) would have negative impacts on the LCOE. Instead of generating a lower LCOE than the baseline case, at these cooling sizes, the GTX system yields higher LCOEs. However, as the size increases the tolerable costs for the GTX and the STM system increases to a maximum of \$245.3 and \$431.6 per kW_{th} with corresponding sizes of 42.85 MW_{th} and 30.15 MW_{th}, respectively. After this maximum, the tolerable costs decrease with the increase in size. A similar pattern is seen for Los Angeles with the GTX and STM systems having maximum values of \$92.8 and \$394 per kW_{th} for cooling sizes 23.12 MW_{th} and 18.18 MW_{th}, respectively. As the size increases beyond these points, the maximum tolerable costs decrease. The main reason for this trend for the STM and GTX systems is that, for both cities, the maximum cooling size sets the operation limits for the systems to cool the gas turbine inlet air to 7°C. By increasing the chiller size beyond these maximum values, a further decrease in overall LCOE cannot be achieved due to increased capital costs associated with installing a larger cooling system. For the FG and VC systems, a different trend is observed. The tolerable cost continues to decrease with the increasing sizes for the FG system for both locations. This decreasing trend for the FG and VC system is because these systems do not affect the net output from the NGCC power plant. The reason the tolerable costs for the VC system is less than the FG system is that the VC system requires electrical power from the power plant.

For VC and FG systems, by installing systems with small chiller sizes, a high allowance in the maximum tolerable costs can be achieved. A low WHR system cost has minimal impact on the overall capital of the power plant (which drives the LCOE), which explains the high tolerable cost at low chiller sizes. Similarly, at high WHR cooling system sizes, the power augmentation would need to increase to maintain a steady tolerable cost, which, for both cities, is not achieved.

So far, the modeling has considered one COP, but there is a range of possible COPs and chiller system costs that yield a lower LCOE than the baseline case. Furthermore, if the power plant owner plans to make an investment on an inlet air chilling unit, but only has a particular amount of capital available, it is possible to use the results from this study to determine the best choice based on the available equipment COP and cost per kW_{th}. Furthermore, this result will provide a basis to compare systems that have various COPs and cost tradeoffs. A combination of systems can be selected based on costs, COP, and size. Thus, a system that costs higher $ per kW of cooling, but with a small size can result in the same investment as a system that costs lower $ per kW of cooling but a larger size. For example, a chiller that costs 1M$ could have a cooling capacity of 20 MW and a cost of $500 per kW_{th} or the system could have a capacity of 10 MW, resulting in a cost of $1000 per kW_{th}.

Figure 4-16 shows the LCOE for waste heat and mechanically driven chiller systems for a fixed investment of $10M in Houston and Los Angeles. The blue plane region represents the breakeven point compared to the baseline case. Clearly, for Houston all four systems breakeven at points where they would generate an LCOE less than at the baseline case. For example, in Houston, a FG system generates a LCOE less than the baseline case if the COP of the system is greater than 0.36 and if the unit cost less than $1217 per kW_{th} of cooling. The breakeven costs for the VC system is $939.9 per kW_{th} of cooling. The breakeven LCOE for the STM system is only possible

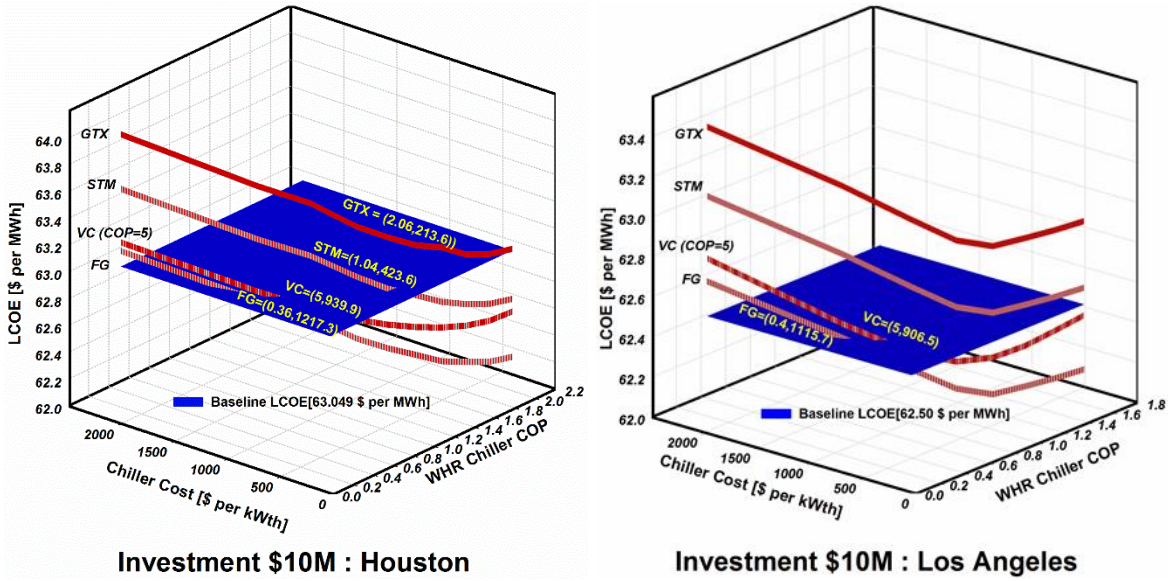

Figure 4-16. Investment based results.

at a COP of 1.04 and the system must cost less ($423.6 per kW_{th}) compared to the VC and the FG system. The corresponding value for the GTX system is a COP of 2.06 and cost of $213.6 per kW_{th}. This result for the GTX system is obtained by extrapolating beyond the studied COP range (0 to 2.0). The COP and cost targets are stringent for the GTX system compared to all other systems and are less likely be implemented.

Figure 4-16 (b) shows the results for Los Angeles. The corresponding COP and $ per kW_{th} values for location of Los Angeles are more stringent compared to the location of Houston for the same investment because the baseline LCOE for Los Angeles is smaller compared to that of Houston. The GTX and STM systems would not be feasible within the studied range of COP and cost targets for an investment of $10M. Also, for all the cooling systems, the LCOE ceases to decrease further beyond a COP of 1.2. The reason for the lack of increase, as mentioned earlier, is that for milder climate conditions in Los Angeles, a cooling system with a COP of 1.2 generates enough cooling to meet 97% of the total cooling hours. Between the FG and the VC systems, the FG system requires a COP of 0.4 and a maximum cost of $1115.7 per kW_{th} to breakeven. The costs

target for a VC system is \$906.5 per $kW_{th.}$ The FG system dominates all other systems in terms of costs and COP requirements; however, it should be noted that a high COP cannot be achieved with low temperature flue gas.

Table 4-4. COP and costs tradeoff targets for different cooling systems and different investments: Houston and Los Angeles.

Investment ($M)	**Houston**						
	GTX		**STM**		**FG**		**VC**
	Min. COP	**Max. Cost ($/kW$_{th}$)**	**Min. COP**	**Max. Cost ($/kW$_{th}$)**	**Min. COP**	**Max. Cost ($/ kW$_{th}$)**	**Max. Cost ($/kW$_{th}$)**
1	0.88	49.9	0.29	153.1	-	-	-
2	0.93	94.4	0.38	232.4	-	-	-
5	1.23	178.4	0.61	359.9	0.03	7322.0	2755.7
10	2.06	213.6	1.04	423.6	0.36	1217.3	939.9
20	3.29	266.6	2.79	314.6	1.16	752.9	381.0
	Los Angeles						
	GTX		**STM**		**FG**		**VC**
1	0.82	53.8	0.32	138.7	-	-	-
2	0.95	93.6	0.38	232.1	-	-	-
5	-	-	0.59	377.5	0.02	14824.5	1021.0
10	-	-	-	-	0.4	1115.7	906.5
20	-	-	-	-	-	-	-

The investment study was extended to different investments of \$1M, \$2M, \$5M, \$10M and \$20M depending on the size of the chiller and \$ per kW_{th}. The results for the different investments are presented in Table 4-4. Some of the COP values did not fall in the range of the values COPs in this study (0-2.0), so a third and fourth order polynomial curve fitting process was used. The missing results in Table 4-4 occur because, at these investments, the minimum COP and maximum tolerable costs could not be solved by using extrapolation methods. It can be noted from Table 4-4 that as the investment increases, the WHR system COP requirements also increase. The COP increase is caused by the increased investments required for the cooling systems, which increases the overall capital cost of the plant. To overcome the capital cost increase and be able to generate a lower LCOE than at the baseline case, a significant increase in the power output must

be created (revenue generated). The possible way to overcome this limitation is to install a cooling system with a higher cooling capacity (higher COP for WHR system). As such, for all the WHR systems, the FG system is feasible for a large number of COP combinations and costs because the FG system does not affect the power plant power compared to other WHR scenarios.

When compared on the basis of tolerable costs, the tolerable costs of the GTX and STM systems ($ per kW_{th}) increase at high investments. Higher investment for both these WHR system is equivalent to having higher cooling and eventually a requirement to have higher COP systems. It is desirable that by extracting the same heat, a higher amount of cooling is provided (thus augmenting more power) instead of losing power output by installing low COP systems. This impact is propagated into the tolerable costs of the systems. For the FG and VC system, the trend is opposite because the FG or the VC system does not negatively impact on the integral performance of the Rankine cycle of the power plant which eventually have costs benefits at lower investments. As the investments increase (larger cooling provided), the corresponding *LCOE* also increases due to higher invested capital resulting in a decreased tolerable costs. From the results in Table 4-4, it can be concluded that for all the WHR systems, the FG system is feasible for many combinations of COP and investment costs. However, it is not always feasible to install a FG system, because, the process of extracting heat from the low temperature flue gas is difficult and requires a large heat exchanger surface area that could increase the capital cost of the cooling system. Also, at these low waste heat temperatures, the only feasible system is a single effect absorption system which has a typical COP range of 0.7 – 0.9. For the STM system, extracting a portion of low pressure steam before it enters the final stage of steam turbine negatively impacts performance, but, the option is better than extraction of gas turbine exhaust gases. At the heat temperatures required for STM and GTX (~330°C for STM and ~630°C for GTX), a double effect

or triple effect absorption chiller can be operated to achieve maximum COPs of 1.2 to 1.8. Future investigations will focus on a more detailed analysis of the costs and COP dependence on waste heat temperature.

The other major objective of the current study is to determine whether the WHR cooling systems are competitive with existing commercial vapor compression systems. One effective way to compare the WHR systems with vapor compression systems is to determine the minimum COP and maximum cost per kW_{th} that yields an equivalent LCOE with a VC system that costs a fixed \$ per kW_{th} of cooling. This method allows the WHR technologies to be compared on a common

Table 4-5. COP and costs targets for WHR systems compared to Vapor Compression system costing \$500 per kW_{th}: Houston and Los Angeles.

Investment ($M)	**Houston**					
	GTX		**STM**		**FG**	
	Min. COP	**Max. Cost ($/kWth)**	**Min. COP**	**Max. Cost ($/kWth)**	**Min. COP**	**Max. Cost ($/kWth)**
2	1.38	63.7	0.73	120.2	0.19	455.5
5	1.97	111.3	1.0	218.4	0.34	630.5
10	3.46	126.9	1.4	313.1	0.65	668.7
	Los Angeles					
	GTX		**STM**		**FG**	
2	-	-	0.55	161.5	0.16	546.7
5	-	-	-	-	0.32	684.8
10	-	-	-	-	0.56	747.4

basis to determine the techno-economic targets that is required to be competitive on the market. For example, the cost of a VC system is assumed to be \$500 per kW_{th}, which is consistent with the cost of a commercially available system (\$ 426.4 for an 1.27 MW system) [68]. This value is chosen as a representative case and actual costs might differ with manufacturers. At an assumed COP of 5, and for a chiller size of 20 MW_{th}, the LCOE for the VC system is lower than the baseline case for both Houston and Los Angeles (i.e., \$62.84 and \$62.36 per MWh, respectively).

The minimum COP and maximum cost requirements for the WHR systems to generate an equal LCOE to the VC system are shown in Table 4-5 at varying investment levels. For example, with a $2M investment at a cost of $500 per kW_{th}, the VC chiller size is 4 MW. If a WHR system was used, however, with the same $2M investment in Houston, a COP of 1.38 (equivalent cooling of 31.4 MW_{th} by extracting 22.76 MW_{th} turbine exhaust heat) would be required, but at a maximum costs of $63.7 per kW_{th} would be allowed to yield the same COP. As shown in Table 4-5, the minimum COP requirement for the FG system is lower than the STM, which is in turn lower than the GTX system. In addition, the FG can tolerate a significantly higher cost than the other two systems. For example, in Houston, at a fixed investment cost of $5M, the minimum COPs required for the FG, STM, and GTX systems are 0.34, 1.0, and 1.97, respectively, while their maximum allowable costs are $630.5, $218.4, and $111.3 per kW_{th}, respectively. If any of these systems can meet these targets at the same investment, then it would be more economical to install them than a VC system. As discussed earlier, for the case of $5M investment, either a GTX chiller with COP of 1.97 (equivalent cooling of 44.84 MW_{th}), STM chiller with COP of 1 (equivalent cooling of 22.76 MW_{th}) or a FG chiller with COP of 0.34 (equivalent cooling of 7.74 MW_{th}) is required to compete with a VC chiller (10 MW_{th} of cooling). Furthermore at this case, the maximum tolerable costs for GTX, STM and FG systems are $111.3, $218.4 and $630.5 per kW_{th} respectively. It is anticipated that the STM and GTX are unlikely to meet these targets compared to a VC system cost ($500 per kW_{th}), because the VC system operates at lower temperatures than GTX systems, likely reducing the material costs for the VC system or the STM system. The FG system likely has the best chance to compete with the VC system, because the FG system has relatively low COP and high maximum costs. The reason the STM and GTX systems are less competitive is because the output of the NGCC power plant decreases when these are implemented.

Similar results are seen for Los Angeles, but there are lower COPs and higher cost thresholds for the WHR cooling systems. For example, while comparing Houston and Los Angeles at a fixed investment of $2M, the minimum COPs for the FG system are 0.19 and 0.16, and the maximum cost is $455.5 and $546.7 per kW_{th}, respectively. The reason the COP targets are lower for Los Angeles is that the number of cooling hours is less because the ambient temperature is not as high compared to Houston. Because of this a comparatively smaller chiller size can be used to generate similar gas turbine inlet temperatures for most of the year. As presented in Table 4-5, to achieve the targets, the WHR systems should have a higher COP in Houston compared to Los Angeles. Furthermore, for the STM and GTX systems in Los Angeles, the cost and COP tradeoff targets were not achieved except for the STM system at a low investments ($2M). The reason is that a GTX or STM system cannot generate an LCOE value less than a VC system at the same investment. For the $2M investment, the GTX system at a COP of 1.6 has a LCOE of $62.46 per MWh while a VC system has a LCOE of $61.99 per MWh. If the costs for the GTX system were reduced to as low as $10 per kW_{th}, the corresponding LCOE for GTX would be $62.41 per MWh, still higher than the VC system. In all of the operating cases tested, the LCOE values for the GTX system were higher than the VC system. For the STM system, the VC system LCOE is achievable at COP and cost targets of 0.55 and $161.5 per kW_{th}, respectively.

For the investment of $5M, the LCOE for the GTX and STM system with a COP of 1.6 are $62.64 and $62.31 per MWh, respectively, which are higher than the VC system ($62.26 per MWh). Hence, for both systems, the LCOE compared to the VC system is not achievable for the same investment. However, if lower investments (lower costs $ per kW_{th}) are considered for both the GTX and STM system, there is a possibility these systems can produce a competitive LCOE. As such, both GTX and STM systems were analyzed for lower investments. For a GTX system

costing as low as \$10 per kW_{th}, the corresponding LCOE is \$62.40 per MWh, still higher than the VC system LCOE. With this result, it can be concluded that the GTX system is not a feasible approach, as VC systems will likely result in a lower LCOE. The STM system, however, can achieve the LCOE at lower investment and at multiple COP values. For example, if a lower investment of \$2M is considered, anything with COP higher than 0.69 and costs less than maximum cost of \$127.7 per kW_{th}, produces an LCOE less than the VC system at \$5M investment. However, it should be noted that the investments for the VC and STM systems are different in this case and cannot be compared on a common investment basis.

Similarly, at the highest investment of \$10M, the GTX and STM systems cannot achieve the LCOE corresponding to a VC system. Even, with a COP of 1.6, the LCOE for GTX and STM systems are \$62.91 and \$62.58 per MWh, respectively, while the value for the VC system is \$62.36 per MWh. Clearly this LCOE is not achievable for either GTX or STM systems at \$10M investment. However, if the investment is reduced to \$5M or \$2M for the STM system, the LCOE targets are achievable with a minimum COP of 0.92 and maximum cost of \$239.9 per kW_{th} and with a minimum COP of 0.56 and maximum costs of \$157.6 per kW_{th}. For the GTX system, neither of the reduced investments yield comparable LCOEs.

From the discussion in the previous paragraphs, it can be concluded that for the same investments (except \$2M for STM), the COP requirements for the GTX and STM systems do not provide a breakeven LCOE compared with a VC system at a VC system cost of \$500 per kW_{th}. By merely increasing the COP of the WHR systems, there is no further gain in power output so the LCOE does not continue to decrease. However, if low investments are considered, the STM system generated comparable breakeven LCOE with that of a VC system. In all cases, the comparable STM system cost tradeoffs were much less compared to the \$500 per kW_{th} cost of a VC system.

Hence, for Los Angeles, the GTX or the STM system are not feasible and probably not preferred compared to a VC system.

An FG system for location Los Angeles produces breakeven results at each investments of \$2M, \$5M and \$10M. The minimum COP for these investments are 0.16, 0.32, and 0.56, respectively. These COPs are equivalent to cooling 3.62 MW_{th}, 7.24 MW_{th}, 12.68 MW_{th}, respectively compared to a VC cooling of 4 MW_{th}, 10 MW_{th}, and 20 MW_{th}, respectively. The maximum cost targets for these FG systems at these investments are \$546.7, \$684.8 and \$747.4 per kW_{th}, respectively, which are higher than \$500 per kW_{th} of VC system. Clearly, the FG system has a higher tolerance and costs benefits at higher investment (and larger cooling duty). This is because a VC system extracts more electric power to achieve more cooling, while a FG system always extracts the normal waste heat. The major limitation for an FG system is that higher COPs can be difficult to achieve at lower waste heat temperatures. Based on the above results, at higher investments, a higher COP is required for the FG system to be effective due to the increased capital.

CHAPTER 5. CONCLUSION AND RECOMMENDATIONS

This study presented a detailed techno-economic assessment of a 565 MW NGCC power plant subjected to different waste heat recovery scenarios and gas turbine inlet chilling conditions. The major difference in this study compared to prior investigations was that the WHR systems were compared on the basis of LCOE instead of a simple payback period analysis. This approach of comparing the systems allowed for all costs, including the capital and operating costs, to be considered alongside the performance of various system combinations throughout the life of the power plant. The results show that gas turbine inlet air chilling is more ideally suited for locations where the temperature is high during the summer months (i.e., Houston compared to Los Angeles). Amongst the different heat source options, for a given WHR system cost, the low temperature flue gas produced the lowest LCOE. The primary explanation is that the flue gas system does not degrade the NGCC performance as compared to the other options. At higher WHR system costs, the LCOE increases rapidly for all systems.

The results from the tolerable cost analysis show that a flue gas driven system can tolerate the highest system cost to yield the same LCOE as the baseline, followed by the mechanical vapor compression, steam driven, and gas turbine exhaust driven cooling systems. The gas turbine exhaust driven system always yields a higher LCOE than the baseline at low cooling capacities. As the cooling capacity is increased, the GTX system becomes more economical because the power reduction from diverting the gas turbine exhaust is offset by the power boost from the turbine inlet air chilling. However, as the capacity increases further (42.85 MW and 30.15 MW for GTX and STM for Houston and 23.12 MW and 18.18 MW for Los Angeles), the tolerable cost reduces because the capital cost of the WHR system increases. Similar trends are observed for the

steam-driven system. For the vapor compression system and the flue gas driven systems, the tolerable costs decreased for higher capacities.

If a power plant owner has a fixed investment amount available, it is likely mechanical vapor compression systems will be more economical than STM or GTX waste heat driven gas turbine inlet chilling systems. The flue gas driven system has the potential to be more economical than the vapor compression system because it does not require a high COP, and it can tolerate a higher cost per kW_{th}. There are some complications with a flue gas driven system, however, because the heat is low temperature which requires relatively complex heat exchanger designs. The results presented here were for only two locations for a single NGCC configuration, and further studies will investigate a wider range of weather patterns and power plant system sizes to determine which system is the best fit for any location.

5.1 Recommendations

This study consisted of multiple assumptions that simplified the performance and financial modeling process of the NGCC power plant. Furthermore, there are other recommendations for future investigations which are beyond the scope of this study. Listed below are the major limitations and specific recommendations for future work.

1. The gas turbine modeling is based on a standard set of equations which might not generate accurate results for gas turbines across a range of different manufacturers. Moreover, to predict the off-design performance of a gas turbine, it is best to use the performance maps generated by the manufacturers for accurate results. Future studies should be focused in using either the performance maps or the performance equations developed by the gas turbine manufacturer to predict the off-design performance.
2. For the ease of calculations, the pressure drops in the gas stream and the steam side of the

HRSG are largely neglected. They are neglected because the pressure drops will be on the order of Pascals, while the steam pressures are in the range of MPa and the gas pressure is in the range of kPa. For more accurate results typical to professional designs, these pressure drops could be added.

3. The comparison of the three waste heat recovery strategies is based on the maximum waste heat that can be extracted from the flue gas stream while the flue gas temperature is dropped to a minimum of 80°C. The amount of cooling generated while keeping a fixed COP for the absorption system is applied to all GTX, STM, and FG systems to calculate the NGCC performance subjected to gas turbine inlet chilling. In real practices, the COP of the absorption system varies as a function of the stack temperature, thus changing the amount of cooling generated. The COP variation is not accounted for in this study. Future investigations should focus on this aspect of COP variations.
4. Since the cost data for absorption cooling systems are not readily available in open literature, a parametric study on the costs of the cooling systems was performed in this study. A more detailed economic study on the installation costs could be performed so that the most accurate results can be obtained.
5. Only two locations were chosen in this study: one representative of an extreme climate during both summer and winter, while the other being a milder climate throughout the year. The primary reason to select only two locations was the computation time required for the analysis. It is recommended that more locations are analyzed to better understand of the best climate for gas turbine inlet chilling.

REFERENCES

[1] BCS, Incorporation., *Waste Heat Recovery- Technology and Opportunities in U.S. Industry*. 2008.

[2] *Modular HRSG*. 2017; Available from: http://www.zeroco2.no/capture/sources-of-co2/combined-cycle-power-plant/MOdularHRSG.jpg/image_view_fullscreen.

[3] Enerdata, *The state of global energy efficiency Global and sectorial energy efficiency trends*. 2013, ABB: Zurich, Switzerland.

[4] Taniguchi, H., et al., *Power generation analysis for high-temperature gas turbine in thermodynamic process.* Journal of Propulsion and Power, 2000. **16**(4): p. 557-561.

[5] U.S., Energy Information Administration(EIA), *U.S. electricity generation by energy source*. 2017; Available from: https://www.eia.gov/tools/faqs/faq.php?id=427&t=3.

[6] U.S., Energy Information Administration(EIA). *Trends in Renewable Energy Consumption and Electricity*. 2012 [cited 2018 Feb 11]; Available from: https://www.eia.gov/renewable/annual/trends/.

[7] U.S., Energy Information Administration(EIA) . *Today in energy*. 2016; Available from: https://www.eia.gov/todayinenergy/detail.php?id=25652.

[8] Institute, G.C. *Power Plant Efficiency*. 2018 [cited 2018 Feb 11]; Available from: https://hub.globalccsinstitute.com/publications/capturing-co2/power-plant-efficiency.

[9] *Combined cycle plant*. 2018 [cited 2018 Feb 23]; Available from: http://cset.mnsu.edu/engagethermo/systems_combinedcycle.html.

[10] Clement, S. *ISO Rating of Gas Turbines*. 2016 [cited 2018 Feb 11]; Available from: https://www.linkedin.com/pulse/iso-rating-gas-turbines-clement-sadjere/.

[11] Paudel, A. and T.M. Bandhauer, *Simulation of Natural Gas Combined Cycle Power Plants at Elevated Temperatures*, in *American Society of Thermal and Fluids Engineering* 2016: Las Vegas.

[12] Ganapathy, V., *Heat-recovery steam generators: Understand the basics.* Chemical Engineering Progress, 1996. **92**(8): p. 32-45.

[13] Ivan, R.G. *The evolution of the combined cycle power plant- I*. 2017; Available from: https://www.turbomachinerymag.com/the-evolution-of-the-combined-cycle-power-plant-i/.

[14] U.S., Energy Information Administration(EIA). *Electricity Data*. 2017 [cited 2017 12 Dec]; Available from: https://www.eia.gov/electricity/data/eia860/index.html.

[15] Alvarez, R.A., et al., *Greater focus needed on methane leakage from natural gas infrastructure.* Proceedings of the National Academy of Sciences of the United States of America, 2012. **109**(17): p. 6435-6440.

[16] Spath Pamela, Mann Margaret, and K. Dawn, *Life Cycle Assessment of Coal-fired Power Production*. 1999, National Renewable Energy Laboratory.

[17] Spath Pamela and M. Margaret, *Life Cycle Assessment of a Natural Gas Combined-Cycle Power Generation System*. 2000, National Renewable Energy Laboratory.

[18] Larson, A., *World's Most-Efficient Combined Cycle Plant: EDF Bouchain*, in *Power*. 2017.

[19] Tenaris. *HRSG*. 2017; Available from: http://www.tenaris.com/en/products/powergeneration/gasfiredpowerplants/gasfiredpowerplants_hrsg.aspx.

[20] El-Wakil, M.M., *Powerplant technology*. 2002, New York: McGraw-Hill Primis Custom Pub. xv, 861 pages.
[21] *Materials of construction for steam temperatures of over 700 °C*. 2018; Available from: http://kraftwerkforschung.info/en/materials-of-construction-for-steam-temperatures-of-over-700-c/.
[22] Paul, B. *Pushing the steam cycle boundaries*. 2012 [cited 2018 Feb 11]; Available from: http://www.powerengineeringint.com/articles/print/volume-20/issue-4/features/pushing-the-steam-cycle-boundaries.html.
[23] Zhai, H.B. and E.S. Rubin, *Performance and cost of wet and dry cooling systems for pulverized coal power plants with and without carbon capture and storage.* Energy Policy, 2010. **38**(10): p. 5653-5660.
[24] Kroger, D.G., *Air-cooled heat exchangers and cooling towers : Thermal-flow performance evaluation and design*. 2004, Tulsa, Okl.: Penwell Corp. xiii, pág. vár.
[25] De Sa, A. and S. Al Zubaidy, *Gas turbine performance at varying ambient temperature.* Applied Thermal Engineering, 2011. **31**(14-15): p. 2735-2739.
[26] Rahman M.M., Ibrahim K. Thamir, and A.N. Ahmed, *Thermodynamic performance analysis of gas-turbine power-plant.* International Journal of the Physical Sciences, 2011. **6**(14): p. 3539-3550.
[27] Gobran, M.H., *Off-design preformance of solar Centaur-40 gas turbine engine using Simulink.* Ain Shams Engineering Journal, 2013. **4**(2): p. 285-298.
[28] Korakianitis, T. and K. Svensson, *Off-design performance of various gas-turbine cycle and shaft configurations.* Journal of Engineering for Gas Turbines and Power-Transactions of the Asme, 1999. **121**(4): p. 649-655.
[29] Al-Hamdan, Q.Z. and M.S.Y. Ebaid, *Modeling and simulation of a gas turbine engine for power generation.* Journal of Engineering for Gas Turbines and Power-Transactions of the Asme, 2006. **128**(2): p. 302-311.
[30] Arrieta, F.R.P. and E.E.S. Lora, *Influence of ambient temperature on combined-cycle power-plant performance.* Applied Energy, 2005. **80**(3): p. 261-272.
[31] *GE Gate Cycle*. 2015; Available from: htpps://gepower.com.
[32] Tiwari, A.K., M.M. Hasan, and M. Islam, *EFFECT OF AMBIENT TEMPERATURE ON THE PERFORMANCE OF A COMBINED CYCLE POWER PLANT.* Transactions of the Canadian Society for Mechanical Engineering, 2013. **37**(4): p. 1177-1188.
[33] Giuma, F., *EFFECT OF AMBIENT TEMPERATURE ON THE THERMODYNAMIC PERFORMANCE OF A COMBINED CYCLE.* Journal of Engineering Research (Al-Fateh University), 2010. **1**(13): p. 35-48.
[34] *Aspen HYSYS* 2018.
[35] Haglind, F., *Variable geometry gas turbines for improving the part-load performance of marine combined cycles - Combined cycle performance.* Applied Thermal Engineering, 2011. **31**(4): p. 467-476.
[36] Nord, L.O. and O. Bolland, *Design and off-design simulations of combined cycles for offshore oil and gas installations.* Applied Thermal Engineering, 2013. **54**(1): p. 85-91.
[37] Lawrence Livermore National Laboratory, *Energy Flow Charts*. 2016 [cited 2017 Dec 15]; Available from: https://flowcharts.llnl.gov/.
[38] Cecilia, A., F. Ed, and P. Kelly. *Industrial Waste-Heat Recovery: Benefits and Recent Advancements in Technology and Applications* in *Summer Study on Energy Efficiency in Industry*. 2007. White Plains, NY: American Council for an Energy-Efficient Economy.

[39] Boonnasa, S., P. Namprakai, and T. Muangnapoh, *Performance improvement of the combined cycle power plant by intake air cooling using an absorption chiller.* Energy, 2006. **31**(12): p. 2036-2046.
[40] Gonzalez-Diaz, A., et al., *Effect of the ambient conditions on gas turbine combined cycle power plants with post-combustion CO2 capture.* Energy, 2017. **134**: p. 221-233.
[41] Popli, S., P. Rodgers, and V. Eveloy, *Gas turbine efficiency enhancement using waste heat powered absorption chillers in the oil and gas industry.* Applied Thermal Engineering, 2013. **50**(1): p. 918-931.
[42] Al-Ibrahim, A.M. and A. Varnham, *A review of inlet air-cooling technologies for enhancing the performance of combustion turbines in Saudi Arabia.* Applied Thermal Engineering, 2010. **30**(14-15): p. 1879-1888.
[43] Nasser, A.E.M. and M.A. Elkalay, *A HEAT-RECOVERY COOLING SYSTEM TO CONSERVE ENERGY IN GAS-TURBINE POWER-STATIONS IN THE ARABIAN GULF*. Applied Energy, 1991. **38**(2): p. 133-142.
[44] AL-Bortmany, J.N., *Assessment of aqua-amonia refrigeration for pre-cooling gas-turbine inlet air*, in *ASME Turbo Expo 2002*. 2002: Amsterdam, The Netherlands. p. 3-6.
[45] Ameri, M. and S.H. Hejazi, *The study of capacity enhancement of the Chabahar gas turbine installation using an absorption chiller.* Applied Thermal Engineering, 2004. **24**(1): p. 59-68.
[46] Mohanty, B. and G. Paloso, *ENHANCING GAS-TURBINE PERFORMANCE BY INTAKE AIR COOLING USING AN ABSORPTION CHILLER.* Heat Recovery Systems & Chp, 1995. **15**(1): p. 41-50.
[47] Dawoud, B., Y.H. Zurigat, and J. Bortmany, *Thermodynamic assessment of power requirements and impact of different gas-turbine inlet air cooling techniques at two different locations in Oman.* Applied Thermal Engineering, 2005. **25**(11-12): p. 1579-1598.
[48] Buecker, B., C. Mieckowski, and Asme, *USING COMBUSTION TURBINE EXHAUST HEAT FOR TURBINE INLET AIR CHILLING*. Proceedings of the 20th International Conference on Nuclear Engineering and the Asme 2012 Power Conference - 2012, Vol 1. 2012, New York: Amer Soc Mechanical Engineers. 289-293.
[49] Rahim, M.A., *Performance and sensitivity analysis of a combined cycle gas turbine power plant by various inlet air-cooling systems.* Proceedings of the Institution of Mechanical Engineers Part a-Journal of Power and Energy, 2012. **226**(A7): p. 922-931.
[50] U.S. Department of Energy, National Energy Technology Laboratory, *Cost and Performance Baseline for Fossil Energy Plants* 2013.
[51] Institute, E.P.R. *F-Class Gas Turbine Technology Summary: Design Features, Reliability Statistics, and Durability Issues*. 2012, Dec 31 [cited 2017 October, 24]; Available from: https://www.epri.com/#/pages/product/1025357/.
[52] Dixon, S.L. and C.A. Hall, *Fluid Mechanics and Thermodynamics of Turbomachinery, 6th Edition.* Fluid Mechanics and Thermodynamics of Turbomachinery, 6th Edition, 2010: p. 1-459.
[53] Kiameh, P., *Power generation handbook : fundamentals of low-emission, high-efficiency power plant operation*. 2nd ed. 2012, New York: McGraw-Hill. xxviii, 704 p.
[54] Kuehn, T.H., et al., *Thermal environmental engineering*. 3rd ed. 1998, Upper Saddle River, N.J.: Prentice Hall. xii, 740 p.

[55] GEA. *GEA-Leader in DeNOx*. 2017 [cited 2018 Feb, 10]; Available from: https://www.gea.com/en/products/gea-scr-plants.jsp.
[56] Moran, M.J. and H.N. Shapiro, *Principles of engineering thermodynamics : SI version*. 7th ed. 2012, Hoboken (NJ): John Wiley & Sons. xiii, 928 p.
[57] *HRSG advances keep GTCC competititve*. 2004 [cited 2018 15 April]; Available from: http://www.modernpowersystems.com/features/featurehrsg-advances-keep-gtcc-competititve/.
[58] Incropera, F.P., et al., *Fundamentals of heat and mass transfer*. [7th ed. 2011, New Delhi: Wiley. xxiii, 840 pages.
[59] Stanciu, M., M. Marcelet, and J.-M. Dorey, *Numerical Investigation of Condenser Pressure Effect on Last Stage Operation of Low Pressure Wet Steam Turbines*, in *ASME Turbo Expo 2013: Turbine Technical Conference and Exposition*. June 3-7, 2013: San Antonio, Texas.
[60] Cale, S.A., *Development of evaporative cooling packing : final report*. Eur. 1982, Brussels ; Luxembourg: Commission of the European Communities; Directorate-general for research Science and education. 66 p.
[61] Bahadori, A., *Estimation of combustion flue gas acid dew point during heat recovery and efficiency gain.* Applied Thermal Engineering, 2011. **31**(8-9): p. 1457-1462.
[62] Kren, C., *Flue gas fired absorption chillers*. 2008. p. XXII, 253 S.
[63] Al-Tahaineh, H., M. Frihat, and M. Al-Rashdan, *Exergy Analysis of a Single-Effect Water-Lithium Bromide Absorption Chiller Powered by Waste Energy Source for Different Cooling Capacities.* Energy and Power, 2013. **3**(6): p. 106-118.
[64] Thermax. *Triple Effect Chiller*. 2017 [cited 2018 Feb, 10]; Available from: http://www.thermaxglobal.com/thermax-absorption-cooling-systems/vapour-absorption-machines/triple-effect-chillers/.
[65] U.S. Department of Energy, National Energy Technology Laboratory, *Cost Estimation Methodology for NETL Assessments of Power Plant Performance*. 2011, The Energy Lab.
[66] Park, C.S., *Contemporary engineering economics*. Sixth edition. Global edition. ed. 1 volume.
[67] U.S. Department of Energy, National Energy Technology Laboratory, *Cost and Performance Baseline for Fossil Energy Plants Volume 1: Bituminous Coal and Natural Gas to Electricity*. 2013.
[68] Barigozzi, G., et al., *Techno-economic analysis of gas turbine inlet air cooling for combined cycle power plant for different climatic conditions.* Applied Thermal Engineering, 2015. **82**: p. 57-67.

APPENDIX A: SAMPLE CALCULATION OF NGCC CYCLE PARAMETERS

In this appendix, the calculations for the NGCC cycle is presented. Table A-1 presents the representative calculations for the gas turbine cycle. Table A-2 presents the representative calculations for the steam cycle at baseline case.

Table A-1. Sample calculation of parameters in gas turbine cycle

Parameter	Equation	Evaluated	EES Calc. Value	Hand Calc. Value	Units
Compressor Efficiency	$\eta_c = \frac{PR^{\left[\frac{\gamma-1}{\gamma}\right]}-1}{PR^{\left[\frac{\gamma-1}{\eta_{poly,c}\gamma}\right]}-1}$	$\eta_c = \frac{20.14^{\left[\frac{1.4-1}{1.4}\right]}-1}{20.14^{\left[\frac{1.4-1}{0.8658\times1.4}\right]}-1}$	0.802	0.802	-
Compressor Pressure Ratio (at 30°C,95 kpa)	$\frac{\left(\dot{m}\sqrt{T_{01}}\right)_{\mathrm{DP}}\left(p_{01}\right)_{ODP}}{\left(\dot{m}\sqrt{T_{01}}\right)_{\mathrm{ODP}}\left(p_{01}\right)_{DP}} = \left(\frac{PR_{\mathrm{DP}}}{PR_{\mathrm{ODP}}}\right)^{1-\left(\frac{\gamma-1}{2\gamma\eta_{\mathrm{p}}}\right)}$	$\frac{\left(876.3\sqrt{273+15}\right)(95)}{\left(781\sqrt{273+30}\right)(101.325)} = \left(\frac{20.14}{PR_{\mathrm{ODP}}}\right)^{1-\left(\frac{1.4-1}{2\times1.4\times0.8658}\right)}$	19.54	19.53	-
Gas Mass flow rate	$\dot{m}_{\mathrm{gas}} = \dot{m}_{\mathrm{air}} + \dot{m}_{\mathrm{NG}}$	$\dot{m}_{\mathrm{gas}} = 876.3 + 21.08$	897.4	897.4	kg s^{-1}
Compressor Work	$W_{\mathrm{c}} = \dot{m}_{\mathrm{air}}(i_2 - i_1)$	$W_{\mathrm{c}} = \frac{876.3(777.5-288.3)}{1000}$	428.7	428.7	MW
Turbine Work	$W_{\mathrm{t}} = (I_3 - I_4)$	$W_{\mathrm{t}} = (356.6-(-484.9))$	841.5	841.5	MW
Net gas turbine electric power	$W_{\mathrm{e}} = \eta_{\mathrm{gen}}\eta_{\mathrm{mech}}(W_{\mathrm{t}} - W_{\mathrm{c}})$	$W_{\mathrm{e}} = 0.977\times0.902\times(841.5-428.7)$	362.2	363.7	MW_e

Table A-2. Sample calculation of parameters in Rankine cycle at 15°C ambient temperature

Parameter	Equation	Evaluated	EES Calc. Value	Hand Calc. Value	Units
HRSG heat exchanger heat duty					
HP superheater	$\dot{Q}_{HP,SPH} = \dot{m}_{HP}(i_{out} - i_{in})$	$\dot{Q}_{HP,SPH} = 104(3362.12 - 2564.17)$	82996	82987	kW
Reheater	$\dot{Q}_{RH} = \dot{m}_{HP}(i_{out} - i_{in})$	$\dot{Q}_{RH} = 104(3618.73 - 2932.9)$	71332	71326	kW
IP superheater	$\dot{Q}_{IP,SPH} = \dot{m}_{IP}(i_{out} - i_{in})$	$\dot{Q}_{IP,SPH} = 13(3484.5 - 2802.2)$	8869	8870	kW
HP evaporator	$\dot{Q}_{HP,EVP} = \dot{m}_{HP}(i_{out} - i_{in})$	$\dot{Q}_{HP,EVP} = 104(2564.17 - 1583.39)$	102010	102001	kW
HP economizer	$\dot{Q}_{HP,ECO} = \dot{m}_{HP}(i_{out} - i_{in})$	$\dot{Q}_{HP,ECO} = 104(1583.39 - 639.49)$	98175	98166	kW
LP Superheater	$\dot{Q}_{LP,SPH} = \dot{m}_{LP}(i_{out} - i_{in})$	$\dot{Q}_{LP,SPH} = 27(3125.5 - 2750.11)$	10135	10136	kW
IP evaporator	$\dot{Q}_{IP,EVP} = \dot{m}_{IP}(i_{out} - i_{in})$	$\dot{Q}_{IP,EVP} = 13(2802.2 - 916.02)$	24519	24520	kW
IP economizer	$\dot{Q}_{IP,ECO} = \dot{m}_{IP}(i_{out} - i_{in})$	$\dot{Q}_{IP,ECO} = 13(916.02 - 618.17)$	3872	3872	kW
LP evaporator	$\dot{Q}_{LP,EVP} = \dot{m}_{LP}(i_{out} - i_{in})$	$\dot{Q}_{LP,EVP} = 27(2750.11 - 624.27)$	57396	57398	kW
LP economizer	$\dot{Q}_{LP,ECO} = \dot{m}_{LP}(i_{out} - i_{in})$	$\dot{Q}_{LP,ECO} = 27(624.27 - 615.14)$	247	247	kW
Preheater	$\dot{Q}_{PH} = \dot{m}_{tot}(i_{out} - i_{in})$	$\dot{Q}_{PH} = 144.01(615.08 - 144.43)$	67777	67778	kW
Condenser	$\dot{Q}_{COND} = \dot{m}_{tot}(i_{out} - i_{in})$	$\dot{Q}_{COND} = 144.01(2400.42 - 143.76)$	324976	324981	kW
Turbine and pump work					
HP turbine work	$\dot{W}_{HPT} = \dot{m}_{HP}(i_{in} - i_{out})$	$\dot{W}_{HPT} = 104(3362.1 - 2932.9)$	44643	44637	kW
IP turbine work	$\dot{W}_{IPT} = \dot{m}_{IPT}(i_{in} - i_{out})$	$\dot{W}_{IPT} = 117(3603.8 - 3131.6)$	55247	55247	kW
LP turbine work	$\dot{W}_{LPT} = \dot{m}_{LPT}(i_{in} - i_{out})$	$\dot{W}_{LPT} = 144.01(3130.5 - 2400.4)$	105137	105141	kW
HP pump work	$\dot{W}_{HP} = \dot{m}_{HP}\frac{(P_{out} - P_{in})}{\rho\eta}$	$\dot{W}_{HP} = 104\frac{(16500 - 480)}{920.8 \times 0.71}$	2549	2548.4	kW
IP pump work	$\dot{W}_{IP} = \dot{m}_{IP}\frac{(P_{out} - P_{in})}{\rho\eta}$	$\dot{W}_{IP} = 13 \times \frac{(2500 - 480)}{920.8 \times 0.71}$	40.2	40.2	kW

Parameter	Equation	Evaluated	EES Calc. Value	Hand Calc. Value	Units
LP pump work	$\dot{W}_{\mathrm{LP}} = \dot{m}_{\mathrm{LP}} \frac{(P_{\mathrm{out}} - P_{\mathrm{in}})}{\rho\eta}$	$\dot{W}_{\mathrm{LP}} = 27 \times \frac{(517.1 - 480)}{920.8 \times 0.71}$	1.5	1.5	kW
Condensate pump work	$\dot{W}_{\mathrm{CP}} = \dot{m}_{\mathrm{tot}} \frac{(P_{\mathrm{out}} - P_{\mathrm{in}})}{\rho\eta}$	$\dot{W}_{\mathrm{CP}} = 144.01 \times \frac{(480 - 6.89)}{994.2 \times 0.71}$	96.5	96.5	kW
Steam turbines net electric work	$\dot{W}_{\mathrm{stm,elec}} = \eta_{\mathrm{elec}} \left(\dot{W}_{\mathrm{HPT}} + \dot{W}_{\mathrm{IPT}} + \dot{W}_{\mathrm{LPT}} \right)$	$\dot{W}_{\mathrm{stm,elec}} = 0.9876 \begin{pmatrix} 44643 \\ +55247 + 105137 \end{pmatrix}$	202486	202485	kW_e
Net power plant output	$\dot{W}_{\mathrm{net,elec}} = \begin{pmatrix} \dot{W}_{\mathrm{stm,elec}} + \dot{W}_{\mathrm{GT,elec}} \\ -\dot{W}_{\mathrm{CP}} - \dot{W}_{\mathrm{HP}} \\ -\dot{W}_{\mathrm{IP}} - \dot{W}_{\mathrm{LP}} \\ -\dot{W}_{\mathrm{aux}} - P_{\mathrm{fan}} \end{pmatrix}$	$\dot{W}_{\mathrm{net,elec}} = \begin{pmatrix} 202486 + 362199 \\ -96.52 - 2549 \\ -40.16 - 1.52 \\ -4135 - 2866 \end{pmatrix}$	554997	554997	kW_e
HHV efficiency	$\eta_{\mathrm{HHV}} = \frac{\dot{W}_{\mathrm{net,elec}}}{\dot{m}_{\mathrm{NG}} \times \mathrm{HHV}}$	$\eta_{\mathrm{HHV}} = \frac{554997}{21.08 \times 52581}$	0.5007	0.5007	-
LHV efficiency	$\eta_{\mathrm{LHV}} = \frac{\dot{W}_{\mathrm{net,elec}}}{\dot{m}_{\mathrm{NG}} \times \mathrm{LHV}}$	$\eta_{\mathrm{LHV}} = \frac{554997}{21.08 \times 47454}$	0.5548	0.5548	-
HRSG heat exchanger NTU					
Reheater	$NTU = -\ln\left[1 + \frac{1}{C_{\mathrm{r}}} \ln\left(1 - \varepsilon C_{\mathrm{r}}\right)\right]$	$NTU = -\ln\left[\begin{matrix} 1 + \frac{1}{0.2191} \times \\ \ln\left(1 - 0.8365 \times 0.2191\right) \end{matrix}\right]$	2.578	2.577	-
HP superheater	$NTU = \frac{1}{C_{\mathrm{r}} - 1} \ln\left(\frac{\varepsilon - 1}{\varepsilon C_{\mathrm{r}} - 1}\right)$	$NTU = \left[\begin{matrix} \frac{1}{0.7313 - 1} \times \\ \ln\left(\frac{0.8281 - 1}{0.8281 \times 0.7313 - 1}\right) \end{matrix}\right]$	3.091	3.090	-

Parameter	Equation	Evaluated	EES Calc. Value	Hand Calc. Value	Units
IP superheater	$NTU = -\ln\left[1+\frac{1}{C_r}\ln\left(1-\varepsilon C_r\right)\right]$	$NTU = -\ln\left[\frac{1+\frac{1}{0.0563}\times}{\ln\left(1-0.8478\times 0.0563\right)}\right]$	2.03	2.03	-
HP evaporator	$NTU = -\ln(1-\varepsilon)$ $NTU = -\ln\left[1+\frac{1}{C_r}\ln\left(1-\varepsilon C_r\right)\right]$	$NTU = -\ln(1-0.737)$ $NTU = -\ln\left[\frac{1+\frac{1}{0.572}\times}{\ln\left(1-0.236\times 0.572\right)}\right]$	1.336 0.292	1.336 0.292	-
HP economizer	$NTU = \frac{1}{C_r - 1}\ln\left(\frac{\varepsilon - 1}{\varepsilon C_r - 1}\right)$	$NTU = \left[\frac{\frac{1}{0.982-1}\times}{\ln\left(\frac{0.85-1}{0.85\times 0.982-1}\right)}\right]$	5.408	5.395	-
LP superheater	$NTU = -\ln\left[1+\frac{1}{C_r}\ln\left(1-\varepsilon C_r\right)\right]$	$NTU = -\ln\left[\frac{1+\frac{1}{0.112}\times}{\ln\left(1-0.802\times 0.112\right)}\right]$	1.84	1.83	-
IP evaporator	$NTU = -\ln(1-\varepsilon)$ $NTU = -\ln\left[1+\frac{1}{C_r}\ln\left(1-\varepsilon C_r\right)\right]$	$NTU = -\ln(1-0.595)$ $NTU = -\ln\left[\frac{1+\frac{1}{0.122}\times}{\ln\left(1-0.122\times 0.377\right)}\right]$	0.905 0.487	0.904 0.487	-
IP economizer	$NTU = -\ln\left[1+\frac{1}{C_r}\ln\left(1-\varepsilon C_r\right)\right]$	$NTU = -\ln\left[\frac{1+\frac{1}{0.058}\times}{\ln\left(1-0.722\times 0.058\right)}\right]$	1.341	1.337	-

Parameter	Equation	Evaluated	EES Calc. Value	Hand Calc. Value	Units
LP evaporator	$NTU = -\ln(1-\varepsilon)$ $NTU = -\ln\left[1+\frac{1}{C_r}\ln\left(1-\varepsilon C_r\right)\right]$	$NTU = -\ln(1-0.705)$ $NTU = -\ln\left[1+\frac{1}{0.241}\times \ln\left(1-0.17\times 0.241\right)\right]$	1.22 0.191	1.22 0.192	-
LP economizer	$NTU = -\ln\left[1+\frac{1}{C_r}\ln\left(1-\varepsilon C_r\right)\right]$	$NTU = -\ln\left[1+\frac{1}{0.120}\times \ln\left(1-0.068\times 0.120\right)\right]$	0.07	0.07	-
Preheater	$NTU = \frac{1}{C_r - 1}\ln\left(\frac{\varepsilon - 1}{\varepsilon C_r - 1}\right)$	$NTU = \left[\frac{1}{0.631-1}\times \ln\left(\frac{0.784-1}{0.784\times 0.631-1}\right)\right]$	2.307	2.303	-
HRSG Heat Exchanger UA					
Reheater	$UA_{RH} = NTU_{RH}\times C_{min}$	$UA_{RH} = 2.578\times 232.4$	599.15	599.12	kW K^{-1}
HP superheater	$UA_{HP,SPH} = NTU_{HP,SPH}\times C_{min}$	$UA_{HP,SPH} = 3.091\times 378.4$	1169.4	1169.6	kW K^{-1}
IP superheater	$UA_{IP,SPH} = NTU_{IP,SPH}\times C_{min}$	$UA_{IP,SPH} = 2.03\times 29.57$	60.03	60.03	kW K^{-1}
HP evaporator	$UA_{HP,EVP,1P} = NTU_{HP,EVP,1P}\times C_{min}$ $UA_{HP,EVP,2P} = NTU_{HP,EVP,2P}\times C_{min}$	$UA_{HP,EVP,1P} = 0.2921\times 505.6$ $UA_{HP,EVP,2P} = 1.336\times 1023$	147.7 1367	147.7 1366.7	kW K^{-1}
HP economizer	$UA_{HP,ECO} = NTU_{HP.ECO}\times C_{min}$	$UA_{HP,ECO} = 5.408\times 485.2$	2623.6	2623.9	kW K^{-1}
LP superheater	$UA_{LP,SPH} = NTU_{LP,SPH}\times C_{min}$	$UA_{LP,SPH} = 1.84\times 56.44$	103.8	103.85	kW K^{-1}
IP evaporator	$UA_{IP,EVP,1P} = NTU_{IP,EVP,1P}\times C_{min}$ $UA_{IP,EVP,2P} = NTU_{IP,EVP,2P}\times C_{min}$	$UA_{IP,EVP,1P} = 0.487\times 59.73$ $UA_{IP,EVP,2P} = 0.905\times 982.3$	29.1 889	29.1 888.9	kW K^{-1}
IP economizer	$UA_{IP,ECO} = NTU_{IP,ECO}\times C_{min}$	$UA_{IP,ECO} = 1.341\times 57.16$	76.6	76.6	kW K^{-1}

Parameter	Equation	Evaluated	EES Calc. Value	Hand Calc. Value	Units
LP evaporator	$UA_{LP,EVP,1P} = NTU_{LP,EVP,1P} \times C_{min}$ $UA_{LP,EVP,2P} = NTU_{LP,EVP,2P} \times C_{min}$	$UA_{LP,EVP,1P} = 0.190 \times 116.5$ $UA_{LP,EVP,2P} = 1.222 \times 972.3$	22.2 1188	22.14 1188.15	kW K^{-1}
LP economizer	$UA_{LP,ECO} = NTU_{LP,ECO} \times C_{min}$	$UA_{LP,ECO} = 0.071 \times 116.2$	8.3	8.25	kW K^{-1}
Preheater	$UA_{PH} = NTU_{PH} \times C_{min}$	$UA_{PH} = 2.307 \times 605.4$	1396.7	1396.6	kW K^{-1}

APPENDIX B: SAMPLE CALCULATION OF COOLING TOWER PARAMETERS

In this section, a sample calculation for determining the heat and mass transfer characteristics in the cooling tower and the fan power calculations are presented.

Table B-1. Parameters for determining cooling tower performance

Parameters	Value	Units
Cooling tower outlet relative humidity (RH_5)	1	
Number of cooling tower units (N_{wc})	10	
Rain zone drop diameter (d_d)	0.0035	m
Total cooling water mass flow rate (m_{cw})	7062.22	kg s^{-1}
Volumetric flow rate of air (V_f)	1021	kg s^{-1}
Fan rotational speed (N_F)	120	
Fan efficiency (η_{fan})	0.9	
Loss coefficient due to inlet louvers (K_{il})	2.5	
Loss coefficient for fill support and contraction (K_{fs})	0.5	
Loss coefficient due to water distribution (K_{wd})	0.5	
Upstream loss coefficient (K_{up})	0.52	
Acceleration due to gravity(g)	9.81	m s^{-2}
Gas constant for water vapor (Rv)	461.52	J $kg^{-1}K^{-1}$
Cooling Tower Dimensions		
Tower height (H_9)	13.5	m
Fan height (H_6)	10.5	m
Tower inlet height (H_3)	4	m
Tower inlet width (W_i)	16	m
Tower breadth (B_i)	16	m
Fill zone height (L_{fi})	2.878	m
Spray zone height (L_{sp})	0.5	m
Plenum chamber height (H_{pl})	2.4	m
Fan diameter (d_F)	10	m

Table B-2. Cooling tower calculations

Parameter	Equation	Evaluated	EES Calc. Value	Hand Calc. Value	Units
Frontal Area	$A_{fr} = B_i \times W_i$	$A_{fr} = 16 \times 16$	256	256	m^2
Air vapor mass flow at exit	$V_f = \frac{\dot{m}_{av5}}{\rho_{av5}}$	$1021 = \frac{\dot{m}_{av5}}{1.179}$	1204	1203.8	kg s^{-1}
Mass flow of dry air	$\dot{m}_{av5} = \dot{m}_a(1+\omega_5)$	$1204 = \dot{m}_a(1+0.01489)$	1186	1186	kg s^{-1}
Air vapor mass flow at inlet	$\dot{m}_{av1} = \dot{m}_a(1+\omega_1)$	$\dot{m}_{av1} = 1186(1+0.006345)$	1194	1193.5	kg s^{-1}
Averaged air vapor mass flow	$\dot{m}_{av15} = \frac{\dot{m}_a(1+\omega_1)+\dot{m}_a(1+\omega_5)}{2}$	$\dot{m}_{av15} = \frac{1186(1+0.006345)+1186(1+0.01489)}{2}$	1199	1199	kg s^{-1}
Make up mass flow	$\dot{m}_{makeup} = \dot{m}_{av5} - \dot{m}_{av1}$	$\dot{m}_{makeup} = 1203.8 - 1193.5$	10.14	10.3	kg s^{-1}
Mass flow of water for unit cell	$\dot{m}_w = \frac{\dot{m}_{cw}}{N_{wc}}$	$\dot{m}_w = \frac{7062.22}{10}$	706.2	706.2	kg s^{-1}
Mass flux of dry air	$G_a = \frac{\dot{m}_a}{A_{fr}}$	$G_a = \frac{1186}{256}$	4.63	4.63	kg $s^{-1}m^{-2}$
Mass flux of air vapor at inlet	$G_{av1} = \frac{\dot{m}_{av1}}{A_{fr}}$	$G_{av1} = \frac{1193.5}{256}$	4.66	4.66	kg $s^{-1}m^{-2}$
Mass flux of air vapor at outlet	$G_{av5} = \frac{\dot{m}_{av5}}{A_{fr}}$	$G_{av5} = \frac{1203.8}{256}$	4.70	4.70	kg $s^{-1}m^{-2}$
Averaged mass flux	$G_{av15} = \frac{\dot{m}_{av15}}{A_{fr}}$	$G_{av15} = \frac{1199}{256}$	4.68	4.68	kg $s^{-1}m^{-2}$

Parameter	Equation	Evaluated	EES Calc. Value	Hand Calc. Value	Units
Mass flux of water	$G_w = \frac{\dot{m}_w}{A_{fr}}$	$G_w = \frac{706.2}{256}$	2.76	2.76	kg $s^{-1}m^{-2}$
Diffusion coefficient	$D = 0.04357 T^{1.5} \frac{\left(\frac{1}{M_a} + \frac{1}{M_b}\right)^{0.5}}{p\left(V_a^{0.333} + V_b^{0.333}\right)^2}$	$D = 0.04357(288)^{1.5} \frac{\left(\frac{1}{28.97} + \frac{1}{18.016}\right)^{0.5}}{101.325 \times 1000\left(29.9^{0.333} + 18.8^{0.333}\right)^2}$	1.9e-5	1.9e-5	m^2 s^{-1}
Schmidt Number	$Sc_1 = \frac{\mu_{av1}}{\rho_{av1} D_1}$	$Sc_1 = \frac{1.8 \times 10^{-5}}{1.216 \times 1.9 \times 10^{-5}}$	0.778	0.779	-
Air vapor velocity before fill	$v_{av3} = \frac{\dot{m}_{av1}}{\rho_{av1} A_{fr}}$	$v_{av3} = \frac{1194}{1.216 \times 256}$	3.83	3.83	m s^{-1}
a coefficients	$a_\mu = 3.061 \times 10^{-6} \left(\frac{\rho_{w,o}^4 g^9}{\sigma_{w,o}}\right)^{0.25}$	$a_\mu = 3.061 \times 10^{-6} \left(\frac{999^4 \times 9.81^9}{0.0733}\right)^{0.25}$	1.0	1.0	-
	$a_\rho = \frac{998}{\rho_{w,o}}$	$a_\rho = \frac{998}{999}$	0.99	0.99	-
	$a_v = 73.298 \left(\frac{g^5 \sigma_{w,o}^3}{\rho_{w,o}^3}\right)^{0.25}$	$a_v = 73.298 \left(\frac{9.81^5 \times 0.0733^3}{999^3}\right)^{0.25}$	1.009	1.008	-
	$a_L = 6.122 \left(\frac{g \sigma_{w,o}}{\rho_{w,o}}\right)^{0.25}$	$a_L = 6.122 \left(\frac{9.81 \times 0.0733}{999}\right)^{0.25}$	1.003	1.002	-

Parameter	Equation	Evaluated	EES Calc. Value	Hand Calc. Value	Units
Rain zone Merkel's number	$Me_{rz} = 3.6\left(\frac{D}{v_{av,o} d_d}\right)\left(\frac{H_i}{d_d}\right)\left(\frac{p_{a1}}{\rho_{w,o} R_v T_{av}}\right) Sc^{0.33} \left[\ln\left(\frac{w_s + 0.622}{w + 0.622}\right) / (w_s - w)\right] \times K$ $K = \left[\begin{array}{l} 4.68851 a_\rho \rho_{av} - 187128.7 a_\mu \mu_{av} \\ -2.29322 + 22.4121\left\{0.350396\left(a_v v_{av,o}\right)^{1.38046} + 0.09\right\} \\ \left\{1.60934\left(a_L H_i\right)^{-1.12083} + 0.66\right\} \\ \times\left\{34.6765\left(a_L d_d\right)^{0.732448} + 0.45\right\} \\ \exp\left\{\begin{array}{l} 7.7389 \exp\left(-0.399827 a_L H_i\right) \\ \ln\left(0.087498 \exp\left(0.026619 a_L W_i\right) + 0.85\right) \end{array}\right\} \end{array}\right]$	$Me_{rz} = 3.6\left(\frac{1.9\times10^{-5}}{3.836\times0.0035}\right)\left(\frac{4}{0.0035}\right)\left(\frac{101325}{999\times461.52\times288}\right) 0.7782^{0.33} \left[\ln\left(\frac{0.01489 + 0.622}{0.006345 + 0.622}\right) / (0.01489 - 0.006345)\right] \times 51.7$ $K = \left[\begin{array}{l} 4.68851 \times 0.99 \times 1.21 - 187128.7 \times 1 \times 0.000018 \\ -2.29322 + 22.4121\left\{0.350396\left(1.009 \times 3.836\right)^{1.38046} + 0.09\right\} \\ \left\{1.60934\left(1.003 \times 4\right)^{-1.12083} + 0.66\right\} \\ \times\left\{34.6765\left(1.003 \times 0.0035\right)^{0.732448} + 0.45\right\} \\ \exp\left\{\begin{array}{l} 7.7389 \exp\left(-0.399827 \times 1.003 \times 4\right) \\ \ln\left(0.087498 \exp\left(0.026619 \times 1.003 \times 16\right) + 0.85\right) \end{array}\right\} \end{array}\right]$	0.335	0.334	-
Spray zone Merkel's number	$Me_{sp} = 0.2 L_{sp}\left(\frac{G_a}{G_w}\right)^{0.5}$	$Me_{sp} = 0.2 \times 0.5\left(\frac{4.634}{2.759}\right)^{0.5}$	0.129	0.129	-
Fill zone Merkel's number	$Me_{fi} = 0.605 L_{fi} G_w^{-0.35} G_a^{0.35}$	$Me_{fi} = 0.605 \times 2.878 \times 2.759^{-0.35} 4.634^{0.35}$	2.088	2.087	-
Total Merkel's	$Me_{tot} = Me_{sp} + Me_{fi} + Me_{rz}$	$Me_{tot} = Me_{sp} + Me_{fi} + Me_{rz}$	2.553	2.550	-

Parameter	Equation	Evaluated	EES Calc. Value	Hand Calc. Value	Units
Intermediate Chebyshev temperatures	$T_{w(1)} = T_{wo} + 0.1(T_{wi} - T_{wo})$	$T_{w(1)} = 16 + 0.1(27 - 16)$	17.1	17.1	°C
	$T_{w(2)} = T_{wo} + 0.4(T_{wi} - T_{wo})$	$T_{w(1)} = 16 + 0.4(27 - 16)$	20.4	20.4	°C
	$T_{w(3)} = T_{wo} + 0.6(T_{wi} - T_{wo})$	$T_{w(1)} = 16 + 0.6(27 - 16)$	22.6	22.6	°C
	$T_{w(4)} = T_{wo} + 0.9(T_{wi} - T_{wo})$	$T_{w(1)} = 16 + 0.9(27 - 16)$	25.9	25.9	°C
Intermediate Chebyshev enthalpy differentials	$\Delta i_{(1)} = (i_{masw_{(1)}} - i_{ma_{(1)}})$	$\Delta i_{(1)} = (48.27 - 33.96)$	14.31	14.31	kJ kg^{-1}
	$\Delta i_{(2)} = (i_{masw_{(2)}} - i_{ma_{(2)}})$	$\Delta i_{(1)} = (58.98 - 42.18)$	16.8	16.8	kJ kg^{-1}
	$\Delta i_{(3)} = (i_{masw_{(3)}} - i_{ma_{(3)}})$	$\Delta i_{(1)} = (66.97 - 47.66)$	19.31	19.31	kJ kg^{-1}
	$\Delta i_{(4)} = (i_{masw_{(4)}} - i_{ma_{(4)}})$	$\Delta i_{(1)} = (80.42 - 55.87)$	24.55	24.55	kJ kg^{-1}
Heat transferred for one cell	$\dot{Q}_{cell} = \dot{m}_w c_p (T_{wo} - T_{wi})$ $\dot{Q}_{cell} = \dot{m}_a (i_{a5} - i_{a1})$	$\dot{Q}_{cell} = 706.2 \times 4.183 \times (27 - 16)$ $\dot{Q}_{cell} = 1186(58.62 - 31.22)$	32.49	32.49	MW
Total condenser cooling load	$N_{wc} = \frac{\dot{Q}_{cond}}{\dot{Q}_{cell}}$	$N_{wc} = \frac{\dot{Q}_{cond}}{\dot{Q}_{cell}}$	324.9	324.9	MW
Fan pressure drop calculation					
Fan area	$A_c = \frac{\pi d_f^{\,2}}{4}$	$A_c = \frac{\pi \times 10^2}{4}$	78.54	78.54	m^2
Characteristic flow parameter	$Ry = \frac{\dot{m}_{av5}}{A_{fr} \mu_{av5}}$	$Ry = \frac{1204}{256 \times 0.0000182259}$	258039	258046	m^{-1}
Water velocity at rain zone inlet	$V_{w3} = \frac{G_w}{\rho_{wi}}$	$V_{w3} = \frac{2.759}{999}$	0.00276	0.00276	m s^{-1}

Parameter	Equation	Evaluated	EES Calc. Value	Hand Calc. Value	Units
Rain zone loss coefficient	$K_{rz} = 1.5 a_v v_{w,i} \left(\frac{H_3}{d_d} \right) \times \left[\begin{array}{l} 0.219164 - 0.30487 a_\rho \rho_{av1} \\ +8278.7 a_\mu \mu_{av1} + 0.954153 \times \\ \left\{ \begin{array}{l} 0.328467 \times \\ \exp\left(135.7638 a_L d_d\right) + 0.47 \end{array} \right\} \\ \times \left\{ \begin{array}{l} 26.28482 \left(a_L H_i \right)^{-2.95729} \right) \\ +0.56 \end{array} \right\} \times m \end{array} \right]$ $m = \left[\begin{array}{l} \exp \left\{ \begin{array}{l} \ln\left(0.204814 \exp\left(0.066518 a_L w_i\right) + 0.21\right) \\ \times \left(3.9186 \exp\left(-0.3 a_L H_i\right)\right) \\ \left(0.31095 \ln\left(a_L d_d\right) + 2.63745\right) \end{array} \right\} \\ \times \left\{ 2.177546 \left(a_v v_{av3} \right)^{-1.46541} + 0.21 \right\} \end{array} \right]$	$K_{rz} = 1.5 \times 1 \times 0.002762 \left(\frac{4}{0.0035} \right) \times \left[\begin{array}{l} 0.219164 - 0.30487 \times 0.999 \times 1.216 \\ +8278.7 \times 1 \times 0.000018 + 0.954153 \times \\ \left\{ \begin{array}{l} 0.328467 \times \\ \exp\left(135.7638 \times 1.003 \times 0.0035\right) + 0.47 \end{array} \right\} \\ \times \left\{ \begin{array}{l} 26.28482 \left(1.003 \times 4 \right)^{-2.95729} \right) \\ +0.56 \end{array} \right\} \times 0.4074 \end{array} \right]$ $m = \left[\begin{array}{l} \exp \left\{ \begin{array}{l} \ln\left(0.204814 \exp\left(0.066518 \times 1.003 \times 16\right) + 0.21\right) \\ \times \left(3.9186 \exp\left(-0.3 \times 1.003 \times 4\right)\right) \\ \left(0.31095 \ln\left(1.003 \times 0.0035\right) + 2.63745\right) \end{array} \right\} \\ \times \left\{ 2.177546 \left(1.009 \times 3.836 \right)^{-1.46541} + 0.21 \right\} \end{array} \right]$	1.831	1.832	-
Rain zone loss coefficient specified to mean fill conditions	$K_{rz,fi} = K_{rz} \left(\frac{\rho_{av15}}{\rho_{av1}} \right) \left(\frac{\dot{m}_{av1}}{\dot{m}_{av15}} \right)^2$	$K_{rz,fi} = 1.831 \left(\frac{1.197}{1.216} \right) \left(\frac{1194}{1199} \right)^2$	1.788	1.787	-

Parameter	Equation	Evaluated	EES Calc. Value	Hand Calc. Value	Units
Fill support loss specified to mean fill conditions	$K_{fs,fi} = K_{fs}\left(\frac{\rho_{av15}}{\rho_{av1}}\right)\left(\frac{\dot{m}_{av1}}{\dot{m}_{av15}}\right)^2$	$K_{fs,fi} = 0.5\left(\frac{1.197}{1.216}\right)\left(\frac{1194}{1199}\right)^2$	0.488	0.488	-
Inlet louvers loss specified to mean fill conditions	$K_{il,fi} = K_{il}\left(\frac{\rho_{av15}}{\rho_{av1}}\right)\left(\frac{W_i B_i}{2H_3 W_i}\right)\left(\frac{\dot{m}_{av1}}{\dot{m}_{av15}}\right)^2$	$K_{il,fi} = 2.5\left(\frac{1.197}{1.216}\right)\left(\frac{16\times16}{2\times4\times16}\right)\left(\frac{1194}{1199}\right)^2$	4.882	4.880	-
Spray zone loss specified to mean fill conditions	$K_{sp,fi} = L_{sp}\left[0.4\left(\frac{G_w}{G_a}\right)+1\right]\left(\frac{\rho_{av15}}{\rho_{av5}}\right)\left(\frac{\dot{m}_{av5}}{\dot{m}_{av15}}\right)^2$	$K_{sp,fi} = 0.5\left[0.4\left(\frac{2.759}{4.634}\right)+1\right]\left(\frac{1.197}{1.179}\right)\left(\frac{1204}{1199}\right)^2$	0.615	0.633	-
Water distribution loss specified to mean fill conditions	$K_{wd,fi} = K_{wd}\left(\frac{\rho_{av15}}{\rho_{av5}}\right)\left(\frac{\dot{m}_{av5}}{\dot{m}_{av15}}\right)^2$	$K_{wd,fi} = 0.5\left(\frac{1.197}{1.216}\right)\left(\frac{1204}{1199}\right)^2$	0.496	0.496	-
Drift eliminator loss specified to mean fill conditions	$K_{de,fi} = 27.4829 Ry^{-0.14247}\left(\frac{\rho_{av15}}{\rho_{av5}}\right)\left(\frac{\dot{m}_{av5}}{\dot{m}_{av15}}\right)^2$	$K_{de,fi} = 27.4829\times258039^{-0.14247}\left(\frac{1.197}{1.179}\right)\left(\frac{1204}{1199}\right)^2$	4.624	4.76	-
Specified fill loss coefficient	$K_{fdm} = 1.103 L_{fi}^{0.32} G_w^{1.1} G_a^{-0.640}$	$K_{fdm} = 1.103\times2.878^{0.32}\times2.759^{1.1}\times4.634^{-0.640}$	1.770	1.770	-

Parameter	Equation	Evaluated	EES Calc. Value	Hand Calc. Value	Units
Actual fill loss coefficient	$K_{fi} = K_{fdm} + \frac{\left(\frac{G_{av5}^2}{\rho_{av5}} - \frac{G_{av1}^2}{\rho_{av15}}\right)}{\frac{G_{av15}^2}{\rho_{av15}}}$	$K_{fi} = 1.77 + \frac{\left(\frac{4.703^2}{1.179} - \frac{4.663^2}{1.197}\right)}{\frac{4.683^2}{1.197}}$	1.818	1.802	-
Effective loss coefficient in the vicinity of fill	$K_{fie} = K_{fs,fi} + K_{fi} + K_{sp,fi} + K_{wd,fi} + K_{de,fi}$	$K_{fie} = 0.4882 + 1.818 + 0.6148 + 0.4966 + 4.624$	8.042	8.041	-
Inlet loss coefficient	$K_{ct} = 0.2339 + \left(3.919\times10^{-3} K_{fie}^2 - 6.84\times10^{-2} K_{fie} + 2.5267\right) \times \exp\left[\frac{W_i}{H_i}\left\{0.5143 - 0.1803\exp\left(0.0163 K_{fi}\right)\right\}\right] - \sinh^{-1} z$ $z = \left[\begin{array}{l} 2.77\exp\left(0.958\frac{W_i}{H_i}\right)\times \\ \exp\left\{10^{-2} K_{fi}\left(2.457 - 1.015\frac{W_i}{H_i}\right)\right\} \\ \times\left(\frac{r_{ir}}{W_i} - 0.013028\right) \end{array}\right]$	$K_{ct} = 0.2339 + \left(3.919\times10^{-3}\times8.042^2 - 6.84\times10^{-2}\times8.042^2 + 2.5267\right) \times \exp\left[\frac{16}{4}\left\{0.5143 - 0.1803\exp\left(0.0163\times1.818\right)\right\}\right] - \sinh^{-1}(1.345)$ $z = \left[\begin{array}{l} 2.77\exp\left(0.958\times\frac{16}{4}\right)\times \\ \exp\left\{10^{-2}\times1.818\times\left(2.457 - 1.015\times\frac{16}{4}\right)\right\} \\ \times\left(\frac{0.4}{16} - 0.013028\right) \end{array}\right]$	7.429	7.428	-
Inlet loss coefficient specified to mean fill conditions	$K_{ct,fi} = K_{ct}\left(\frac{\rho_{av15}}{\rho_{av1}}\right)\left(\frac{\dot{m}_{av5}}{\dot{m}_{av15}}\right)^2$	$K_{ct,fi} = 7.378\left(\frac{1.197}{1.216}\right)\left(\frac{1204}{1199}\right)^2$	7.378	7.323	-
Upstream loss coefficient specified to mean fill conditions	$K_{up,fi} = K_{up}\left(\frac{\rho_{av15}}{\rho_{av5}}\right)\left(\frac{\dot{m}_{av5}}{\dot{m}_{av15}}\right)\left(\frac{A_{fr}}{A_c}\right)^2$	$K_{up,fi} = 0.52\left(\frac{1.197}{1.179}\right)\left(\frac{1204}{1199}\right)\left(\frac{256}{78.54}\right)^2$	5.487	5.632	-

Parameter	Equation	Evaluated	EES Calc. Value	Hand Calc. Value	Units
Pressure drop across fan	$dP = \begin{pmatrix} K_{il,fi} + K_{rz,fi} + K_{fs,fi} \\ +K_{fi} + K_{sp,fi} + K_{wd,fi} \\ +K_{de,fi} + K_{ct,fi} + K_{up,fi} \end{pmatrix} \left[\frac{\left\{ \frac{\dot{m}_{av15}}{A_{fr}} \right\}^2}{2\rho_{av15}} \right]$	$dP = \begin{pmatrix} 4.882 + 1.788 + 0.4882 \\ +1.818 + 0.6148 + 0.4966 \\ +4.624 + 7.378 + 5.487 \end{pmatrix} \left[\frac{\left\{ \frac{1204}{256} \right\}^2}{2 \times 1.197} \right]$	252.6	254.8	Pa
Fan power	$P = \frac{\dot{m}_{av5}}{\rho_{av5}} \left(\frac{dp}{\eta_{fan}} \right)$	$P = \frac{1204}{1.179} \left(\frac{254.8}{0.9 \times 1000} \right)$	286.6	289.1	kW
Total fan power	$P_{total} = P \times N_{WC}$	$P_{total} = 289.1 \times 10$	2866	2891	kW

APPENDIX C: LCOE CALCULATION DATA

Table C-1. Capital costs of 555 MW_e NETL Case-13 plant escalated to 2017 base year

S.N.	Item/Description	Equipment Cost	Material Cost	Labor		Sales Tax	Bare Erected Cost $(BEC)	Engineering CM H.O & Fee	Contingency Project	Total Plant Cost	
				Direct	Indirect					$ x1000	$/kW
1	Feed Water and Miscellaneous BOP System	30,162.86	5,995.21	8,756.96	0.00	0.00	44,915.03	3,788.50	7,770.52	56,474.05	101.76
2	Combustion Turbine/Accessories	101,188.84	966.28	7,456.05	0.00	0.00	109,611.16	9,302.59	12,104.65	131,018.41	236.07
3	HRSG, Ducting and Stack	45,961.94	1,276.72	7,253.12	0.00	0.00	54,491.78	4,640.54	6,214.27	65,346.59	117.74
4	Steam Turbine Generator	43,110.15	1,072.45	12,585.78	0.00	0.00	56,768.37	4,791.06	6,939.98	68,499.42	123.42
5	Cooling Water System	7,423.79	5,776.15	5,179.45	0.00	0.00	18,379.40	1,528.03	2,830.29	22,737.72	40.97
6	Accessory Electric Plant	22,361.42	4,933.52	11,907.10	0.00	0.00	39,202.04	3,006.34	4,475.24	46,683.62	84.11
7	Instrumentation and Control	7,765.15	796.94	6,452.14	0.00	0.00	15,014.23	1,249.84	1,864.01	18,128.09	32.66
8	Improvements to site	2,314.22	1,256.56	6,157.82	0.00	0.00	9,728.61	860.11	2,118.01	12,706.73	22.90
9	Buildings and Structures	0.00	5,583.97	5,936.08	0.00	0.00	11,520.05	936.71	1,868.04	14,324.80	25.81
10	Waste Heat Recovery Retrofit	0.00	0.00	0.00	0.00	0.00	0.00	0.00	0.00	0.00	0.00
	TOTAL COST	260,288.38	27,657.80	71,684.50	0.00	0.00	359,630.68	30,103.73	46,185.03	435,919.44	785.44
	Owner's Cost										
	Preproduction Costs										
	6 Months All Labor									4,326.72	7.80
	1 Month Maintenance Materials									503.18	0.91
	1 Month Non-fuel Consumables									189.47	0.34
	1 Month Waste Disposal									0.00	0.00
	25% of 1 Months Fuel Cost at 100% CF									3,004.78	5.41
	2% of TPC(Total plant costs)									8,718.39	15.71
	TOTAL									16,742.53	30.17
	Inventory Capital										
	60 day supply of consumables at 100% CF									230.44	0.42
	0.5% of TPC(Spare Parts)									2179.597182	3.93
	TOTAL									2,410.04	4.34
	Land									403.1749138	0.73
	Other Owner's Costs(15% TPC)									65387.92	117.82
	Financing Costs (2.7% TPC)									11769.82	21.21
	TOTAL OVERNIGHT COSTS(TOC)									532,632.92	959.70
	TASC Multiplier							IOU , Low Risk,33 years		1.078	0.00
	TOTAL AS SPENT COST (TASC)									574,125.03	1,034.46

Table C-2. Fixed and Variable operation and maintenance costs of 555 MW_e plant escalated to base year 2017

	Fixed Operating Cost		
S.N	Items/ Description	Annual Cost ($)	
1	Annual Operating Labor Cost	3,563,405.09	
2	Maintenance Labor Cost	3,541,722.28	
3	Administrative and Support Labor	1,548,307.25	
4	Property Taxes and Insurance	11,716,785.41	
	Total	20,370,220.03	
	Variable Operating Cost		
S.N	Items/ Description	Annual Cost($) (100%CF)	Annual Cost($) (At given CF)
1	Maintenance Material Cost	6,038,101.54	6038101.54
2	Water/1000 gallons	871,742.99	871742.9948
3	Chemicals	1,401,864.24	1401864.244
4	WHR Retrofit	0.00	0
	Total	8,311,708.78	8311708.779
4	Fuel	144,229,446.74	144229446.7
	Total	152,541,155.52	152541155.5

Table C-3. Financial and economic assumptions

Description	**Value**
Capital Structure	
Percentage Debt	45%
Percentage Equity	55%
Total Debt Amount	$258,408
Project Debt Terms	
Loan Amount (Thousand $)	$258,408
Interest Rate	5.5%
Repayment Term (in Years)	15
First Year of Principal Repayment	2020
Depreciation	
Capital Costs (Years)	20
Financing (Years)	20
Type	150% DB
ECONOMIC ASSUMPTIONS	
Cash Flow Analysis Period	
Plant Economic Life (Operational Period) in Years	30
Nominal Inflation Rate	3%
Escalation Factors	
Electricity: Energy Payment	3.0%
Gas	3.0%
Variable O&M	3.0%
Fixed O&M	3.0%
Capital Cost escalation during the capital expenditure period	3.6%
Tax Assumptions	
Income Tax Rate	38.0%

Table C-4. Income Statement for 30 operating years for the power plant without waste heat being considered

Year Ending	**2020**	**2021**	**2022**	**2023**	**2024**	**2025**	**2026**	**2027**	**2028**	**2029**	**2030**	**2031**	**2032**	**2033**	**2,034**	**2,035**
Revenues	$258,142	$265,886	$273,863	$282,078	$290,541	$299,257	$308,235	$317,482	$327,006	$336,816	$346,921	$357,329	$368,048	$379,090	$390,463	$402,176
Operating Expenses	$193,354	$199,154	$205,129	$211,283	$217,621	$224,150	$230,874	$237,801	$244,935	$252,283	$259,851	$267,647	$275,676	$283,946	$292,465	$301,239
Operating Income	$64,788	$66,732	$68,734	$70,796	$72,920	$75,107	$77,360	$79,681	$82,072	$84,534	$87,070	$89,682	$92,372	$95,143	$97,998	$100,938
Less: Total Interest Expense	$14,212	$13,578	$12,909	$12,203	$11,458	$10,673	$9,844	$8,969	$8,047	$7,073	$6,046	$4,963	$3,820	$2,614	$1,342	$0
Less: Depreciation & Amortization	$21,534	$41,454	$38,342	$35,471	$32,806	$30,349	$28,069	$25,967	$25,623	$25,617	$25,623	$25,617	$25,623	$25,617	$25,623	$25,617
Income Before Taxes	$29,042	$11,699	$17,483	$23,122	$28,655	$34,086	$39,448	$44,745	$48,402	$51,844	$55,401	$59,102	$62,930	$66,912	$71,033	$75,321
Less: Carry Forwards Used	$0	$0	$0	$0	$0	$0	$0	$0	$0	$0	$0	$0	$0	$0	$0	$0
Taxable Income w/o Tax Holiday	$29,042	$11,699	$17,483	$23,122	$28,655	$34,086	$39,448	$44,745	$48,402	$51,844	$55,401	$59,102	$62,930	$66,912	$71,033	$75,321
Taxable Income	$29,042	$11,699	$17,483	$23,122	$28,655	$34,086	$39,448	$44,745	$48,402	$51,844	$55,401	$59,102	$62,930	$66,912	$71,033	$75,321
Less: Income Taxes	$11,036	$4,446	$6,643	$8,786	$10,889	$12,953	$14,990	$17,003	$18,393	$19,701	$21,052	$22,459	$23,913	$25,427	$26,993	$28,622
Net Income	$18,006	$7,254	$10,839	$14,336	$17,766	$21,133	$24,458	$27,742	$30,009	$32,143	$34,348	$36,643	$39,016	$41,486	$44,041	$46,699

Table C-4. Income Statement for 30 operating years for the power plant without waste heat being considered

Year Ending	**2036**	**2037**	**2038**	**2039**	**2040**	**2041**	**2042**	**2043**	**2044**	**2045**	**2046**	**2047**	**2048**	**2049**
Revenues	$414,242	$426,669	$439,469	$452,653	$466,233	$480,220	$494,626	$509,465	$524,749	$540,492	$556,706	$573,407	$590,610	$608,328
Operating Expenses	$310,276	$319,584	$329,172	$339,047	$349,218	$359,695	$370,486	$381,600	$393,048	$404,840	$416,985	$429,494	$442,379	$455,651
Operating Income	$103,966	$107,085	$110,297	$113,606	$117,014	$120,525	$124,141	$127,865	$131,701	$135,652	$139,721	$143,913	$148,230	$152,677
Less: Total Interest Expense	$0	$0	$0	$0	$0	$0	$0	$0	$0	$0	$0	$0	$0	$0
Less: Depreciation & Amortization	$25,623	$25,617	$25,623	$25,617	$0	$0	$0	$0	$0	$0	$0	$0	$0	$0
Income Before Taxes	$78,343	$81,468	$84,675	$87,989	$117,014	$120,525	$124,141	$127,865	$131,701	$135,652	$139,721	$143,913	$148,230	$152,677
Less: Carry Forwards Used	$0	$0	$0	$0	$0	$0	$0	$0	$0	$0	$0	$0	$0	$0
Taxable Income w/o Tax Holiday	$78,343	$81,468	$84,675	$87,989	$117,014	$120,525	$124,141	$127,865	$131,701	$135,652	$139,721	$143,913	$148,230	$152,677
Taxable Income	$78,343	$81,468	$84,675	$87,989	$117,014	$120,525	$124,141	$127,865	$131,701	$135,652	$139,721	$143,913	$148,230	$152,677
Less: Income Taxes	$29,770	$30,958	$32,176	$33,436	$44,465	$45,799	$47,173	$48,589	$50,046	$51,548	$53,094	$54,687	$56,328	$58,017
Net Income	$48,573	$50,510	$52,498	$54,553	$72,549	$74,725	$76,967	$79,276	$81,654	$84,104	$86,627	$89,226	$91,903	$94,660

Table C-5. Cash flow statement for 30 operating years of the power plant

Year Ending	**2017**	**2018**	**2019**	**2020**	**2021**	**2022**	**2023**	**2024**	**2025**	**2026**	**2027**	**2028**	**2029**	**2030**	**2031**	**2032**	**2033**	**2034**	**2035**
Plus: Operating Revenues	$0	$0	$0	$258,142	$265,886	$273,863	$282,078	$290,541	$299,257	$308,235	$317,482	$327,006	$336,816	$346,921	$357,329	$368,048	$379,090	$390,463	$402,176
Less: Operating Expenses	$0	$0	$0	$193,354	$199,154	$205,129	$211,283	$217,621	$224,150	$230,874	$237,801	$244,935	$252,283	$259,851	$267,647	$275,676	$283,946	$292,465	$301,239
Cash From Operations	$0	$0	$0	$64,788	$66,732	$68,734	$70,796	$72,920	$75,107	$77,360	$79,681	$82,072	$84,534	$87,070	$89,682	$92,372	$95,143	$97,998	$100,938
Less: Income Taxes	$0	$0	$0	$11,036	$4,446	$6,643	$8,786	$10,889	$12,953	$14,990	$17,003	$18,393	$19,701	$21,052	$22,459	$23,913	$25,427	$26,993	$28,622
Less: Total Interest Expense	$0	$0	$0	$14,212	$13,578	$12,909	$12,203	$11,458	$10,673	$9,844	$8,969	$8,047	$7,073	$6,046	$4,963	$3,820	$2,614	$1,342	$0
Less: Total Principal Repayment	$0	$0	$0	$11,532	$12,166	$12,835	$13,541	$14,286	$15,071	$15,900	$16,775	$17,697	$18,671	$19,698	$20,781	$21,924	$23,130	$24,402	$0
Operating Cash Flow	$0	$0	$0	$28,008	$36,542	$36,346	$36,265	$36,287	$36,410	$36,626	$36,934	$37,935	$39,089	$40,273	$41,479	$42,715	$43,973	$45,261	$72,316
Less: Capital Cost	$53,987	$336,904	$183,348	$0	$0	$0	$0	$0	$0	$0	$0	$0	$0	$0	$0	$0	$0	$0	$0
Net Cash Flow After Investments	($53,987)	($336,904)	($183,348)	$28,008	$36,542	$36,346	$36,265	$36,287	$36,410	$36,626	$36,934	$37,935	$39,089	$40,273	$41,479	$42,715	$43,973	$45,261	$72,316
Plus: Loan Draws	$24,294	$151,607	$82,506	$0	$0	$0	$0	$0	$0	$0	$0	$0	$0	$0	$0	$0	$0	$0	$0
Net Cash Flow After Debt Financing	($29,693)	($185,297)	($100,841)	$28,008	$36,542	$36,346	$36,265	$36,287	$36,410	$36,626	$36,934	$37,935	$39,089	$40,273	$41,479	$42,715	$43,973	$45,261	$72,316
Plus: Equity Draws	$29,693	$185,297	$100,841	$0	$0	$0	$0	$0	$0	$0	$0	$0	$0	$0	$0	$0	$0	$0	$0
Net Cash Flow For Equity Distribution	$0	$0	$0	$28,008	$36,542	$36,346	$36,265	$36,287	$36,410	$36,626	$36,934	$37,935	$39,089	$40,273	$41,479	$42,715	$43,973	$45,261	$72,316
Cash Available for Equity Distribution	$0	$0	$0	$28,008	$36,542	$36,346	$36,265	$36,287	$36,410	$36,626	$36,934	$37,935	$39,089	$40,273	$41,479	$42,715	$43,973	$45,261	$72,316
Less: Equity Paid in Cash	$29,693	$185,297	$100,841	$0	$0	$0	$0	$0	$0	$0	$0	$0	$0	$0	$0	$0	$0	$0	$0
Equity Participants Cash Flow	($29,693)	($185,297)	($100,841)	$28,008	$36,542	$36,346	$36,265	$36,287	$36,410	$36,626	$36,934	$37,935	$39,089	$40,273	$41,479	$42,715	$43,973	$45,261	$72,316

Table C-5. Cash flow statement for 30 operating years of the power plant

Year Ending	**2036**	**2037**	**2038**	**2039**	**2040**	**2041**	**2042**	**2043**	**2044**	**2045**	**2046**	**2047**	**2048**	**2049**
Plus: Operating Revenues	$414,242	$426,669	$439,469	$452,653	$466,233	$480,220	$494,626	$509,465	$524,749	$540,492	$556,706	$573,407	$590,610	$608,328
Less: Operating Expenses	$310,276	$319,584	$329,172	$339,047	$349,218	$359,695	$370,486	$381,600	$393,048	$404,840	$416,985	$429,494	$442,379	$455,651
Cash From Operations	$103,966	$107,085	$110,297	$113,606	$117,014	$120,525	$124,141	$127,865	$131,701	$135,652	$139,721	$143,913	$148,230	$152,677
Less: Income Taxes	$29,770	$30,958	$32,176	$33,436	$44,465	$45,799	$47,173	$48,589	$50,046	$51,548	$53,094	$54,687	$56,328	$58,017
Less: Total Interest Expense	$0	$0	$0	$0	$0	$0	$0	$0	$0	$0	$0	$0	$0	$0
Less: Total Principal Repayment	$0	$0	$0	$0	$0	$0	$0	$0	$0	$0	$0	$0	$0	$0
Operating Cash Flow	$74,195	$76,127	$78,121	$80,170	$72,549	$74,725	$76,967	$79,276	$81,654	$84,104	$86,627	$89,226	$91,903	$94,660
Less: Capital Cost	$0	$0	$0	$0	$0	$0	$0	$0	$0	$0	$0	$0	$0	$0
Net Cash Flow After Investments	$74,195	$76,127	$78,121	$80,170	$72,549	$74,725	$76,967	$79,276	$81,654	$84,104	$86,627	$89,226	$91,903	$94,660
Plus: Loan Draws	$0	$0	$0	$0	$0	$0	$0	$0	$0	$0	$0	$0	$0	$0
Net Cash Flow After Debt Financing	$74,195	$76,127	$78,121	$80,170	$72,549	$74,725	$76,967	$79,276	$81,654	$84,104	$86,627	$89,226	$91,903	$94,660
Plus: Equity Draws	$0	$0	$0	$0	$0	$0	$0	$0	$0	$0	$0	$0	$0	$0
Net Cash Flow For Equity Distribution	$74,195	$76,127	$78,121	$80,170	$72,549	$74,725	$76,967	$79,276	$81,654	$84,104	$86,627	$89,226	$91,903	$94,660
Cash Available for Equity Distribution	$74,195	$76,127	$78,121	$80,170	$72,549	$74,725	$76,967	$79,276	$81,654	$84,104	$86,627	$89,226	$91,903	$94,660
Less: Equity Paid in Cash	$0	$0	$0	$0	$0	$0	$0	$0	$0	$0	$0	$0	$0	$0
Equity Participants Cash Flow	$74,195	$76,127	$78,121	$80,170	$72,549	$74,725	$76,967	$79,276	$81,654	$84,104	$86,627	$89,226	$91,903	$94,660

Table C-6. Sample calculation of *LCOE* from *IRR* and *COE* values

Parameters	Equation	Evaluated	Value	Units
COE	Assumed and calculated for 12% IRR	49.31	49.31	$ MWh^{-1}
IRR	*IRR=IRR(Net Cash flows, Guess)*, Calculated from MS Excel	12.02	12.02	%
A	$A = \frac{D(1+D)^{LPn}}{(1+D)^{LPn} - 1}$	$A = \frac{0.1202(1+0.1202)^{30}}{(1+0.1202)^{30} - 1}$	0.1243	
K	$K = \frac{1+N}{1+D}$	$K = \frac{1+0.03}{1+0.1202}$	0.9194	
Levelization Factor	$LF = \frac{A(1 - K^{LPn})}{(D - N)}$	$LF = \frac{0.1243(1 - 0.9194^{30})}{(0.1202 - 0.03)}$	1.2672	
Levelized Cost of Electricity	$LCOE = COE \times LF$	$LCOE = 49.31 \times 1.2672$	62.485	$ MWh^{-1}
First year revenue	$REV = MWh_{avg} \times COE \times 8760 \times CF$	$REV = 547 \times (49.31 \times 1.03^{2020-2017}) \times 8760 \times 1$	258.18	M$

LIST OF ABBREVIATIONS

CCGT	Combined Cycle Gas Turbine
CCF	Capital Charge Factor
CF	Capacity Factor
COE	Cost of Electricity
COP	Coefficient of Performance
DB	Declining Balance
DOE	Department of Energy
EIA	Energy Information Administration
FG	Flue Gas
GTX	Gas Turbine Exhaust
HHV	Higher Heating Value
HP	High Pressure
HRSG	Heat Recovery Steam Generator
IP	Intermediate Pressure
IPT	Intermediate Pressure Turbine
IRR	Internal Rate of Return
ISO	International Organization for Standardization
LCOE	Levelized Cost of Electricity
LHV	Lower Heating Value
LP	Low Pressure

LPT	Low Pressure Turbine
LF	Levelization Factor
NETL	National Energy Technology Laboratory
NGCC	Natural Gas Combined Cycle
OC	Operation Costs
STM	Steam
TOC	Total Overnight Capital
TMY	Typical Meteorological Year
TTD	Terminal Temperature Difference
VC	Vapor Compression
WHR	Waste Heat Recovery